THE RADIO AND ELECTRONIC ENGINEER

The Journal of the Institution of Electronic and Radio Engineers

FOUNDED 1925 INCORPORATED BY ROYAL CHARTER 1961

"To promote the advancement of radio, electronics and kindred subjects by the exchange of information in these branches of engineering."

VOLUME 28 DECEMBER 1964 NUMBER 6

UNIFYING THE ENGINEERING PROFESSION

ONE of the objects of the Council of Engineering Institutions is to promote common standards of admission to the thirteen Chartered Engineering Institutions. In pursuance of this object, proposals for a common scheme of examination for all engineering institutions are now being considered by the Councils of the Institutions. These proposals involve a common entrance requirement, and a common Part 1 examination of a standard equivalent to that reached at the end of the first year of a university engineering degree and consisting of six compulsory subjects.

No specific proposals have been made about Part 2, except that this should be of degree standard and should give a sufficient choice of papers to meet the requirements of the individual institutions. There is also a tentative suggestion of a Part 3, which would be entirely specific to each institution, and would be unlikely to take the form of a written examination.

The suggested common entrance requirement, at G.C.E. "A" level in physics and pure and applied mathematics, and, possibly, "O" level in chemistry, is unlikely to arouse great opposition, but the proposals for the new Part 1 examination have far-reaching implications, and may well give rise to many objections. These objections will certainly not be limited to the actual content of the examination, but will extend to the whole principle of 'common' examinations at this level. It is felt strongly by many people that there is insufficient common ground between engineers of the different disciplines—ranging as they do from mining to electronics—for a common examination to be realistic at this comparatively advanced level.

If one subscribes to this latter view there are two alternative methods of dealing with the problem: the first is to offer in Part 1 either a choice of subjects or a wide choice of questions.

The other method is represented by the opinion, held by some members of our own Institution's Council, that it is unwise and unnecessary for the C.E.I. to design an examination based chiefly on common papers. They consider that the C.E.I. should instead become the custodian of a common standard of professional engineering qualification, in the manner in which the senate of a university strives to secure that the standard of, say, an Honours B.Sc. degree is uniform whatever the subject and faculty.

Quite apart, however, from the desire of C.E.I. to unify the profession, a need has been expressed for a 'broader based' engineer, for instance by Dr. A. C. Copisarow of N.E.D.C. in his recent address to the Institution.* Certain universities also are setting up engineering courses designed to train engineers, who can specialize after graduation, rather than 'civil' engineers or 'electronic' engineers. It is claimed that in industry there is a demand for these broader-based engineers, who are said to be easier to promote into management positions involving many different engineering disciplines.

These two requirements should not necessarily be completely opposed; and it should be possible to devise a scheme of training for all engineers which will be sufficiently broadly based, but yet allow for treatment in depth of each particular field of engineering.

A. J. K.

* "Enhancing the Contribution of the Engineer to the Economy", *Proc.I.E.R.E.* (To be published.)

INSTITUTION NOTICES

Convention on 'Advances in Automatic Control'

A Convention on 'Advances in Automatic Control' will be held at Nottingham University from 5th to 9th April, 1965. Arrangements are being made jointly by the Institutions of Mechanical, Electrical, Chemical, Production and Electronic and Radio Engineers, the Royal Aeronautical Society, and the Society of Instrument Technology, under the aegis of the United Kingdom Automation Council. (See *The Radio and Electronic Engineer*, January 1964, p. 64.)

There will be 25 to 30 papers on a wide range of topics, including a number of review papers; the sessional papers will be introduced by rapporteurs. It is hoped to include local visits in the programme. Accommodation for delegates will be available at the University.

Further details of arrangements may be obtained from the Conference Section of the Institution of Mechanical Engineers, 1 Birdcage Walk, Westminster, London, S.W.1.

I.E.C. General Meeting 1965

The next General Meeting of the International Electro-Technical Commission will be held in Tokyo from 10th to 23rd October, 1965.

Several Committees concerned with work in the fields of Electronics and Telecommunications are likely to meet in Tokyo, among them the following:

Radio-communication (TC 12); Radio Receiving Equipment (SC 12A); Safety (SC 12B); Electronic Tubes and Valves (TC 39); Capacitors and Resistors for Electronic Equipment (TC 40); Waveguides and their accessories (SC 46B); Semiconductor Devices (TC 47); Electromechanical Components for Electronic Equipment (TC 48); Environmental Testing (TC 50); Shock and Vibration Tests (SC 50A); Climatic Tests (SC 50B); Printed Circuits (TC 52); Reliability of Electronic Components and Equipment (TC 56).

The previous General Meeting of the I.E.C. was held in Venice from May to June 1963; a short note on some of the work of interest to electronic and radio engineers was published in the *Proceedings of the I.E.R.E.* for March-April 1964.

Royal Society to Increase Annual Elections

In his Anniversary Address in November, Sir Howard Florey, President of the Royal Society, announced that the Society intended to increase the number of annual elections to Fellowship from 25 to 32.

He said that it was the firm intention of this year's Council that a substantial number of new places should be given to electing some Fellows in some of the disciplines currently not represented or, if represented, inadequately so.

Sir Howard continued, "It is certain that there are many applied scientists particularly in Government and industrial environments who, if they became Fellows, would greatly strengthen the Society in its relationship to the contemporary milieu. It is for the Society to devise machinery by which their originality and contributions to contemporary civilizations can be assessed as against the more familiar claims of those who have hitherto formed the great majority of our potential Fellows."

Later in his Address Sir Howard referred to the acceptance by the Government of proposals put forward by the Royal Society for the setting-up of research and advisory councils. He also mentioned the Society's collaboration with the Engineering Institutions Joint Council (now the Council of Engineering Institutions) in arranging a conference for headmasters and others interested in education, to make known as widely as possible the intellectually satisfying careers which were presented by the applied sciences.

World Congress on Engineering Education

A World Congress on Engineering Education will be held in conjunction with the 73rd Annual Meeting of the American Society for Engineering Education at the Illinois Institute of Technology, Chicago, Illinois, from 21st to 25th June, 1965. This educational meeting is being sponsored by the Engineers' Council for Professional Development, the Engineers' Joint Council, the Conference of Engineering Societies of Western Europe and the United States, the Pan-American Federation of Engineering Societies, and the American Society for Engineering Education.

The programme for this Congress will cover all phases of engineering education—from the post-secondary two-year engineering technician programmes, through the first degree (diploma engineer) for professional engineers, and including post-graduate doctoral research and university teaching.

Further information may be obtained from the World Congress on Engineering Education, American Society for Engineering Education, University of Illinois, Urbana, Illinois, U.S.A.

Index to Volume 28

This issue completes Volume 28 of *The Radio and Electronic Engineer* which covers the period July–December 1964. An Index to the volume will be circulated with the February 1965 issue.

U.D.C.621.396.677

Wideband, High-gain, Variable Time-delay Techniques for Array Antennae

By

First-Lieutenant
J. B. PAYNE, M.S., Ph.D.,
U.S.A.F.†

Reprinted from the Proceedings of the Symposium on "Signal Processing in Radar and Sonar Directional Systems", held in Birmingham from 6th–9th July, 1964.

Summary: The purpose of this paper is to present two improved techniques for obtaining a wideband, high-gain, non-dispersive, variable time-delay device to steer array antennae. The first time-delay technique utilizes two wideband helix structures separated by a cylindrical drift tube to obtain a variable delay of 20 ns or more with a gain of 20 to 30 dB. An electron beam passes through the two helices and drift region. Signal energy coupled on to the beam at the input helix is decoupled at the output helix. A variable delay is obtained by controlling the beam velocity through the drift region by varying the drift tube potential. Gain variation is minimized by maintaining constant beam velocity through the helices. The gain of the device is proportional to output helix length.

The second method for obtaining a variable time-delay is realized by switching different time-delay elements into the signal path. Such a technique is controlled digitally and is referred to as a digital delay line. In this technique each switch is replaced by a wideband amplifier. It is the bandwidth of these amplifiers that determines the system bandwidth (200 to 800 Mc/s). Each bit is capable of producing 12 dB gain. The amplifiers can be easily gated on or off.

1. Introduction

The introduction of missiles and satellites into our defence environment has greatly increased the demands placed on modern radar technology. Longer detection ranges of smaller target cross-sections and higher data rates have necessitated investigations into array antenna design. Array systems have the advantage of greater power handling capability and rapid single- or multiple-beam scanning from stationary structures.

Array antennæ have been used for many years in both the communication and radar fields. Until recent years this type of antenna was designed primarily to handle narrow-band signals and as such was referred to as a phased array. Their characteristics in this mode have been extensively studied and are well understood.

In adopting the array system, range resolution has suffered due to the limited bandwidth problems encountered when narrow pulses or pulse compression like linear or quadratic frequency-time waveforms are incorporated into the phase-steered system.

In array antennæ it is desirable to steer the position of the main beam by varying the time delay between elements. However, in narrow-band systems it has been shown that steering by varying the relative phase shift between elements produces the same result with negligible loss in the signal/noise ratio. The relative phase shift method is simple and inexpensive to implement.

As the bandwidth of a phase steered array system is increased, a point is quickly reached where the loss in signal/noise ratio can no longer be neglected. This deterioration in system performance of a phase-steered array is caused by two main factors. The first and most important factor is due to the finite propagation or transient time across the array aperture for off-broadside beam positions. For a narrow pulse it is this effect that produces a finite build-up and decay of the signal. For instance, when the pulse length is equal to array transit time, the signal/noise ratio will be down 3 dB. For certain types of pulse compression this finite transit time prevents coherent element-to-element summation off-boresight.

The second factor that can contribute to signal deterioration is the increase in half-power beamwidth (decreased antenna gain) due to an increase in the pulse bandwidth. Assuming wideband elements and phase shifters, this effect is usually of secondary importance and is highly dependent on the feed system

† Rome Air Development Center, Griffiss Air Force Base, New York.

used. At most this effect is about 10% of the transit effect degradation. In a series-fed array antenna where the phase is inserted between elements (compared with the parallel-fed system) the beam is phased to steer at a single carrier frequency. Power radiated at different frequencies in the spectrum will be steered to different directions. Thus, wider spectrum of transmitted frequencies results in beam broadening. In a parallel-fed system (element-feed line lengths are the same) the element-to-element phase is also a function of frequency. In this case the frequency dependence is a function of beam position off-boresight and the type of phasing employed.

Both of the above problems can be overcome by the proper use of true time-delay steering. Methods have been devised for compensating phased arrays in order that they might handle wideband signals; however, the added complexity makes such techniques questionable.

The major component problem in building a wideband array system is the realization of a lossless, wideband, non-dispersive, variable time-delay device.

Work sponsored by R.A.D.C. up to the present has been limited to the Philco lumped-parameter delay-line technique at i.f. which utilizes all-pass networks similar to the symmetrical lattice phase-correction network.[1] Another technique which appears to be attractive is the cross-field technique described by Klüver.[2]

Work at Lincoln Laboratory has concentrated on the diode-switched digital delay technique at both i.f. and r.f.[3] Other proposed digital techniques include the use of new ferrite switches for the higher microwave frequencies.

The purpose of this paper is to present two improved techniques for obtaining a wideband variable time delay device to steer array antennæ.

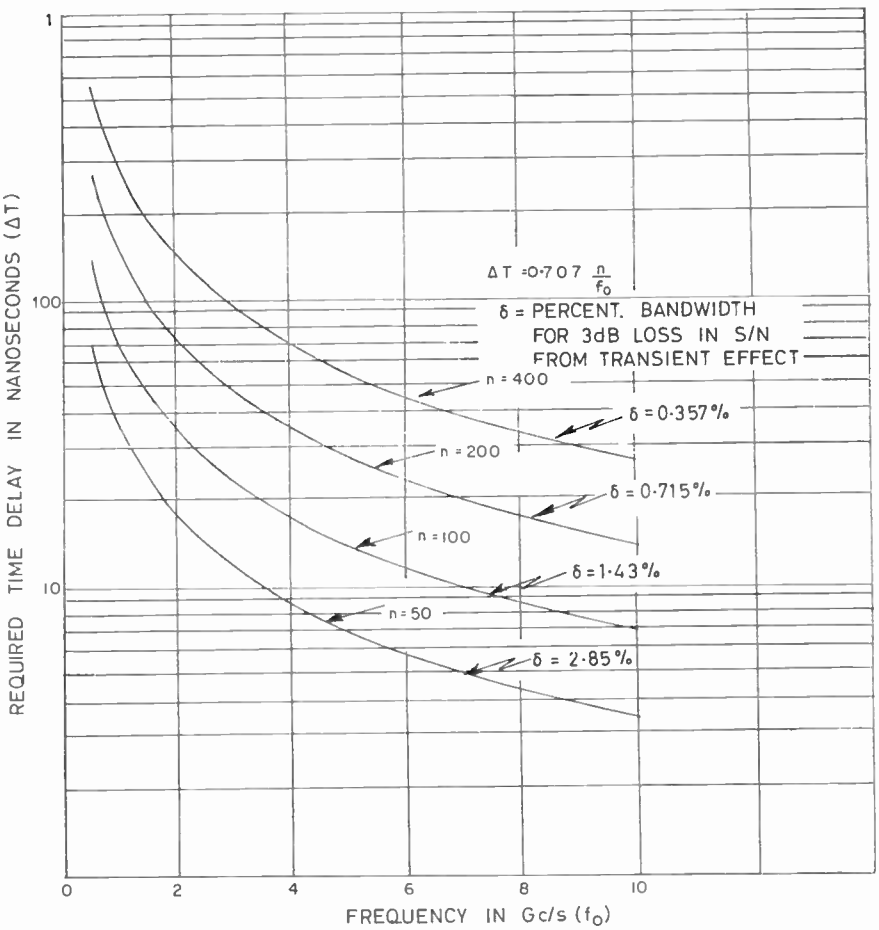

Fig. 1. Maximum delay as a function of the centre frequency of operation and array length.

2. Variable Time Delay Requirements

In order to time-delay-steer the beam of an array antenna off-boresight by an angle α, a differential time delay, ΔT, must be introduced into each element or sub-group signal path. It can be shown that the desired differential time-delay for the Mth element or sub-group signal path ($M = 0$ is taken as the centre element or sub-group with a total count of $(2M+1)$ in the array) is given by the expression:

$$\Delta T = M\Delta T_0 \sin\alpha = \frac{M\Delta X_0}{c}\sin\alpha \qquad \ldots\ldots(1)$$

where c = speed of light in free space

ΔT_0 = propagation time between elements or sub-groups

ΔX_0 = element or sub-group spacing.

Notice that the total differential delay required to scan $\pm\alpha$ would be twice ΔT.

If we assume the array is $n\lambda$ long (i.e. $2M+1 = n\lambda$), then for a scan angle of ± 45 deg coverage, the maximum delay variation required can be written as

$$\Delta T_{max} = 0{\cdot}707 n\frac{\lambda}{c} = 0{\cdot}707\frac{n}{f_0} \qquad \ldots\ldots(2)$$

Here the array is scanned about the centre element.

This expression gives the maximum delay as a function of both the centre frequency of operation and array length n in terms of wavelength. Figure 1 is a plot of this equation for array lengths of 50, 100, 200, and 400λ as a function of the operating frequency. Also indicated is the percentage bandwidth where the signal is down 3 dB due to the lack of time delay steering. This is indicated by δ.

As an example, for 100λ array at 4 Gc/s (24·6 ft) the maximum delay variation required is 17·65 ns. In the absence of delay steering the signal would be down 3 dB for a bandwidth greater than 1·43% or 57 Mc/s.

There are two basic ways for obtaining variable time delay. One logical way would be to vary the propagation velocity, v_p, down a transmission or guide structure. If the structure was a conventional waveguide, variable delays could be obtained by operating the guide near cut-off and varying either the physical dimension of the guide or the radio frequency. However, waveguide structures generally are not satisfactory for wideband signals since they introduce dispersion and loss. Physical movement of components is too slow. However, this method has been used with narrow-band signals. The first time-delay technique to be discussed below obtains a variable time-delay by controlling the signal propagation velocity down a broadband, non-dispersive structure. It is also possible to obtain gain at the same time from this device.

Another method for obtaining variable time-delay can be realized by switching different time-delay elements into the signal path. Such a technique is usually controlled digitally and is referred to as a digital delay line. The second delay technique discussed below realizes a wideband, high gain, variable delay by this digital technique.

3. Velocity-controlled Electron-beam Time Delay

If, instead of trying to vary the propagation velocity of electromagnetic waves down a guiding medium, we control the velocity of a modulated electron beam down a drift region, then it appears feasible to build a true variable time-delay device (delays greater than 20 ns) for array antennæ. The basic configuration is shown in Fig. 2.

An electron beam emitted by the cathode is accelerated toward the first helix by the accelerating potential V_a. The beam, which is confined by magnetic focusing, passes through the input coupling helix at a constant velocity. Upon leaving helix 1, the beam is further accelerated or decelerated by the potential V_b between the helix and drift region. The beam moves through the drift region at its new velocity and is then decelerated or accelerated by $-V_b$ as it passes into the second helix.

Energy coupled to helix 1 is in turn coupled to the beam. V_a is adjusted so the beam velocity and helix phase velocity are nearly synchronous. The length of helix 1 is made to correspond to the Kompfner dip length.[4] This is the length for which all of the helix energy is transferred to the beam.

The variable time-delay is obtained by varying the beam velocity in the drift region, L_d. The beam velocity, v_b, is a function of the two potentials and can be written as

$$v_b \simeq \sqrt{V_a + V_b} = \sqrt{V_d} \qquad \ldots\ldots(3)$$

Normally V_a would be held constant and V_b varied.

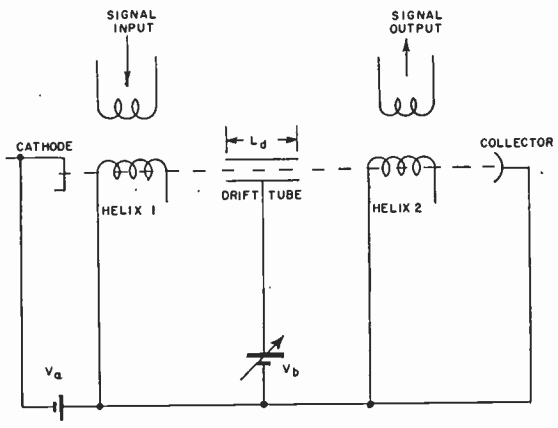

Fig. 2. Travelling-wave variable delay tube.

The time T required for the beam to traverse L_d is

$$T = \frac{L_d}{v_b} \qquad \text{.....(4)}$$

A change in beam velocity through the drift tube will result in a change in delay. That is

$$\Delta T = T_1 - T_2 = \frac{v_{b_2} - v_{b_1}}{(v_{b_1} v_{b_2})} L_d \qquad \text{.....(5)}$$

The beam velocity, v_b, is related to the accelerating potential V_d by the expression

$$v_b = \sqrt{\frac{2eV_d}{m}} \qquad \text{.....(6)}$$

Here e/m is the electron charge/mass ratio.

The change in time delay, ΔT, produced by varying the drift tubes potential from V_{d1} to V_{d2}, can be written as

$$\Delta T = L_d \sqrt{\frac{m}{2e}} \left[\frac{\sqrt{V_{d_2}} - \sqrt{V_{d_1}}}{\sqrt{V_{d_1} V_{d_2}}} \right]$$

or

$$\Delta T = L_d 42{\cdot}8 [V_{d_2}^{-\frac{1}{2}} - V_{d_1}^{-\frac{1}{2}}] \text{ ns} \qquad \text{.....(7)}$$

where L_d is in inches and V_d is in volts.

For a 300-V change (± 150) in V_d centred about 200 V and a drift length of 6 in, a variable time delay of $\Delta T = 23{\cdot}1$ ns is obtained. Lower drift velocities will enable large ΔT's to be obtained.

The beam is accelerated or decelerated back to the helix synchronous velocity before entering helix 2. R.f. energy will be coupled to the helix. If the helix is long enough, amplification will be obtained.

Since travelling-wave tubes are inherently broadband devices, bandwidths of up to 50% should be realizable.

The use of t.w.t. structures for phased-array steering is not a new concept and has received limited investigation in the past. These techniques were used in narrow-band systems where a maximum shift of 360 deg was all that was required. Larger amounts of phase shift are redundant and could be eliminated. However, in wideband steering systems time delays greater than that equivalent to 360 deg of phase shift are necessary. Some of these earlier techniques are briefly discussed below.

The t.w.t. technique employed by Illinois Institute of Technology,[5] Buchmiller at Stanford,[6] and early Hughes work[7] utilized a conventional t.w.t. and placed a number of equally spaced couplers along the length of the helix. The relative phase shift between adjacent couplers was varied by controlling the d.c. helix voltage (beam velocity down the helix). Array phase-steering was demonstrated in each case. Although the multiple output (or input) phase shifting technique appears to be quite satisfactory and simple, it has several severe disadvantages. The major problems are:

(1) The location of the couplers is very critical.

(2) Matching each coupler over a wide bandwidth is very difficult if not impossible.

(3) The gains of the devices vary 6 to 10 dB when the array beam is steered off-boresight by 45 deg. This gain change is a result of varying the beam velocity above and below the synchronous velocity.

A different approach taken by the General Electric Company at C-band utilized a split-helix t.w.t. amplifier.[8] This low-noise amplifier was strictly a 2-port device in which the helix was separated 0·75 to 2 inches to form a drift region. The drift region was simply an open space between the two halves of the helix. The input helix was maintained at the voltage for optimum noise figure. Phase shift was accomplished by varying the d.c. potential between the two helices. This drift region was not a true drift space since the beam experiences a constant accelerating force due to the potential difference between helices. A shift of 360 deg in phase resulted in a gain variation of 2 to 3 dB. This gain variation was primarily due to the variation of beam velocity through the output helix.

A more recent development has been the travelling-wave phase shifter developed by Hughes[9] at X-band. Its basic configuration is identical to the technique depicted in Fig. 2. The two helices are maintained at constant potentials and thus no gain variation is experienced due to beam velocity variation within the helix. Again, however, the Hughes device is intended to introduce a very limited variation in phase and thus the drift region is only about 1·5 in. Figure 3 shows the variation in phase as a function of drift tube voltage for this tube. The gain was measured to be in the range of 35 to 43 dB at frequencies of from 8 to 12 Gc/s. The maximum gain variation as a function of drift tube voltage was about ± 1 dB with a static drift tube potential of 300 V. It differs from the General Electric split-helix tube in that a constant potential (constant velocity-zero acceleration) drift region is obtained by surrounding the region between helices with a cylinder whose potential is varied to control the beam velocity through it.

The drift region of the variable time-delay tube pictured in Fig. 2 is being extended to about 7 in at X-band. In order to obtain large delay variations the lower limits of the drift tube potentials will have to approach the 20 to 30 volt range.

As the variation in delay is increased by either lowering the minimum drift tube potential or by increasing the drift region length, two major problems arise. At low drift tube potentials beam defocusing

becomes important, particularly when the drift region length is increased. This results in excessive beam intercept current on the drift tube cylinder and output helix. The effect can be reduced by increasing the axial magnetic confinement field or by using beam-forming or electrostatic focusing techniques either between the input helix and drift region or within the drift space itself. A simple electrostatic focusing technique within the input helix to drift tube transition region would be to optimize the helix to drift tube diameter ratio. For very long drift spaces the drift cylinder itself could be divided into several lens sections of varying diameter and potentials.

From published experimental results the defocusing effect is not expected to present a major problem. Caulton, Hershenov, and Paschke[10] in their experiments with Landau damping passed electron beams ranging from 50 μA to 0·5 mA down a 20-cm drift space with the relatively low drift potential of 50 V. A magnetic focusing field of 1000 gauss was used.

The second and more serious problem involves the variation of overall gain as a function time delay (beam velocity through the drift space). Ideally, the electron beam, upon entering the drift space, should be density modulated by the input signal. The beam should be bunched with all electrons having the same velocity. Finite velocity modulation of the beam results in two propagating waves (the slow and fast space-charge waves) whose phase velocities are less and greater respectively, than the electron beam velocity. These waves have been termed the Hahn-Ramo waves.[11,12] A spatially periodic interference pattern results along the beam, with minima at every half-plasma wavelength, if both waves are excited with equal amplitude.[13] Such patterns are clearly indicated from the experimental results of Beam[14], and Caulton et al.[10]

The fundamental plasma wavelength varies with both beam current and drift potential. Therefore, as the delay is varied by altering the drift space potential

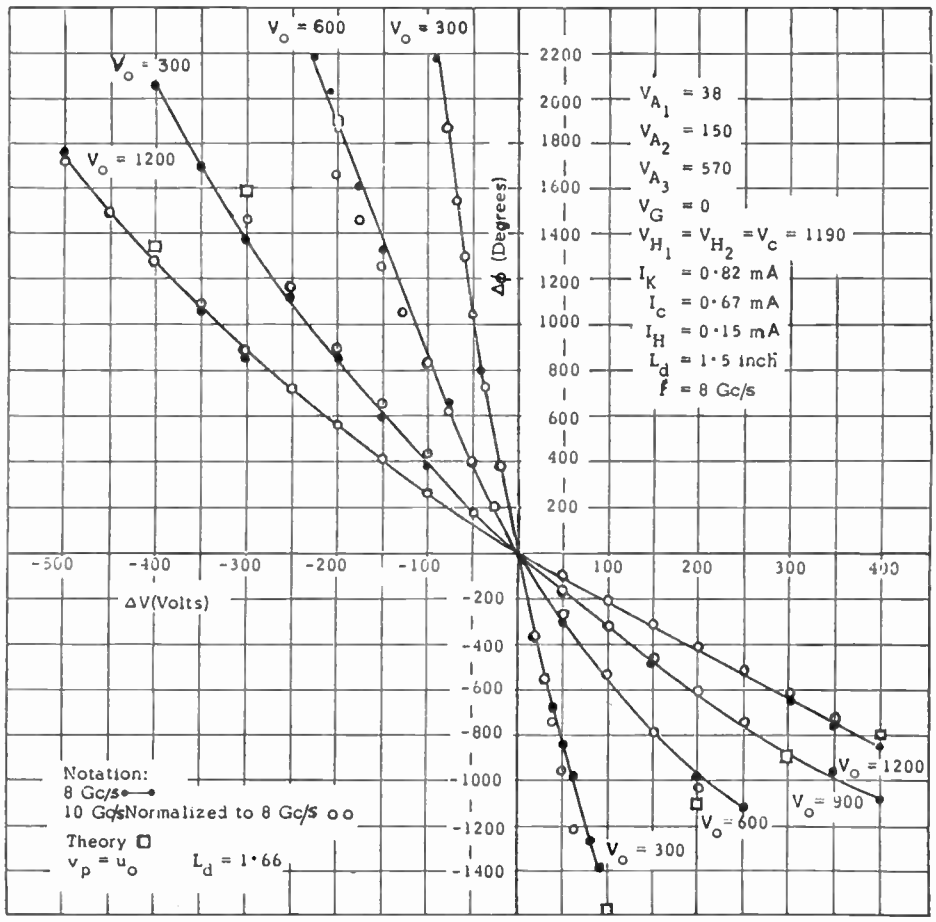

Fig. 3. Phase shift ($\Delta\phi$) as a function of incremental change in drift tube voltage (ΔV) with the static drift-tube voltage (V_0) as a parameter.

the amplitude of the output signal (gain) will vary. Most modulating techniques introduce some velocity spread within the beam. The end objective is to minimize this velocity spread. Density modulation of the beam with a gridded structure introduces minimum velocity spread, however, in the microwave region such a broadband structure is not easily realizable. Beam modulation by a narrow-gap resonator, besides being relatively narrowband, velocity-modulates the beam as in a klystron, causing large variations in gain, and therefore, is very undesirable. The broadband helix structure appears to be a reasonable compromise. The helix will density-modulate the beam to a degree; however, it will still introduce velocity modulation.

Other coupling techniques are being considered but the helix structure appears superior at this time.

Fortunately, but paradoxically, the amplitude of the spatially periodic interference pattern decreases at large distances from the modulating source. Such a phenomenon is referred to as Landau damping[15] and has been analysed by Dawson[16] and Berghammer[13] and experimentally verified by Caulton et al.[10] Berghammer has shown that the decay of the velocity modulation is attributable to a spatial Landau damping of the 'fast' space-charge wave.

Mihran[17] investigated the propagation of an r.f. signal, instituted as density modulations (grid) with some velocity modulation present. He found that the amplitude of the spatial interference pattern could be controlled by changing the magnetic focusing field when the beam was viewed 15 to 20 cm from the modulating point.

From the above considerations a delay variation in excess of 20 ns with maximum fluctuations in gain of several decibels is considered realizable by this technique of an extended drift space region.

Once the bunched beam enters the second or output helix useful gain of 20 to 30 dB can be obtained.

4. Wideband Digitally Controlled Delay Line for Phased Array Steering

Digitally controlled delay lines or phase shifters have been used for the past several years in steering phased array antennae. Lincoln Laboratory has conducted an extensive programme in the development of such devices. Much of Lincoln's work can be found in their technical reports.[3]

Most digital delay-line or phase-shift devices use diodes to switch the signal through or around a length of transmission line cut to give the desired incremental delay or phase shift. A commonly used technique is shown in Fig. 4. The input signal can be delayed through path 1 simply by closing S1, S2, and opening S3, S4. Path 2 is selected by closing S3, S4, and opening S1, S2. However, high-speed switching requires the elimination of mechanical switching devices. Switching devices in the past have utilized simple diodes with small forward impedance and a high back impedance. Replacing S1, S2, S3, S4, with diodes D1, D2, D3, D4, and controlling the magnitude and direction of current flow through the diodes one is able to direct the input signal through either path 1 or path 2.

These diodes, however, have a finite series resistance when forward biased and therefore produce loss.

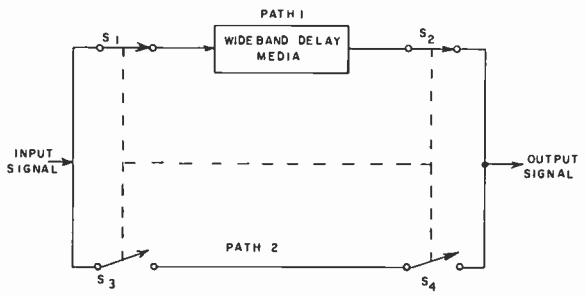

Fig. 4. Single-bit digital delay line.

Additional loss is usually introduced so as to reduce the fluctuation in amplitude as the signal path is changed.

The matching of these diodes and the proper termination of the incremental delay units is accomplished at the expense of bandwidth. Series diode resistance plus diode reactance also results in poor matching and s.w.r. between the incremental delay units.

A typical 6-bit, 28-Mc/s digital phase shifter or delay line is described in Reference 3. It was designed to produce a total of 360 deg phase shift at 28 Mc/s by switching either through or around 6 lengths of coaxial cable by the use of diode switches. Total insertion loss was 11 dB. The set-up time ran about 3 μs with a maximum amplitude error of 0·25 dB and phase error of 2 deg. Input power capacity was limited to 1 watt. Each diode switch required about 40 mA in order to reduce the diode series resistance to a useable value.

The wideband digital delay line to be described utilizes the basic technique indicated by Fig. 4. However, in this case each mechanical switch is replaced by a wideband amplifier. It is the bandwidth of these amplifiers that determine the system bandwidth (200 to 800 Mc/s). These amplifiers can be gated on or off. By using wideband amplifiers in place of the diode switches three advantages are gained:

(1) Each delay line (coaxial) is properly terminated into its characteristic impedance over the frequency

band of interest; this prevents loss due to excessive s.w.r.

(2) Each delay line increment is isolated from the next due to the presence of amplifiers.

(3) With the inclusion of amplifiers the total input-output gain can be made equal to or greater than unity (gains as high as 100 dB for a 10-bit device are achievable with bandwidths of 200 Mc/s. However, 100 dB is more than is normally required with such bandwidths).

The wideband digital delay line is inherently a low-frequency device. By low frequency we mean intermediate frequencies up to 600 or 800 Mc/s. If we wish to process a signal with a 200 or 300 Mc/s bandwidth the i.f. centre frequency would more than likely be located in the range of 200 to 300 Mc/s.

4.1. *High-gain Wideband Digital Delay*

The basic building block for the high-gain wideband delay device is a stable wideband amplifier that can be gated on or off. One such amplifier will replace each diode switch of Fig. 4. The wideband amplifiers to be described utilized transistors operated in the common-base configuration; however, vacuum tubes could be used if necessary.

The basic common-base amplifier configuration is shown in Fig. 5. The input signal power is:

$$P_{in} = Z_{in}(\Delta i)^2 \qquad \text{.....(8)}$$

where Z_{in} is the input impedance which is approximately equal to r_e ($r_e \simeq 25$ to 100 ohms). In the grounded-base configuration the emitter signal current is approximately equal to the collector signal current. Therefore, the amplifier's output signal power is:

$$P_{out} = R_2(\Delta i)^2 \qquad \text{.....(9)}$$

The amplifier power gain then becomes

$$G_p = \frac{R_2}{Z_{in}} \qquad \text{.....(10)}$$

The amplifier gain is thus fixed by the ratio of the input impedance to output load. This relationship is valid as long as the cut-off frequency of the transistor is not exceeded. The figure of merit for amplifiers is normally given as the gain × bandwidth product, f_t, in Mc/s. Thus, the upper bandwidth limitation, f_c, on the grounded-base amplifier can be written as

$$f_c = \frac{f_t}{G_p} \qquad \text{.....(11)}$$

The amplifier can easily be gated off by either grounding the base directly or by applying a small negative bias to the base. When reverse biased the opened switch produces at least 25 dB isolation in the band of interest.

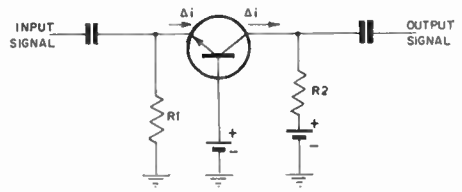

Fig. 5. Grounded base amplifier.

In this particular application it is desirable to have the amplifier's input and output impedances matched to a transmission line of characteristic impedance Z_0. When resistive coupling is used as shown in Fig. 5 such that $Z_0 = Z_{in} = R_2$, unit gain is obtained from eqn. 10. Since longer lengths of coaxial cable used for delay lines produce attenuation it is desirable that this amplifier should provide gain instead of having to add additional amplifiers at the delay units output. Gain can be obtained by increasing the load impedance seen by the collector. Such an increase in load impedance can be obtained by using broadband transformers like those described by Ruthroff[18] to transform Z_0. The particular transformer useful in this case is the 4:1 impedance transformer shown in Fig. 6, which is wound to form a transmission line. Ruthroff obtained bandwidths of over 700 Mc/s at the 3-dB points with the lower cut-off at 200 kc/s and the upper cut-off at 715 Mc/s.

If this transformer were combined with the grounded-base amplifier of Fig. 5, a power gain of 4 (6dB) would be possible when the amplifier's input and output are matched to Z_0. Figure 7 is a schematic of the wideband amplifier.

The transistor shown (2N709) has a typical f_t of 800 Mc/s. The input impedance Z_{in} was measured at about 31 Ω. With the 4:1 impedance transformer coupled to 52 Ω, a bandwidth of over 200 Mc/s has been observed. This was verified with several 2N709

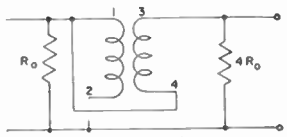

(a) Transmission line form.

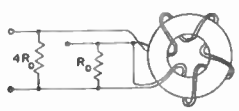

(b) Wiring diagram.

Fig. 6. 4:1 impedance transformer.

transistors, which indicates that the devices tested had a better f_t than the typical sample. When the input signal was taken directly from the sweep generator output the response to 200 Mc/s was within 1 dB of being flat. A 10-ft length of 52 Ω coaxial cable was then connected between the generator and amplifier input. No attempt was made to match the cable. The amplifier output showed ripples of about 2 dB amplitude due to the non-ideal termination. The 3 dB drop-off was above 250 Mc/s.

Since loss will vary from bit to bit due to the different lengths of delay line the amplification must be controlled without disturbing the line match. Gain variation can be accomplished by several techniques. Since the input impedance to the transistor is smaller than Z_0, a small resistance pad added to the input would control the gain as well as the termination of the line. This technique should be avoided if possible by using either a transistor with higher grounded-base input impedance or a lower impedance transmission line. Increasing the input to the transistor by the addition of a series resistor tends to reduce the upper cut-off frequency.

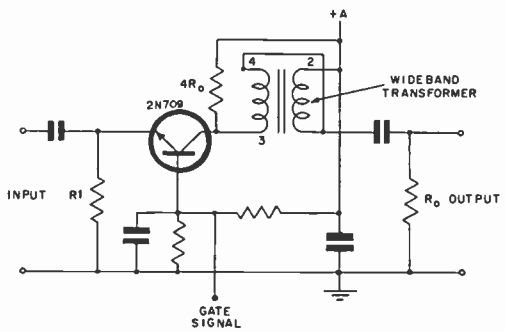

Fig. 7. Wideband amplifier.

A second and more profitable technique for lowering the gain of the amplifier is to load the transformer. If either side of the transformer is loaded the other must be loaded accordingly to maintain the 4:1 impedance ratio. For maximum bandwidth it is important that this 4:1 match be maintained. However, a small mismatch will produce a slight rising or falling with frequency that can be used to cancel the attenuation of the delay line as a function of frequency. If each stage gain were reduced to 5 dB, a 10-bit delay line would produce 100 dB (two amplifiers per bit) of gain over the band required. In a wideband system the overall gain would depend on the bandwidth and front-end noise figure. If only 50 dB of gain were required one stage could be operated at unity gain without the transformer. If less bandwidth is desired a filter could be placed at the input and output of the overall delay unit. The bandwidth of each bit could be extended at the expense of gain. As new transistors become available the bandwidth will be extended for a fixed gain. Devices at present available include: 2N2857–$f_t \simeq$ 1200 Mc/s; 2N2808A–$f_t \simeq$ 1500 Mc/s. These devices are fairly expensive, however. The 2N2966 claims a typical gain of 10·5 dB at 800 Mc/s, and is relatively inexpensive.

It should be noted that this digital delay and amplifier device does not require intricate tuning. The transformer is easily wound and the 2N709 transistor is not expensive. If a bandwidth of 150 Mc/s is desired a 2N708 could be used at a cost of about $2 each (approx. 14s. 0d.), which is quite reasonable for the job it performs.

Four such wideband amplifiers connected as shown in Fig. 8 would form one bit of the digital delay device. Notice that a common emitter resistor is used for both inputs. Since both VT1 and VT3 are not on at the same time, a single emitter resistor provides better matching of the preceding stage as well as fewer components, shorter stray lead length and capacitance which could reduce bandwidth and increase s.w.r. Also, it should be noted that the output transistors, VT2 and VT4, have their collectors connected. Since only one of these stages is on at a time this also provides better matching to the following delay bit stage. As before this reduces component and stray-lead inductance and capacitance. The gain of each path (that is in VT1 or VT3) can be adjusted by changing R1 and R2. The delay bit stage gain can be controlled by introducing resistor R4 in series with the input or by changing R3.

It can be seen that if the digital delay line device produced sufficient gain then an additional wideband i.f. amplifier is no longer required. This would reduce the cost per element.

The angular beam coverage generally required is ±45 deg or a total of 90 deg. If the array is 100λ then the 3 dB beam width would be about 0·5 deg. If the beam were moved in 0·1 deg increments the resultant scanning would closely resemble a continuous scanning system. This would require 900 beam positions. If each digital delay line had 10 bits this would give 1024 discrete positions. Nine bits would give 512 positions or about 0·2 deg incremental beam steps.

4.2. *Wideband Delay Elements*

Previously, the wideband delay line for insertion between amplifiers VT1 and VT2 has not been considered. Any delay device considered should not have too great a loss; however, this is of secondary importance with the addition of amplifiers. Of primary importance is the dispersion of these devices. They should be operated well in the nondispersive region. The most obvious method for realizing a wideband delay line would be the use of a fixed length of coaxial

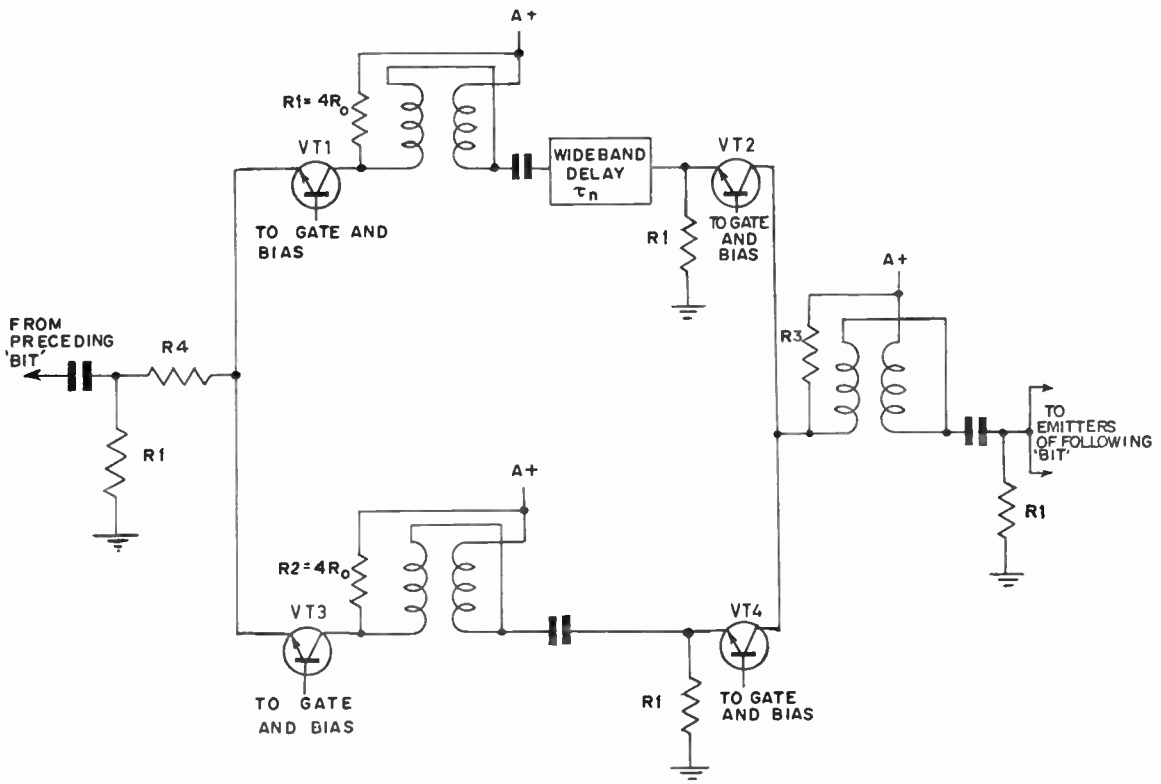

Fig. 8. Schematic diagram of single bit of wideband digital delay device.

cable. Different lengths of cable would produce different delay times.

Over a wide frequency range the attenuation of coaxial cable is a function of frequency. For instance, RG-8/U which has a characteristic impedance of 52Ω and a capacitance of 29·5 pF/ft, has an attenuation per 100 ft of 0·16 dB at 1 Mc/s; 0·55 dB at 10 Mc/s; 2·0 dB at 100 Mc/s; 8·6 dB at 1 Gc/s. A second consideration would include the size of the cable since a 50-ft coil could take up considerable space. There are some manufacturers who produce small low-capacitance cable.

A coaxial cable with a high dielectric constant is desirable since this will reduce the propagation velocity and thus result in shorter lengths of cable. RG-8/U has a relative velocity of propagation of 65·9%.

By mismatching the wideband transformer, it can be made to give a slight increase in gain with frequency. This effect could be used to compensate to a limited degree the attenuation characteristics of the cable.

Generally, helical high-impedance delay cables (centre conductor wound like a helix) are dispersive above a critical frequency. This upper critical frequency is seldom above 10 Mc/s, which would eliminate it from consideration. However, variations of this technique could no doubt be devised to extend this frequency to several hundred megacycles.

The Philco Corporation under R.A.D.C. sponsorship has been developing an electronically variable time-delay technique using an all-pass network similar to the symmetrical lattice phase-correction network. Although a description of this device has not been published a similar delay technique has been described by R. W. Calfee.[1] The lumped-parameter delay line technique appears attractive as a delay device. A typical network is capable of producing delays from 8 to 15 ns or a variation of 7 ns with a bandwidth of 30 to 40 Mc/s. The variation in delay is produced by replacing the fixed capacitors with matched varactors. To extend the bandwidth to several hundred megacycles requires high-quality diodes that can be quite expensive. As the frequency is increased the delay is decreased approximately proportionally. If the expensive varactors were replaced by small adjustable capacitors, the total delay through the device could be used to obtain a desired incremental delay. With adjustable capacitors each increment of delay could easily be adjusted to the proper value.

The coaxial cable technique could be combined with the adjustable lumped constant network. This would reduce the complexity of final adjustment by providing a simple method of line stretching.

5. Conclusions

Two variable time-delay devices have been discussed. Both techniques although still in the construction stage appear capable of producing the required delay variation with a large gain and bandwidth.

The t.w.t. technique has the advantage of:

(1) operating at the radiating frequency;

(2) octave instantaneous bandwidth capabilities;

(3) producing gain (at moderate noise figures) and delay within the same envelope;

(4) occupying a relatively small space behind each element;

(5) large dynamic range.

If the beam current were increased (incompatible with long delays) then such a tube could be used in the transmit array. Such a device would probably be used to time-steer sub-groups of elements instead of one per element. With appropriate high-power amplifiers in each sub-group it is desirable that the t.w.t. delay amplifiers provide at least several kilowatts of peak output power.

Disadvantages of the t.w.t. technique include:

(1) high power and multi-voltage sources;

(2) requirement for excellent voltage stability, particularly for the drift tube potential;

(3) heat dissipation problem.

To maintain good phase stability, especially if the tube is operated at higher power levels, a closed-loop stabilization system should be considered.

The digital delay technique is capable of much better phase stability since fixed delays are required in each bit. About the only parameter requiring control in order to maintain phase stability is temperature. In addition to the phase stability, this delay technique has the advantage of very low power requirements, minimum heat dissipation, and high gain and wide bandwidths.

Disadvantages of the digital delay technique include:

(1) limited power handling capacity (this is primarily a receiving technique but could be used in the transmitter with appropriate power gain following it);

(2) operation at i.f. (if radiated frequency is above 1 Gc/s additional mixers and local oscillator phase shifters are required);

(3) larger in size than the t.w.t., although power requirements are *considerably* reduced.

With either or both of these variable delay techniques wideband time-steered array antenna systems capable of handling any type of signal waveform (short pulse, chirp, etc.) would be possible.

6. References

1. R. W. Calfee, "An active network equivalent to the constant-resistance lattice with delay circuit applications", *I.E.E.E. Transactions on Circuit Theory*, **CT-10**, No. 4, pp. 532–3, December 1963.
2. J. W. Klüver, "An electronically variable delay line", *Proc. I.R.E.*, **50**, p. 2487, December 1962.
3. "Phased Array Radar Studies", Lincoln Laboratory, Tech. Reports 228 August 1960, AD-249 470; 236 November 1961, AD-271 724; 299 February 1963.
4. R. G. E. Hutter, "Beam and Wave Electronics in Microwave Tubes", p. 332 (Van Nostrand, New York, 1960).
5. G. I. Cohn, "Theoretical Study and Investigation of Techniques for an Electronic Rapid-Scan Antenna", Phase I, Ia, II, Electronics Research Laboratory, Illinois Institute of Technology, Contract No. DA-36-039 SC-70114, 1st April, 1959.
6. L. D. Buchmiller, "A Multiple Input Travelling Wave Tube Phase Shifter", Stanford University, Tech. No. 558–1, Contract No. DA 36-039-SC-78296, 10th October, 1960.
7. "High Speed Electronic Antenna Scanning in the Microwave Region", Hughes Aircraft Co.; Tech. Report RADC-TR-61-197, AF30(602)-2156, April 1961.
8. "Low-Noise C-Band Travelling-Wave Amplifier", General Electric Company; RADC-TDR-62-445, AF30(602)-2436, 11th September, 1962.
9. "Travelling-Wave Phase Shifter", Hughes Aircraft Co., RADC-TDR-63-498, AF30(602)-3005, December 1963 (Confidential).
10. M. Caulton, B. Hershenov and F. Paschke, "Experimental evidence of Landau damping in electron beams", *J. Appl. Phys.*, **33**, pp. 800–3, March 1962.
11. W. C. Hahn, "Small-signal theory of velocity-modulated electron beams", *General Electric Rev.*, **42**, pp. 258–70, 1939.
12. S. Ramo, "Space charge and field waves in an electron beam", *Phys. Rev.*, **56**, pp. 278–83, 1939.
13. J. Berghammer, "Landau damping of space-charge waves", *J. Appl. Phys.*, **33**, pp. 1499–1504, April 1962.
14. W. R. Beam, "On the possibility of amplification in space-charge-potential-depressed electron streams", *Proc. I.R.E.*, **43**, pp. 454–62, April 1955.
15. L. Landau, *J. Phys. U.S.S.R.*, **10**, p. 25, 1946.
16. J. Dawson, "On Landau damping", *Phys. of Fluids*, **4**, pp. 869–74, July 1961.
17. T. G. Mihran, "R.f. current behavior in electron beams with d.c. velocity spread", *J. Appl. Phys.*, **33**, pp. 1582–90, April 1962.
18. C. L. Ruthroff, "Some broad-band transformers", *Proc. I.R.E.*, **47**, pp. 1337–42, August 1959.

Manuscript received by the Institution on 17th February 1964. (Paper No. 945/RNA38.)

DISCUSSION

Under the Chairmanship of Mr. W. K. Grimley, O.B.E.

Dr. D. E. N. Davies: I think that it is worth drawing attention to the fact that time-delay beam-steering can only compensate for one direction at any time, therefore, if the main beam is compensated the side-lobes are not. The significance of this is that there may be transient side-lobe levels greater than the steady-state values. However, the time-average value of the side-lobes should be given by the wideband directional pattern which has the usual effect of filling in the zeros of the pattern.

The author (*in reply*)*:* Dr. Davies' statement in general is true. Reference is made to a report.† Here the antenna pattern of a phased array is plotted at fixed periods of time during the build up of a wideband signal. It can be clearly seen how the side-lobe levels and positions vary as a function of time during the build-up and decay of wideband signals on such an antenna.

Mr. B. W. Osborne: Is the use of the t.w.t. as a variable time delay device affected by its limited life compared with the switched delay?

The author (*in reply*)*:* T.w.t. will definitely be affected by its limited life compared with the switched delay. For this reason the switched delay technique appears more feasible as far as its use in a receiving system. In the transmitter other considerations may override the life-time considerations, for instance, power handling capability.

Mr. J. Ponsonby: Transient response apart, it is important for side-lobe reduction for the gain to be held closely constant. Can you put a figure to the degree of gain stability of such a digital system?

The author (*in reply*)*:* The gain stability of such a digital system can be held to within a fraction of a decibel.

Mr. B. M. Chisholm: What combination of phase shifting and time delay is used at i.f. to achieve time delay steering?

The author (*in reply*)*:* It can be shown that in order to time-delay-steer at i.f. an additional phase shift must be introduced. That is, the envelope is delayed at the i.f. by the proper amount to cause the leading edges to coincide, however, in order to obtain coherent summation a phase shift (independent of frequency) must be introduced into each channel. This is best done by shifting the phase of the l.o. signal. The required phase shift in each channel (l.o.) is just enough to cause the antenna, if operated at the l.o. frequency, to point in the desired direction. In other words, the l.o. is phased to look in the desired direction.

Dr. D. H. Davies: The author mentioned 1000 Mc/s as a design objective for the digital delay amplifiers. Is this the target for individual elements or for a complete digital switching chain?

The author (*in reply*)*:* The 1000 Mc/s is a design objective for each amplifier (3 dB). Since the amplifier will be essentially flat to about 750 Mc/s the overall design objective is about 750 Mc/s at this time.

Mr. K. L. Fuller: Does digital scanning introduce noise analogous to quantization noise in analogue/digital conversion?

The author (*in reply*)*:* A digitally steered array sweeping in discrete steps through a continuous source will produce an output with step modulation superimposed, and this modulation may be regarded as noise. For example, an aerial with 2 deg 20 dB beamwidth sweeping in 0·1 deg steps will produce an output signal with 10 steps up and down, and hence a maximum possible signal/noise ratio of 20 dB. This only applies to signals of length greater than the 'dwell' time of the aerial. In the 'track' condition where a larger signal/noise ratio is required, this quantization noise would be absent.

Mr. B. N. Alcock: What is the phase stability of the travelling wave delay tube?

The author (*in reply*)*:* The phase stability of this t.w.t. is poor. At this time a phase stabilization loop is anticipated.

† "Transit Time Effects in Phased Arrays", Tech. Report RADC-TDR-63-67, AD 405-974, 1963.

Letter to the Editor

SIR,

Electronic Drawing

In the recent report of the Education and Training Committee of the Institution† some emphasis is laid on the functional structure of diagrams. The Committee found that professional electronic engineers do not pay sufficient attention to numerous principles and practices, the first of which was 'Laying out a circuit diagram. The fundamental principle, which should be observed, but frequently is not, is that the layout should show the function of the various parts of the circuit and of the circuit overall'. In the proposed syllabus for academic courses at all levels the following item was included, 'Application of functional flow principles to block schematics and circuit diagrams'.

What may be difficult to interpret from these recommendations is the difference between diagrams drawn on a functional basis and other types of diagram. What are 'functional flow principles'? B.S. 530 does not help: Supplement No. 4, 1956, defines a functional diagram as 'A diagram to illustrate the function of a piece of equipment. This is often partly electrical and partly mechanical and therefore does not conveniently fall under any of the other headings'. The proposed amalgamated version of B.S. 108 and B.S. 530 does not include a definition for functional diagrams but quotes a functional diagram as being an example of a block diagram.

The Royal Air Force is always interested in improving the quality of technical diagrams, in order to ease the training task and provide improved job aids

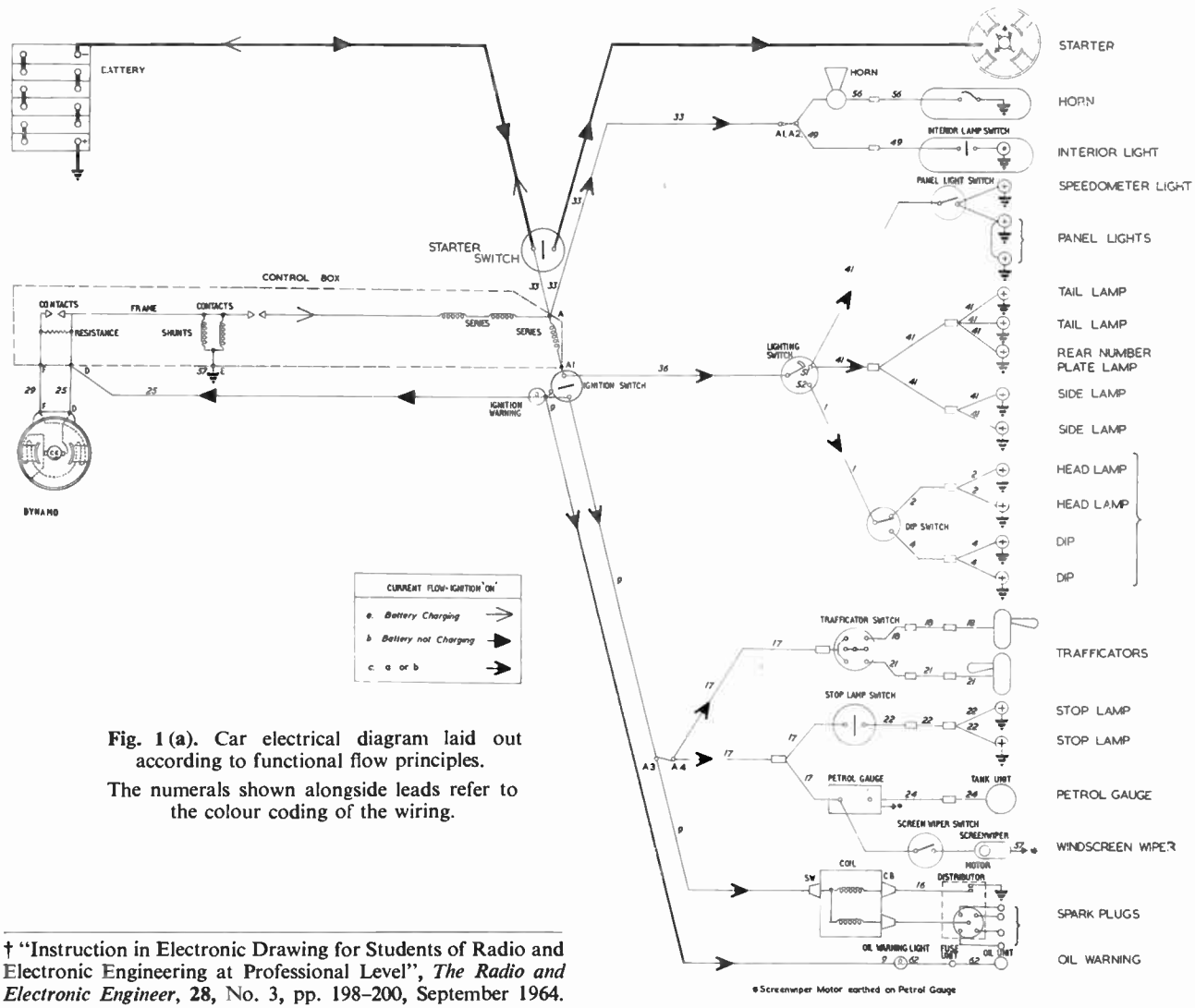

Fig. 1 (a). Car electrical diagram laid out according to functional flow principles.

The numerals shown alongside leads refer to the colour coding of the wiring.

† "Instruction in Electronic Drawing for Students of Radio and Electronic Engineering at Professional Level", *The Radio and Electronic Engineer*, **28**, No. 3, pp. 198–200, September 1964.

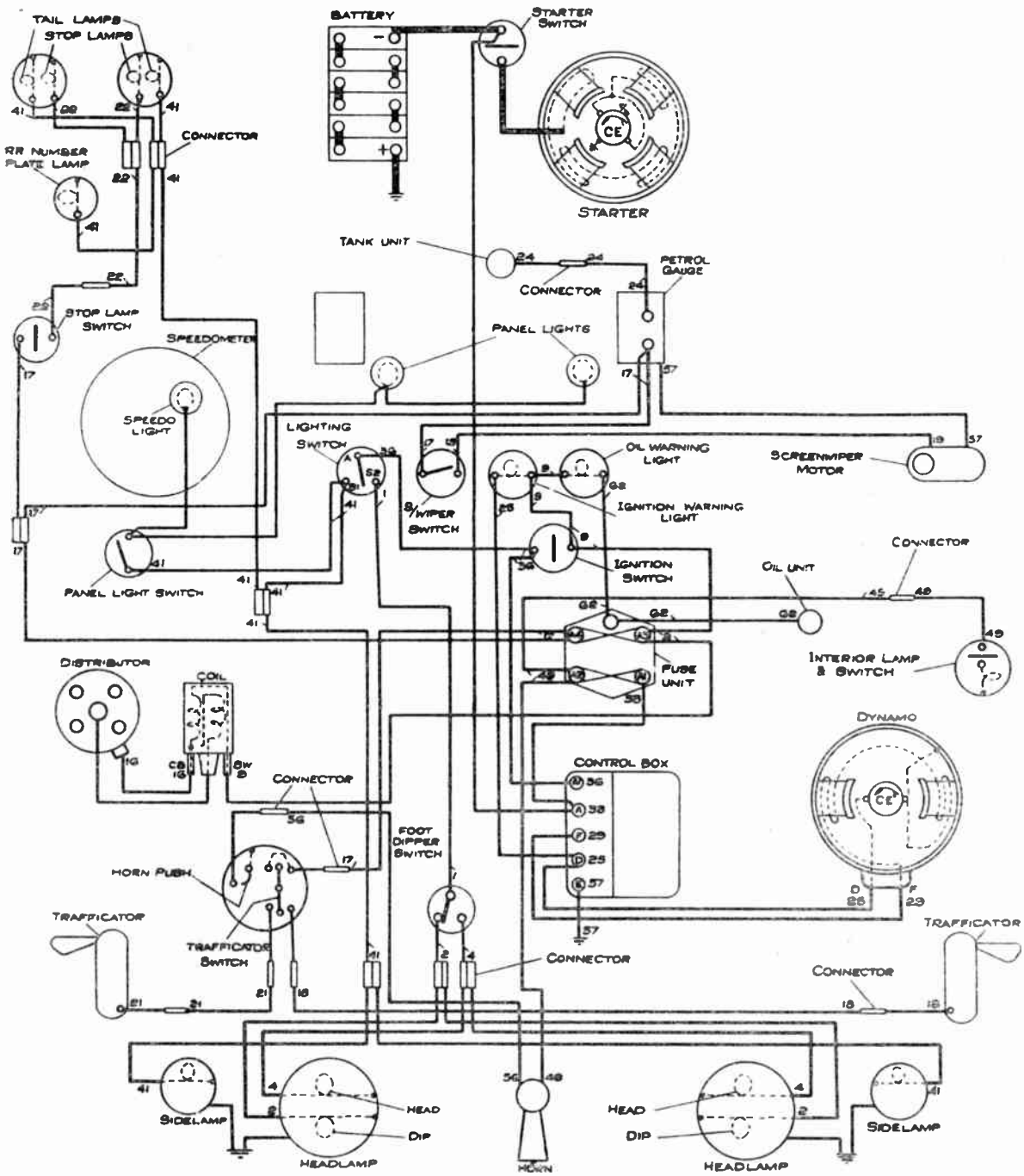

Fig. 1 (b). The conventional style of car electrical diagram from which **Fig. 1** (a) on the opposite page was derived.

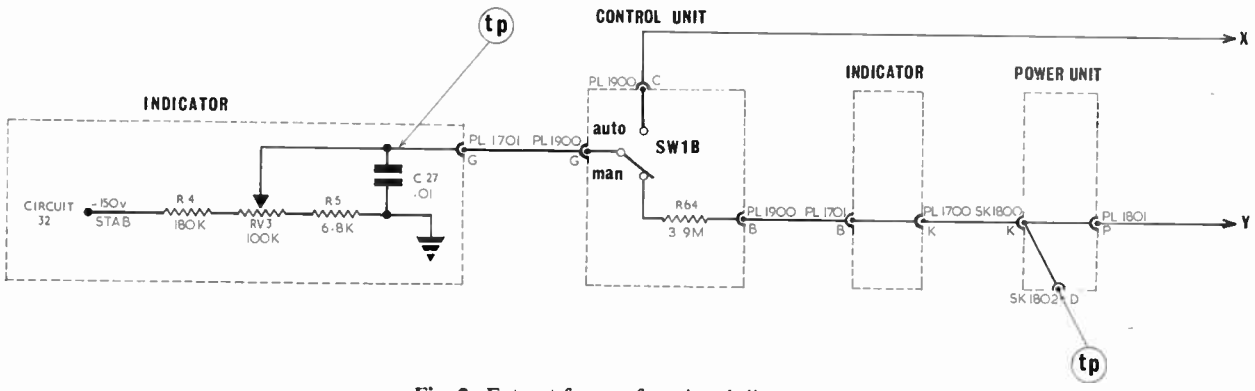

Fig. 2. Extract from a functional diagram.

for modern complex equipment. Greater use is now being made of the functional approach which is being applied to both the preparation of new diagrams and the re-drawing of old ones. Although no definitions or rules have been formally issued by the Ministry of Defence, diagrams have been drawn to satisfy the following definition:—

> A functional diagram illustrates, in a simple form, the functions of a device irrespective of its physical structure. It emphasizes the signal or functional flow paths and the main sequence of cause to effect goes from left to right. Functional diagrams may be drawn for any logically structured device and at any level from component detail to overall function.

Figures 1 and 2 illustrate the main points contained in the definition. Figure 1 shows how a car electrical diagram can be simplified and put on a functional basis to make it more easily understood and usable as a diagnostic aid. Figure 2 is an example in which the physical boundaries have been arranged so that they do not destroy a clear presentation of the circuit's function. This particular diagram was originally spread over four separate diagrams appearing in different parts of the publication of which it was part.

The examples given show one attempt to improve technical diagrams by putting them on a functional basis. I would be interested to see any other interpretations of this part of the Committee's report, or an expansion of the recommended syllabus content to define the 'functional flow principles' mentioned.

F. W. STAINER

Headquarters, Technical Training Command,
(Research Branch),
Royal Air Force,
Brampton, Hunts.

2nd October 1964.

Comment on papers or other technical material published in *The Radio and Electronic Engineer* is welcomed, either in the form of a letter or as 'written discussion'. Contributions should be addressed to The Editor.

U.D.C. 621.387.33: 621.394.346

Cold Cathode Trigger Tubes in Logic Control Circuits and Memory Matrices

By

G. F. BRUNN, P.Eng.†

Reprinted from the Proceedings of the Symposium on "Cold Cathode Tubes and their Applications", held in Cambridge from 17th–19th March 1964.

Summary: Cold cathode trigger tubes are fast acting, gas controlled switches. In slow speed computers, where their relatively low duty cycle is tolerable, they may be combined with solid-state components, such as transistors, diodes, and silicon controlled switches. In such combinations the gas switches can be visually observed in operation, so that fault location is considerably simplified.

Several unique advantages and various techniques of designing such logic control circuits are outlined. Examples of applications of their circuits in telecommunication control equipments are described. An economical and unsophisticated modular packaging is illustrated, which has proved to be suitable for servicing of complex equipments by technicians of ordinary skills.

1. Introduction

Among the reasons for using cold cathode tubes in computer and control circuits is the advantage that visual indication of circuit operations makes it possible for technicians of ordinary skills to service complex equipments from fault/symptom charts. This is accomplished in slow motion operation, using step-by-step instructions. Speedy maintenance is greatly facilitated by modular packaging. In timing chains, decade, or ring counters, the neon glow of cold cathode trigger tubes may be observed flashing from module to module during normal operation. In the extremely rare event of a malfunction, a steady bright glow is emitted by the module closest to the break in the circuit chain. This glow very effectively pinpoints and announces the trouble area. Due to slow de-ionizing effects it is possible to observe even extremely short pulses. As an example, single 'carry' pulses of 100 μs duration at half width can be consistently seen by the eye.

Design economy is a primary consideration for any project. Cold cathode trigger tubes serve simultaneously as neon indicators and as logic control elements. Moreover, because of its bistable mode of operation, a single trigger tube performs the functions of two transistors. These combined features make the use of cold cathode tubes very attractive in slow-speed binary computer circuits.

Reliability is a function of the number of components used, apart from their quality. If one were to assume that cold cathode tubes have only one half of the life of transistors in a particular binary circuit, it is obvious from the above that the equipment service life would be equal, due to the smaller number of tubes used.

Solid-state components, such as transistors and silicon controlled rectifiers, and cold cathode tubes complement each other in various circuit applications. They should each be used to their best advantage. Frequently it is desirable to utilize one to control the other.

The widespread use of transistors and other solid-state components in high-speed computers has given them a certain prestige which has unjustly obscured the many advantages inherent in the use of cold cathode trigger tubes in circuits where a lower speed of operation can be tolerated. The latter is really a gas controlled switch and not one of the common types of vacuum tubes. The gas controlled switch has a current gain which is unexcelled by either thermionic tubes or transistors. In sophisticated terms one might call it a plasma switch rather than a tube. The term gas controlled switch, which is analogous to the term silicon controlled switch, is frequently used in this paper to designate cold cathode trigger tubes in logic circuits.

2. Preferred Circuits

2.1. *Component Selection for Logic Control Circuits*

The control circuits to be described in this paper make extensive use of the type Z70U cold cathode trigger tube manufactured by Philips. All diodes are the rugged glass rectifier Texas Instrument type TI60 with 400 V p.i.v. rating. Transistors are 2N404 and s.c.r's are Transitron SW1242.

† Philco Corporation of Canada Ltd., Don Mills, Ontario.

A Z70U functions as a single-pole, single-throw switch. To close the switch a difference of potential is required between the starter electrode (grid) and the cathode. This type of gas switch fires if a steady direct potential between 135 and 152 V is applied. More frequently it is advantageous to superimpose a pulse on a steady direct voltage in such a fashion that they must both be simultaneously present, in order to cause the tube to fire. Typically, the pedestal is in the order of 90–100 V and the pulse peak is approximately the same.

AND gate functions are reliably and economically achieved by this combination of pulse and d.c. pedestal. There is a choice of outputs from this AND gate, consisting of either a steady direct voltage from the cathode of the trigger tube or alternately of a single output pulse. The latter is produced by arranging the tube circuit in such a fashion that the voltage drops below the value required for continuous 'burning', immediately after firing.

Turn-off from external control circuits is likewise achieved by dropping or removing the anode voltage on the tube to be controlled. This can be accomplished by the use of a suitable relay. Generally, the burning voltage level of the tube is so arranged that the cathode is about 120 V above ground. Typically, this requires a 20 kΩ anode resistor and a 47 kΩ cathode resistor, with 285 V h.t. For turn-off control two or more tubes have their anodes connected together, while using separate cathode resistors, each shunted with a 0·0047 μF bypass capacitor. Assuming that one of the tubes is burning with its cathode level at +120 V, if either of the associated tubes is then fired, its bypass capacitor will initially have zero impedance, until it charges up. As the voltage drop between anode and cathode remains constant on this type of gas tube, the common anode lead drops from +240 V to +120 V. This momentary drop safely extinguishes the tube originally burning, because its cathode is at the 120 V level, leaving the second tube in the 'on' state. As a third alternative for turn off control, the anode voltage can be held constant, while raising the cathode level. This is possible, although it is not commonly used.

2.2. *Programmed Counter Circuits*

Counting circuits of various types can be designed by combining the turn-on and turn-off conditions outlined above. The most common designations are ring counters, binary counters, shift registers, etc. Typical circuits are published by the tube manufacturer. A number of such counters or counting chains can be interconnected in such a fashion that the output of one chain causes one or more other counters to step ahead in a predetermined manner (Fig. 1). The simple AND gate and OR gate circuits available with gas controlled switches enable the designer to achieve complex slow-speed computer control functions with a minimum of circuit elements. This type of computer is usually semi-permanently programmed by internally controlled reflex action, making external step-by-step instructions unnecessary. This fixed program is useful in process control.

CARRY circuits are one-shot pulse generators. Typically, the anode of the trigger tube is directly connected to h.t.+ and the cathode resistor is chosen to be so high (typically 680 kΩ) that the current flow is too small to sustain the tube operating after firing. The small cathode bypass capacitor, while charging up, draws a high peak current which is in the order of one ampere, or more, for microsecond duration. The cathode delivers a high output voltage to a differentiating network. This voltage is determined by the difference between the h.t.+ and the burning voltage of the tube. It is in the order of 160 V peak. The output from one CARRY tube is sufficient to trigger a considerable number of associated tubes.

An alternate CARRY circuit uses an RC network in the anode lead so that a small amount of energy is stored for single shot operation.

2.3. *Pulse Generator Circuits*

Pulse generators use the same circuit as the CARRY tube, except that the starter electrode is usually held at a d.c. level high enough to cause relaxation type oscillation. When the starter voltage is clipped by means of a voltage regulator tube, the frequency stability is in the order of 1% or better. The relaxation oscillators are used to provide clock pulses to the various counters and logic control circuits. Using suitable d.c. or a.c. feedback it is possible to prolong the time intervals between clock pulses in an aperiodic fashion to suit slow operating relays or to provide sync periods in start/stop systems, between code groups.

2.4. *Delay and Interval Timing Circuits*

Delay and interval timing circuits can be achieved by one of several design approaches:

(i) The delay tube may be fired with +160 V d.c. applied to the starter electrode via an RC network. This starter voltage can be controlled from the cathode of another trigger tube, using a diode switch in the bottom end of a voltage divider. Typically, the tap connected to the starter electrode is between a 2·2 MΩ and a 1·5 MΩ resistor on 285 V. The lower end of the 1·2 MΩ resistor is connected to ground via a diode and via the 47 kΩ cathode resistor of the control tube. When the latter is not fired the tap of the voltage divider provides approximately 115 V d.c. to the starter electrode of the delay tube, which is insufficient for triggering. As the control tube fires, its cathode voltage rises to a value which reverse biases the diode, causing the tap voltage to rise proportionally. If a capacitor is connected to the anode side of the diode,

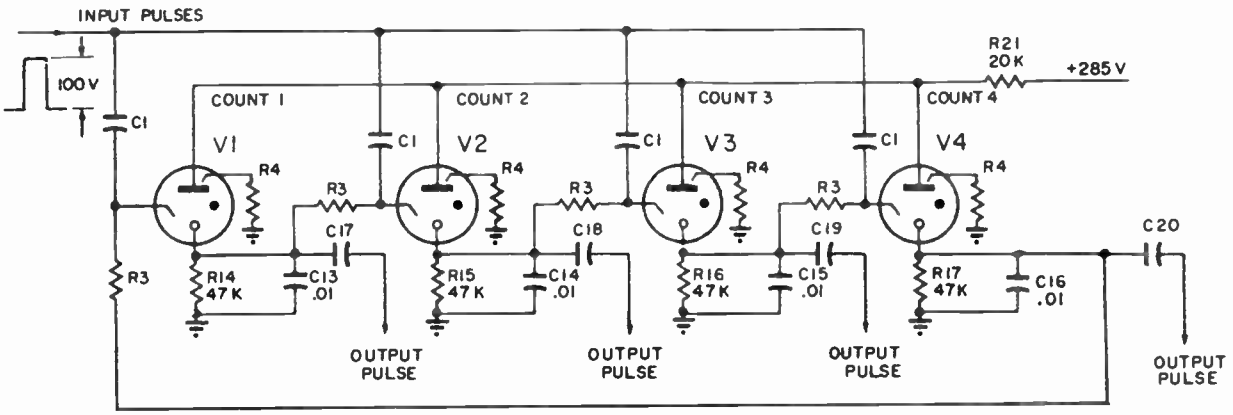

Fig. 1. Typical control counter circuit.

or to the tap of the voltage divider, it causes a delay in firing. Practical delay values range from microseconds up to the order of seconds.

(ii) Staircase counters are capable of producing longer delays up to several minutes. One trigger tube operates as a pulse generator. Its output is integrated in an RC network, so that an associated delay tube fires after a predetermined time interval. The accuracy of triggering is improved by feeding a small amount of ripple to the starter electrode of the delay tube.

(iii) Binary counters are useful for long delays requiring very accurate timing. As an example, 180 seconds +0−5 seconds control timing was achieved in this manner.

2.5. *Monitor Circuits*

In a remote control system it was found desirable to monitor the control loops provided by telephone companies in such a fashion that partially open or shorted loops would cause an alarm to be triggered in the control centre. A single cold cathode trigger tube is arranged in a monitor circuit in such a fashion that an open line, or a considerable increase in loop resistance causes the starter voltage to rise above the firing point. This is accomplished in the manner outlined in the previous section, except that a 31-kΩ termination resistor is used at the far end of the line in place of the 47 kΩ. The starter voltage divider is so arranged that the tube fires when the line resistance rises above 75 kΩ, although its cathode is held at about +40 V from a second voltage divider.

If the line resistance falls below about 8·5 kΩ the cathode voltage is reduced, while the starter voltage is maintained, so that the total potential difference again fires the monitor tube. As a further refinement the polarity of the supply voltage is reversed between the monitoring and control phase of the circuit by means of a relay. At the far end of the line a diode is used in series with the control relay, so that it is not biased by the monitor current.

2.6. *Pulse Gate Circuits*

Diode conductance can be inhibited by means of a reverse bias derived from the cathode of a control tube. Two types of reliable pulse gates can be designed in this manner. One uses a series circuit, while the other one functions as a shunt circuit. The former blocks the pulse path in the presence of back bias, whereas the latter shorts the pulse output in the absence of back bias. AND and NAND pulse gates can be designed with diode-trigger tube combinations.

2.7. *Bit Memory Circuits*

Bit memories with non-destructive read-out have been used in several designs of data processing equipments, and utilize a number of the shunt type pulse gates. Each bit register is packaged into a plug-in module and the required number of modules is laid out in the form of an array which permits visual check-out of its functions. The array has separate control inputs for each row and each column.

Typically each column of trigger tubes in the array has its starter electrodes primed in turn from the cathode of an associated column control tube. Only the primed bit register tubes are conditioned to be fired. The firing is caused by pulses which are simultaneously fed to each row of bit registers via coupling capacitors connected to a common pulse feed bus.

The column control tubes are arranged in the form of a counter. Once the bit information is stored, the

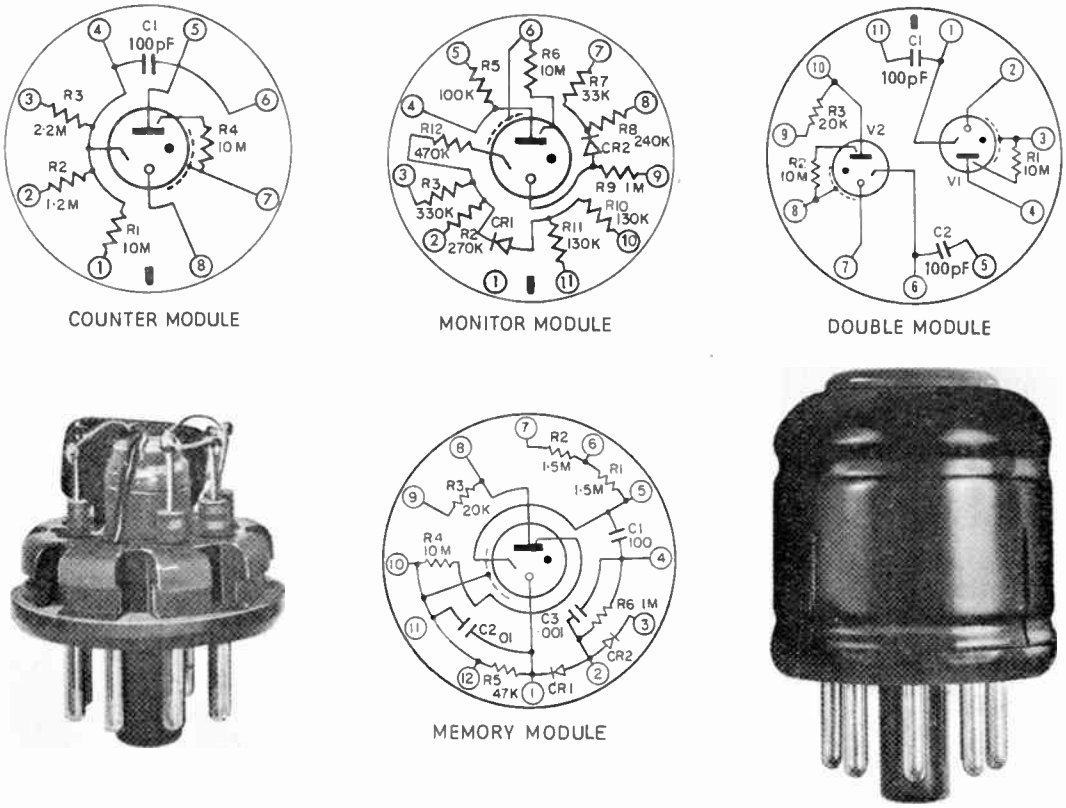

Fig. 2. Trigger tube modules.

bit register tubes which are fired open a gate for the read-out pulses. This path can be maintained for any desired length of time or for any number of read-outs.

The complete array can be cleared by momentary removal of the anode voltage. This is accomplished by a mercury wetted relay, the coil of which is connected between the cathode of a trigger tube and earth, while the contact is in the h.t.+ supply line feeding the array.

2.8. *Circuits combining Trigger tubes with Transistors or S.C.R.'s*

Cold cathode trigger tubes are well suited for control of transistors. Such combinations are particularly effective where higher currents are required at low impedance. In one application the current rating of the Z70U was insufficient to drive an associated telegraph relay. This was overcome by feeding a d.c. bias through the relay coil from the h.t.+ source. In the 'off' state the bias was effectively removed by shunting the relay coil with a transistor.

In another application where 25 monitor circuits were contained in a common package, it was necessary to recognize that one, or more, or all, of the monitor tubes had fired. In the 'off' state each monitor tube was drawing approximately 10 μA priming current. When fired, each tube used 1 mA anode current. A small resistor was inserted into the common h.t.+ line for the 25 tubes in such a fashion that the priming current was producing a small 0·4 V bias between base and emitter of a transistor. The resistor was shunted by a diode which does not conduct at fractions of 1 V. When either or all of the monitor tubes fired, the diode started to conduct, shorting out the transistor bias. This caused the transistor to actuate an associated alarm relay.

Silicon controlled rectifiers use gate currents in the order of a few milliamperes to break down the main control path which may draw amperes of current. The gate current can be provided by connecting the s.c.r. or s.c.s. into the cathode circuit of a trigger tube.

3. Modular Packaging of Trigger Tube Circuits

3.1. *Printed Wiring Boards*

Printed wiring boards are commonly used in packaging standardized circuits, such as decade counters, clock pulse generators, etc. This is advantageous where multiple numbers of the same circuit are used in an equipment. Sufficient spare assemblies must be provided for servicing with each equipment. Competent personnel are required to carry out repair work on printed wiring boards.

3.2. *Plug-in Modules*

Plug-in modules containing only one or two trigger tubes, as well as their associated components, were found more readily acceptable in applications where the service personnel are not highly skilled. Large numbers of modules have been produced which are packaged into octal type plugs (Fig. 2). A plastic lens in the module cover facilitates the visual observation of circuit operation. The number of socket pins is peculiar to each type of module. Various plugs with 4 to 12 pins were used. Although this type of packaging is by no means sophisticated by current standards, it is reliable, economical and functional, in equipments using up to 1000 modules.

3.3. *Chassis Layout*

Up to 160 of the above plug-in modules are arranged on a common chassis in such a fashion that related circuit functions are clearly recognizable, typically in the form of straight line flashing operation. On the front plate of each chassis a tube layout label displays all major circuit functions as an aid to the service man.

3.4. *Cabinet Design*

In the equipment cabinet the module chassis are arranged as horizontal and vertical drawers which pull forward for convenience of servicing.

4. Logic Control Circuits and Memory Matrices

4.1. *Encoder Circuits*

Encoder circuits are sometimes used in conjunction with memory matrices, for reasons of design economy. In a typical application, an 11×30 memory matrix was required to control selectively the operation of 11 teleprinters to any one of 30 routes. As this would have required 330 bit memory modules it was found economical to encode the input, using a 2^4 binary code. A small diode matrix had 11 selective inputs which were each connected to the cathode of a gas switch. The four encoder outputs each fed into a row of 30 gas switches in the memory. In this fashion only 120 bit memory modules were required. At the memory output a decoder restored selective printer control.

Diode matrices in conjunction with gas switches (trigger tubes) can be used in a variety of control circuits. For transmission of fixed format messages a gas switch counter feeds from each stage to a different input on the diode matrix, so that the latter provides the desired character code sequence.

4.2. *Decoder Circuits*

Parallel code can be decoded by feeding into two complementary diode matrices (Fig. 3). One matrix provides enabling d.c. pedestal to the starter electrodes

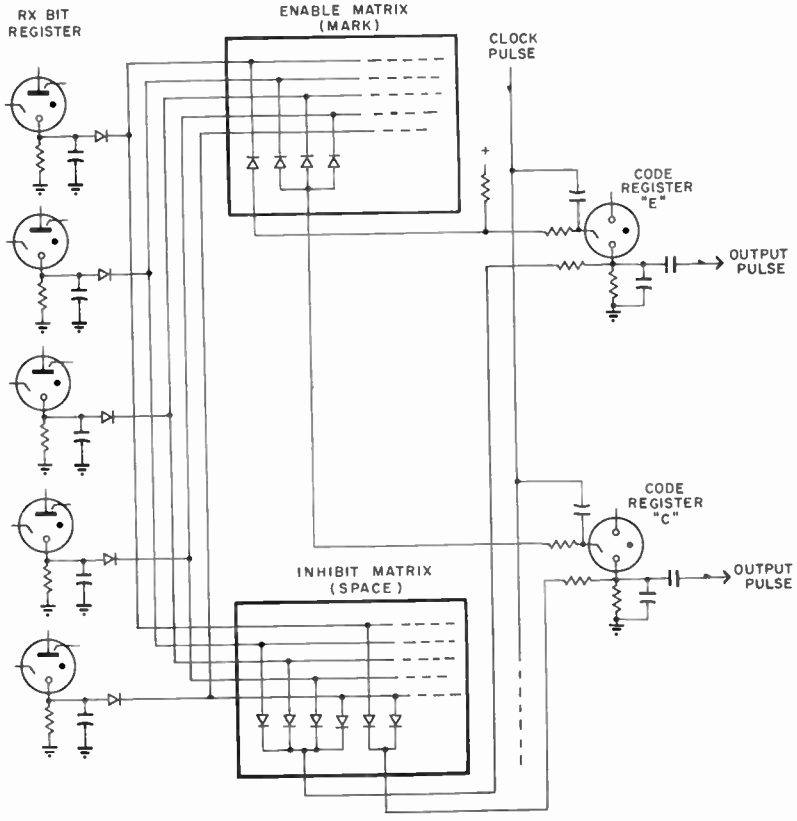

Fig. 3. Decoder circuit.

of the gas switches serving as code output registers. The other matrix simultaneously feeds an inhibiting voltage to the cathodes of the code output registers. The circuit is so arranged that for each input code combination only a single one of the output registers can be operated.

The code output registers must be erased after each cycle of operation. This can be accomplished by a gas switch driving a mercury wetted contact relay which has its normally closed contact in the h.t.+ line feeding the output registers and the erase control.

4.3. *Code Buffer Store*

At the interface between parallel and sequential code operation, gas switches can serve as code bit registers. As the code bits are received in sequence the bit registers are selectively operated according to the code combination. At the end of the receive cycle the code combination is transferred to a second set of code bit registers serving as a buffer store. Subsequently, the first set of registers is cleared for the next cycle, during the sync. period. A block diagram of a typical arrangement is given in Fig. 4.

The reverse process of feeding parallel code during the sync. period into a transmit register for sequential code output control can likewise be accomplished with gas switches.

4.4. *Sequence Control*

Counter circuits can be adapted to sequence control functions by controlling the triggering of each stage from different building blocks in the system. A typical process control uses a counter which has its '0' tube fired when the regulated power supply is first turned on. Pushing the manual 'start' button advances the count to '1'. This, in turn, causes a tape reader and the associated code recognition circuits to operate. As a predetermined code combination is recognized, count '2' is actuated. It enables a transmit function to start. At the end of the transmission the '0' tube in sequence control counter is once more turned on.

4.5. *Labyrinth Logic*

In slow speed applications trigger tube logic circuits can serve as an alternative to magnetic memories. As an example cable addresses may be automatically sorted by comparing their code with a multitude of different codes stored on a magnetic drum or in a core memory until coincidence is established. A much more economical solution has been developed with

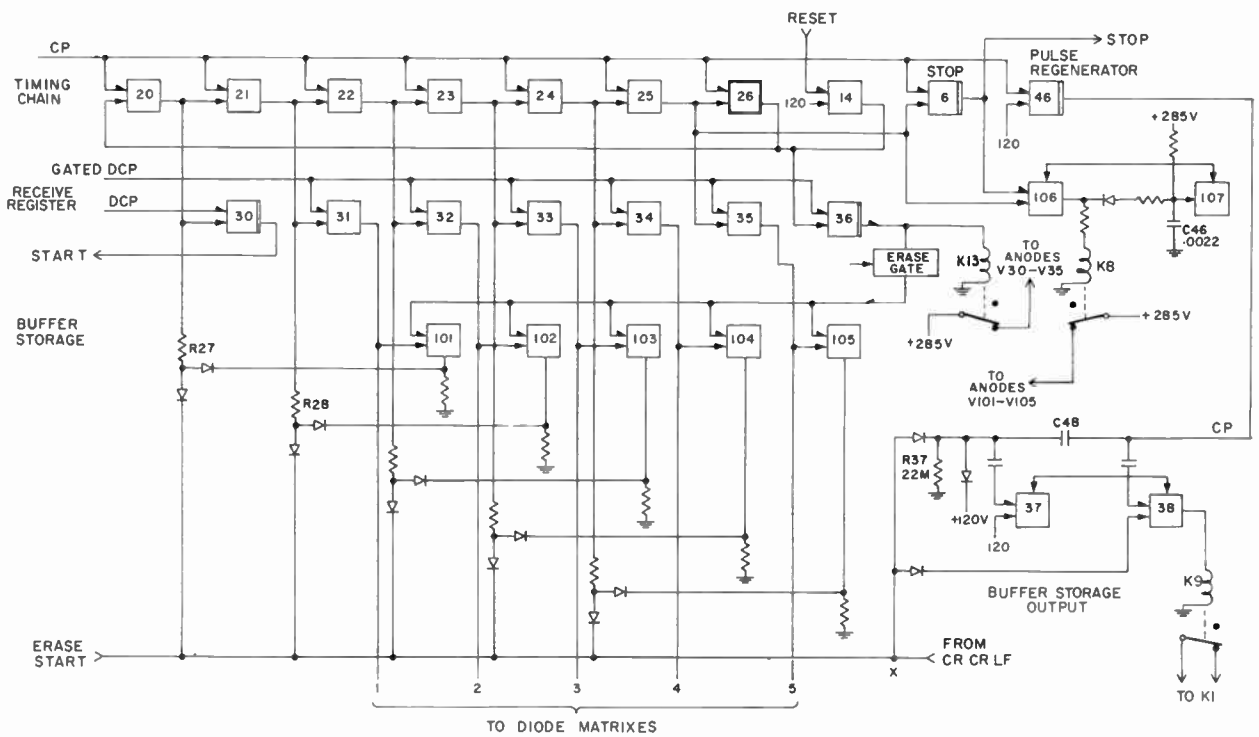

Fig. 4. Buffer storage.

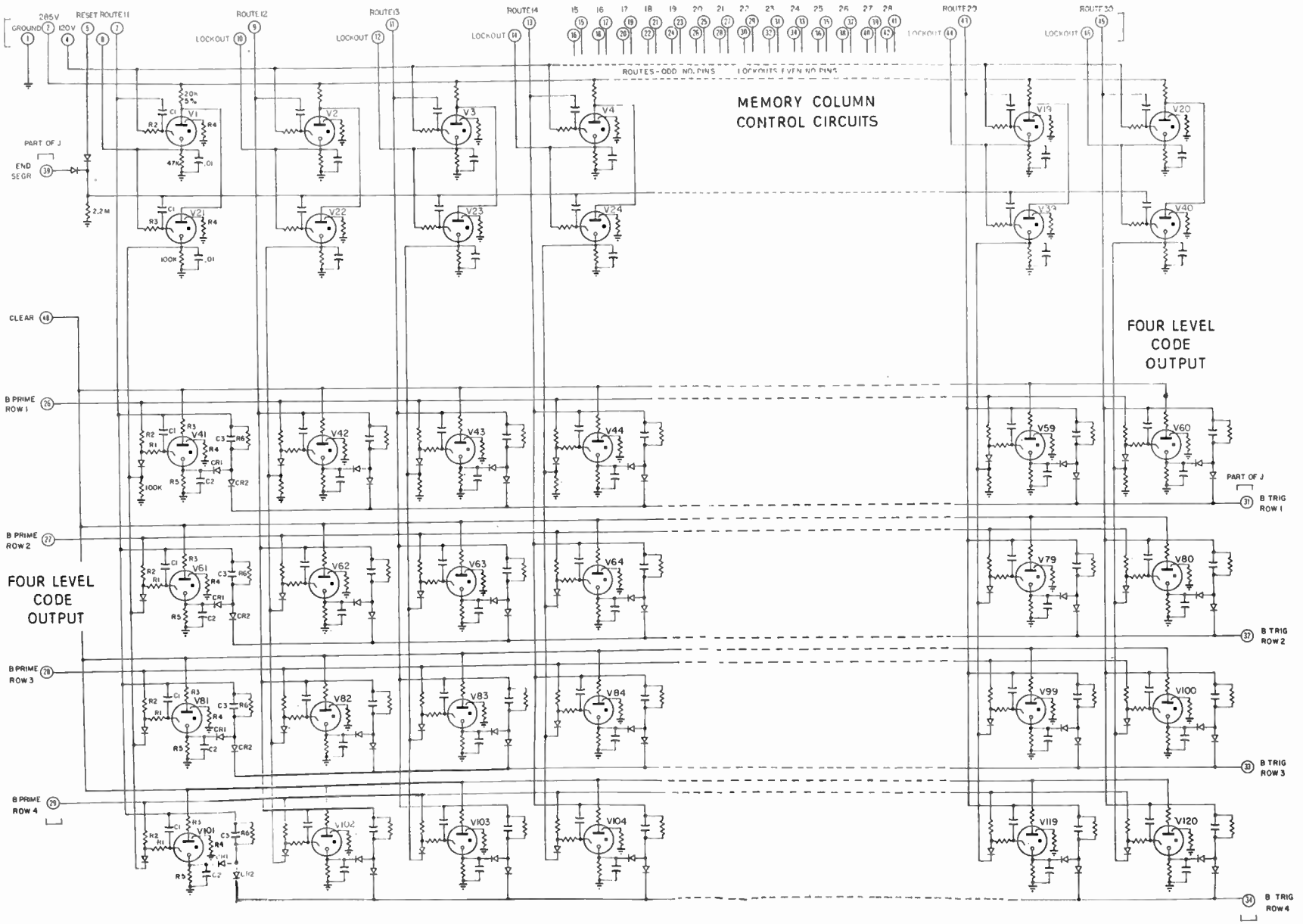

Fig. 6. Typical 4 × 10 memory matrix circuit.

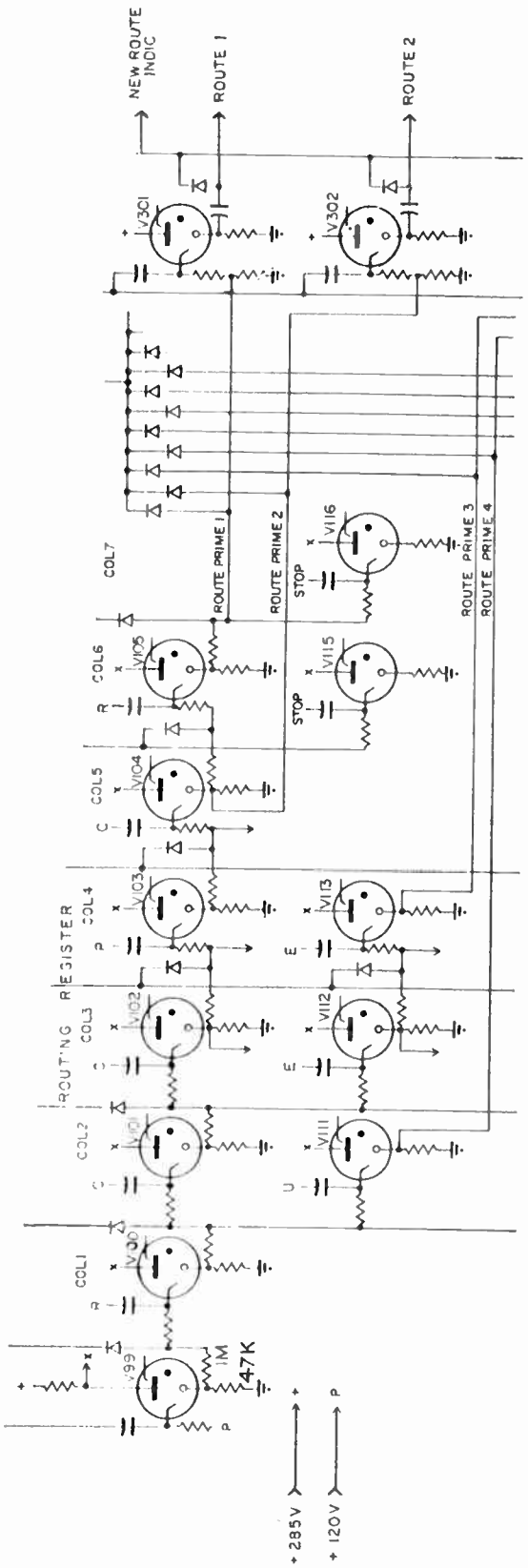

Fig. 5. Basic labyrinth logic circuit.

cold cathode trigger tube counter circuits which are programmed to recognize only those code elements of the cable address which determine the message routing at the equipment location. This is accomplished by combining a decoder circuit with a sequence control counter in such a fashion that the latter proceeds one step when its control input is fed from the associated decoder output. A basic circuit is shown in Fig. 5.

This shift register circuit combination can be so arranged that it fans out into multiple control paths. These form a labyrinth, as only one of several output gates opens for any particular combination of decode input. In this manner predetermined character sequences can be recognized to actuate control functions of the 'lock and key' type.

4.6. *Code Memory Matrix*

The trigger tube bit memory modules described in Section 2.7 are utilized in a Canadian-designed message routing equipment. The message heading consists of 13 teletype characters in 5 level code. It is followed by several routing sequences (cable addresses), each between 4 and 7 characters in length. Each character sequence is temporarily stored in a matrix of bit memory modules which are arranged in 5 rows and 20 columns, as shown in Fig. 6.

In each of the 5 rows, the starter electrodes are connected to a common code input bus, via coupling capacitors. The cathodes are connected, via isolation diodes, to a common code output bus in each row. Column control tubes are provided for character-by-character read-in and read-out, in parallel code, as called for by the main sequence control. Read-out is accomplished by gating a clock pulse from the code input bus to the code output bus under control from those bit memory modules in each column which were fired during the read-in phase. For test purposes any character sequence can be stored and read-out under manual step by step control. The stored code is visibly indicated by the neon glow in the appropriate memory modules.

5. Bibliography

"Cold Cathode Trigger Tubes for Industrial Applications", Philips Electron Tube Division 20/092/D–E–1–62.

"The Basic Operation of Cold-Cathode Glow Discharge Tubes", Philips Electron Tube Division A.I. 419, released 13th March 1963.

M. E. Bond, "The life expectancy of cold-cathode tubes", *Electronic Engineering*, **34**, pp. 798–803, December 1962.

J. Das, "An electronic coder and decoder for teleprinter signals", *Electronic Engineering*, **31**, pp. 156–60, March 1959.

Manuscript received by the Institution on 29th February 1964. (Paper No. 946.)

U.D.C. 621.375 : 621.376.33

Equivalent Variable Centre-frequency Amplifiers

By

B. R. DAVIS, B.E., B.Sc.†

Summary: This paper attempts to demonstrate the equivalence of two variable centre-frequency amplifiers. The first consists of an i.f. amplifier preceded by a mixer and a voltage-controlled oscillator; the second consists of a tuned amplifier whose centre frequency is altered by the use of voltage-controlled capacitors across the resonant circuits. The first is the type normally employed in frequency feedback detectors, whilst the second is the basis of 'dynamic selector' or 'dynamic filter' systems. A method of analysing the response of a dynamic filter to a frequency-modulated signal is developed using this equivalence.

The application of the dynamic filter to f.m. detection is considered and it is shown that one possible circuit arrangement is equivalent to a feedback f.m. detector.

1. Introduction

In frequency-modulation receivers, a rapid increase in the noise output occurs if the i.f. signal/noise ratio falls below a certain value, usually about 12 dB.[1,2] This threshold effect sets a lower limit for the signal strength required for satisfactory operation.

It has been shown that the required signal strength may be reduced by the use of frequency feedback.[2,3] In this system, the local oscillator frequency is forced by feedback to follow the incoming signal frequency, as shown by the block diagram of Fig. 1. The effect of feedback is to make the i.f. deviation much less than the incoming signal-frequency deviation. Whereas without feedback an i.f. bandwidth which can handle the full signal-frequency deviation is necessary, with frequency feedback the i.f. bandwidth may be smaller because of the reduced deviation. Reduction of the i.f. bandwidth will improve the signal/noise ratio, and hence the threshold will occur at a lower signal level when frequency feedback is used. Improvement cannot be obtained indefinitely by increasing the amount of feedback for two reasons. Firstly, the i.f. bandwidth must be at least twice the modulation bandwidth, and secondly there is another threshold effect which occurs when the r.m.s. phase deviation of the local oscillator due to noise exceeds a value of 0·32 rad. This additional threshold effect was first noticed by Enloe.[2]

The action of the feedback f.m. system may be considered to be that of tuning a narrow-band amplifier continuously so that the incoming signal frequency always falls within its passband. The mixer, i.f. amplifier and the voltage-controlled oscillator (v.c.o.) constitute a variable centre-frequency amplifier.

† Electrical Engineering Department, University of Adelaide, South Australia.

Another type of variable centre-frequency amplifier may be achieved by varying the actual tuning of the resonant circuits. It is the purpose of this paper to compare the characteristics of these two types of variable centre-frequency amplifier.

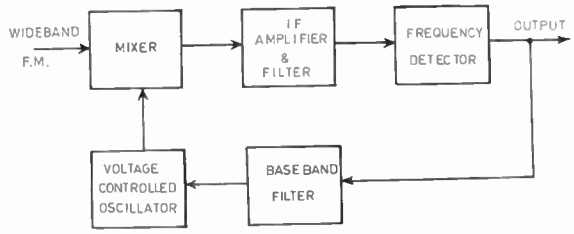

Fig. 1. Block diagram of a feedback f.m. system.

2. Variable Centre-frequency Amplifiers

Figure 2 shows block diagrams of these two types of variable centre-frequency amplifier. Frequency detectors and feedback circuitry have been omitted from the diagrams, since there are several feedback configurations possible.

The two systems may be considered identical, except that in one case the oscillator frequency is voltage controlled, and in the other the i.f. amplifier centre frequency is voltage controlled. Of particular interest is the behaviour of the systems when the incoming signal is frequency modulated.

For the purposes of this investigation it is assumed that when the control voltages are zero, the two systems are identical. The response to a frequency-modulated signal is then the same for both systems and may be found by conventional methods.[4] If

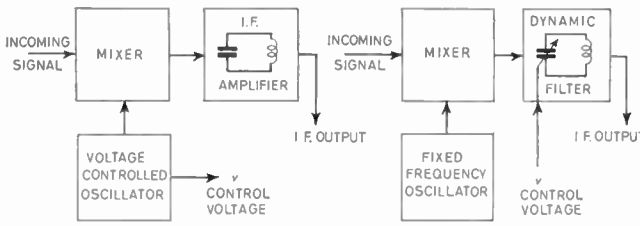

(a) V.c.o. fixed i.f.

(b) Dynamic filter

Fig. 2. Variable centre-frequency amplifiers.

the control voltages are not zero, then the systems are no longer identical.

Consider the response of the v.c.o. fixed-i.f. system of Fig. 2(a) to a sinusoidal frequency modulation. By modulating the v.c.o. such that its instantaneous frequency differs from the instantaneous signal frequency by a constant amount at all times, the frequency deviation of the i.f. signal may be reduced to zero. This is shown in Fig. 3(a). In the vicinity of the i.f. filter centre frequency, therefore, the input to the i.f. amplifier consists of a constant frequency sine wave. The output of the i.f. amplifier is therefore also a sine wave of the same frequency, whose amplitude and phase differ from that at the input by the amplitude and phase characteristics of the i.f. filter at that frequency.

The response of the dynamic filter of Fig. 2(b) to the same input is considered. By modulating the dynamic filter so that its instantaneous centre frequency differs from the instantaneous intermediate frequency by a constant amount at all times, the frequency deviation of the i.f. signal with respect to the i.f. filter centre-frequency may be reduced to zero.

If the modulating frequency is low, then it is easily seen that the instantaneous frequency of the i.f. input always lies in the same position in the i.f. passband relative to the centre frequency. This is shown in Fig. 3(b). It is not obvious, however, that the tuning of the filter can follow the instantaneous frequency of the signal at higher modulation rates, particularly when this approaches or exceeds the bandwidth of the filter. It should seem intuitively that the energy storage of the i.f. tuned circuits would resist any changes faster than their bandwidth. Also since a wideband f.m. wave consists of a wide spectrum of sidebands, some of these would be excluded for part of the time by the narrow bandwidth of the i.f. filter, and hence the wave at the output might not be expected to be a replica of the input. However, it can be demonstrated that the dynamic filter will respond to modulation rates in excess of its bandwidth and that the i.f. output differs from the i.f. input only by an amplitude and phase determined by the difference of the input frequency and the i.f. centre frequency (this difference was arranged to be constant).

2.1. *Theoretical Derivation of Dynamic Filter Response*

The variation of the capacitance across a tuned circuit can alter the stored energy very rapidly and independently of the tuned circuit bandwidth. The stored energy is $\frac{1}{2}CV_{pk}^2$, which may be changed rapidly by varying C, instead of relying on the dissipation of the tuned circuit.

The proof for the case of a high-Q tuned circuit is found by considering the steady state solution of the following integro-differential equation.

$$C_0\frac{de}{d\tau} + G_0 e + \frac{1}{L_0}\int e\,d\tau = I_0 \cos\omega_1\tau \quad \text{.....(1)}$$

If τ is the time variable, this equation describes the response of a parallel tuned circuit to an exciting sine wave. The frequency ω_1 will be considered to be not far removed from the resonant frequency

$$\omega_0 = \frac{1}{\sqrt{L_0 C_0}}$$

A change of variable is performed by substituting for τ as follows:

$$\tau = t + \frac{\varepsilon}{p}\sin pt \quad \text{.....(2)}$$

where $\varepsilon \ll 1$ and $p \ll \omega_1$. Equation (1) then becomes, after a little manipulation:

$$\frac{d}{dt}[vC(t)] + vG(t) + \frac{1}{L_0}\int v\,dt = I_0 \cos\left[\omega_1\left(t + \frac{\varepsilon}{p}\sin pt\right)\right] \quad \text{.....(3)}$$

where

$$v = e(1+\varepsilon\cos pt) \quad \text{.....(4)}$$

$$C(t) = \frac{C_0}{(1+\varepsilon\cos pt)^2} \quad \text{.....(5)}$$

$$G(t) = \frac{G_0}{(1+\varepsilon\cos pt)} - \frac{\varepsilon p C_0 \sin pt}{(1+\varepsilon\cos pt)^3} \quad \text{.....(6)}$$

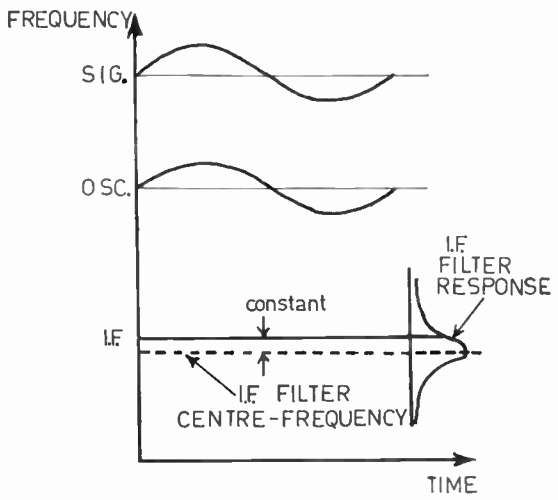

(a) V.c.o. fixed i.f.

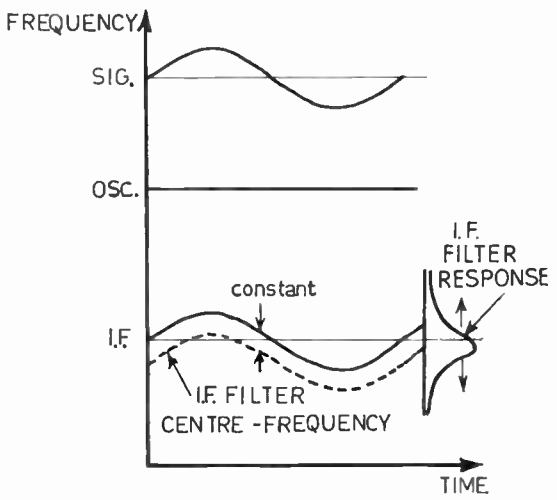

(b) Dynamic filter

Fig. 3. Comparison of variable centre-frequency amplifiers.

If t is now regarded as the time variable, it is immediately apparent that eqn. (3) is the integro-differential equation describing the response of a tuned circuit with varying capacitance and conductance to a frequency modulated signal of peak deviation $\varepsilon\omega_1$ and modulation frequency p.

The instantaneous centre frequency is given by:

$$\omega_c(t) = \frac{1}{\sqrt{L_0 C(t)}} = \omega_0(1+\varepsilon\cos pt) \quad \ldots\ldots(7)$$

The instantaneous frequency of the exciting wave is

$$\omega_i(t) = \omega_1(1+\varepsilon\cos pt) \quad \ldots\ldots(8)$$

The difference between the instantaneous input frequency and the instantaneous centre frequency of the filter is therefore approximately constant since ε is small

$$\omega_d(t) = (\omega_1-\omega_0)(1+\varepsilon\cos pt) \simeq (\omega_1-\omega_0) \quad \ldots\ldots(9)$$

The variation in $G(t)$ may be shown to be small by writing it in the form:

$$G(t) = G_0\left[\frac{1}{(1+\varepsilon\cos pt)} - \frac{p}{\Delta\omega}\cdot\frac{\varepsilon\sin pt}{(1+\varepsilon\cos pt)^3}\right] \quad (10)$$

where $\Delta\omega = G_0/C_0$ = full 3 dB bandwidth of tuned circuit. Since the modulation frequencies of interest are normally not much greater than $\Delta\omega$, then $G(t) \simeq G_0$. The small variation in $G(t)$ may be neglected since it has a negligible effect on the tuned circuit. The variation in $G(t)$ produces an infinitesimal variation in the tuned circuit bandwidth.

The steady-state solution to eqn. (1) is given by:

$$e(\tau) = A\cos(\omega_1\tau+\phi) \quad \ldots\ldots(11)$$

where A and ϕ are constants which depend on the frequency difference $(\omega_1-\omega_0)$ and the tuned-circuit bandwidth $\Delta\omega$. The solution to eqn. (3) is therefore given by eqn. (11) with the appropriate substitution for τ being made

$$v(t) = A(1+\varepsilon\cos pt)\cos\left[\omega_1\left(t+\frac{\varepsilon}{p}\sin pt\right)+\phi\right] \quad (12)$$

The amplitude modulation may be ignored since ε is small and hence:

$$v(t) \simeq A\cos\left[\omega_1\left(t+\frac{\varepsilon}{p}\sin pt\right)+\phi\right] \quad \ldots\ldots(13)$$

The output voltage is a replica of the exciting signal except that it differs in amplitude and phase.

In arriving at this result a number of approximations have been made, the errors becoming smaller as ε tends to zero. Determination of the errors is not feasible using this simplified analysis. Exact analysis involves the use of Matthieu functions,[5] and becomes exceedingly complex due to the fact that the response to each sideband of the f.m. wave must be calculated and these summed to obtain the overall response. Practical tests described in the next section indicated that the errors were negligible.

2.2. *Practical Tests on the Dynamic Filter*

Verification of the foregoing theory was obtained by testing a dynamic filter tuned by varactor diodes. The frequency/voltage characteristic obtained by direct biasing of the diodes was slightly non-linear, so this was corrected by placing a non-linear network between the diodes and the bias source. The output/input characteristic of this network was adjusted so

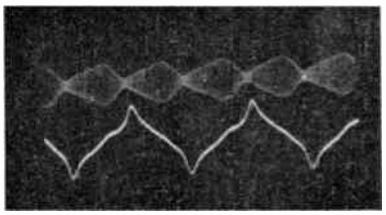

(a) $f_d = 30$ kc/s, $f_m = 8{\cdot}5$ kc/s

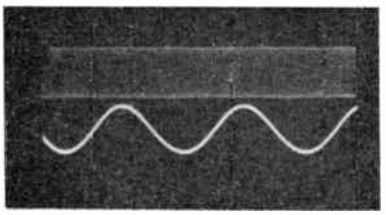

(f) $f_d = 30$ kc/s, $f_m = 8{\cdot}5$ kc/s

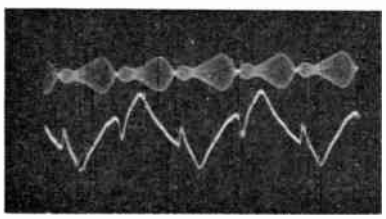

(b) $f_d = 50$ kc/s, $f_m = 8{\cdot}5$ kc/s

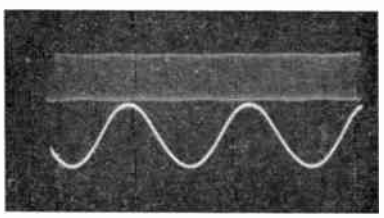

(g) $f_d = 50$ kc/s, $f_m = 8{\cdot}5$ kc/s

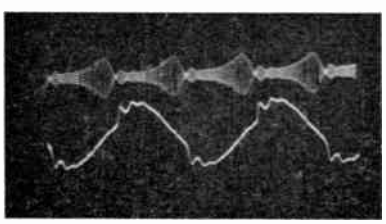

(c) $f_d = 50$ kc/s, $f_m = 4{\cdot}3$ kc/s

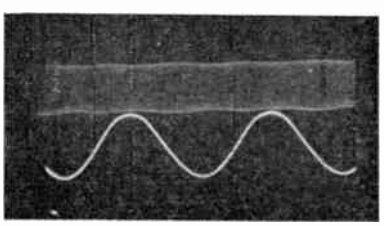

(h) $f_d = 50$ kc/s, $f_m = 4{\cdot}3$ kc/s

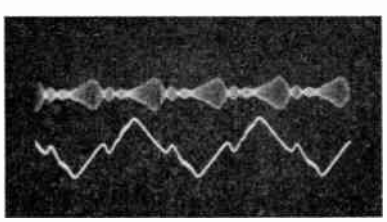

(d) $f_d = 85$ kc/s, $f_m = 8{\cdot}5$ kc/s

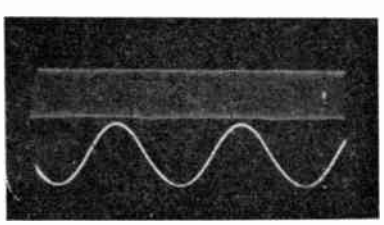

(i) $f_d = 85$ kc/s, $f_m = 8{\cdot}5$ kc/s

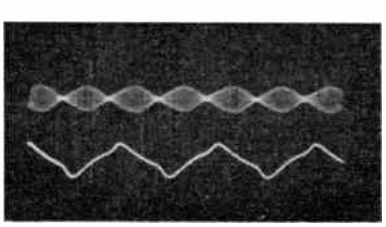

(e) $f_d = 50$ kc/s, $f_m = 20$ kc/s

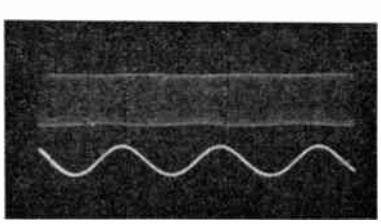

(j) $f_d = 50$ kc/s, $f_m = 20$ kc/s

(i) No capacitor modulation

(ii) Correct capacitor modulation

Fig. 5. R.f. envelope and instantaneous frequency of filter output.

that the overall frequency/voltage characteristic was linear over the required range. The experimental set-up is shown in Fig. 4.

The resonant frequency of the filter was 1·5 Mc/s and the bandwidth 17 kc/s. The frequency/voltage characteristic was linear to within 1% for deviations up to ± 100 kc/s and the discriminator was linear to within 1% for deviations up to ± 150 kc/s.

The first experiment consisted of making the centre frequency of the filter equal to the instantaneous input frequency. According to the theory of the previous section, under these conditions the output wave should be identical to the input with no amplitude change or phase shift. Figure 5 shows oscillograms of the r.f. envelope and the instantaneous frequency for different frequency deviations and modulation rates. The output with the filter unmodulated is also shown. With correct capacitor modulation, there is no discernible distortion of the instantaneous frequency and the amplitude modulation of the envelope is negligible.

The second experiment determined whether the instantaneous frequency suffered any phase or amplitude change in passing through the dynamic filter. At a fixed frequency deviation of 50 kc/s, the amplitude and phase characteristics were measured from the modulator input to the discriminator output. These were measured with the dynamic filter in the circuit (with correct capacitor modulation) and with the dynamic filter omitted. The difference of these two measurements gave the dynamic filter characteristics shown in Fig. 6. It is evident that the dynamic filter did not significantly affect the amplitude or phase of the instantaneous frequency. This again is consistent with the foregoing theory.

The third experiment compared the harmonic distortion of the discriminator output with the dynamic filter in circuit (with correct capacitor modulation) and with the dynamic filter omitted.

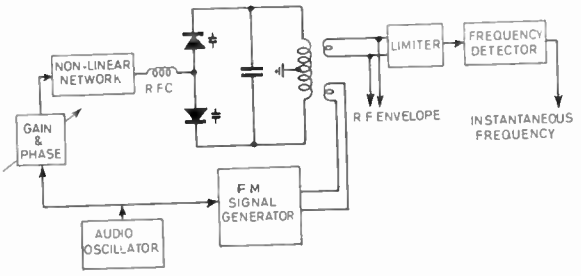

Fig. 4. Dynamic filter test circuit.

A frequency deviation of 100 kc/s was used. These results are shown in Fig. 7, from which it is evident that the amount of distortion caused by the filter was negligible. The increase in fourth harmonic was due to the non-linearity correction circuit which had a fourth-order error ripple. The total harmonic distortion was of the order of 1% or less at all modulation frequencies.

In the fourth experiment the discriminator output was measured when the dynamic filter was correctly modulated but detuned by varying amounts. The harmonic distortion of the output and the amplitude of the output r.f. envelope were also measured. These

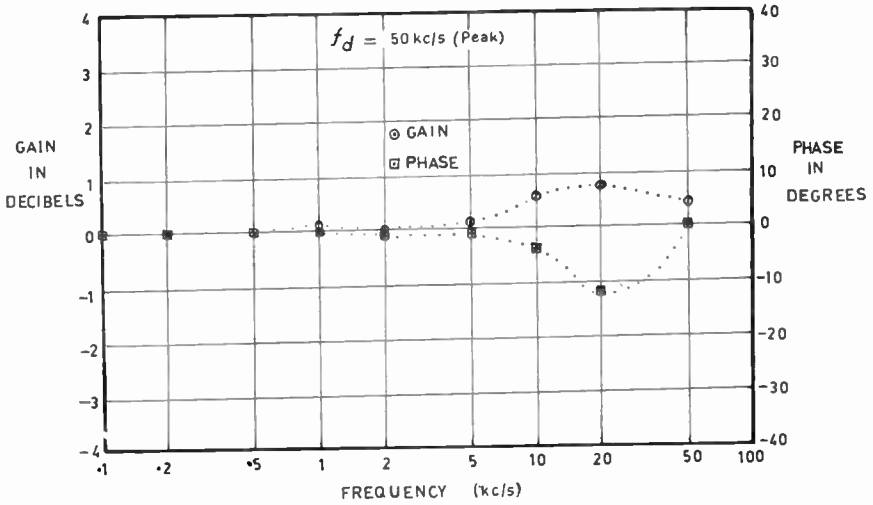

Fig. 6. Effect of dynamic filter on instantaneous frequency.

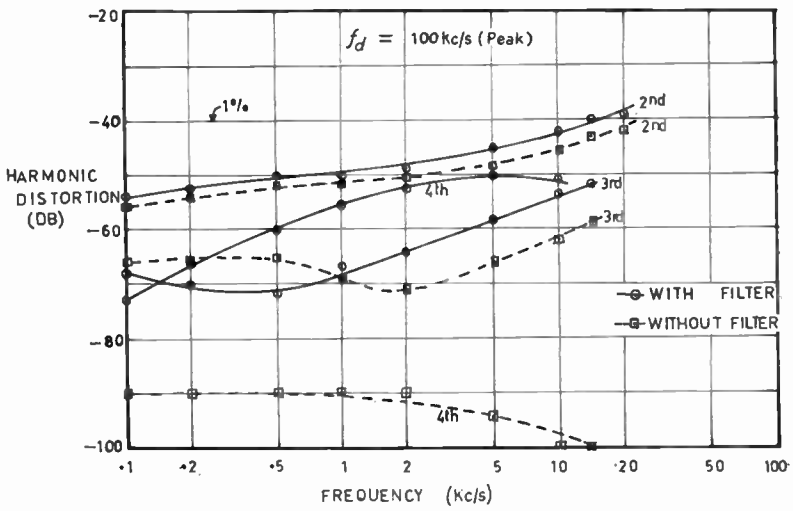

Fig. 7. Harmonic distortion of instantaneous frequency.

results are shown in Fig. 8. The fundamental component was constant and the harmonic distortion small. The r.f. amplitude variation was that expected of a single tuned circuit of 17 kc/s bandwidth. A deviation of 50 kc/s and a modulation frequency of 5 kc/s were used. The results obtained were consistent with the foregoing theory.

2.3. *Development of Equivalence*

2.3.1. V.c.o. fixed i.f. response to f.m.

If the oscillator frequency deviation is different from the signal frequency deviation, then the intermediate frequency no longer has zero deviation. The response could be found by the following steps.

(i) Determination of the instantaneous signal and oscillator frequencies and hence the instantaneous intermediate frequency.

(ii) Resolving the i.f. signal into sidebands and calculating the effect of the i.f. filter on each in turn.

(iii) Reassembling the modified sidebands to give the output signal. For example, suppose the signal and oscillator voltages are as follows:

$$e_{sig} = \cos[\omega_s t + m_1 \sin(pt+\phi)] \quad \text{.....(14)}$$

$$e_{osc} = \cos[\omega_0 t + m_2 \sin pt] \quad \text{.....(15)}$$

The i.f. signal is therefore a sine wave of frequency equal to the difference of the signal and oscillator frequencies, namely,

$$e_{i.f.} = \cos[\omega_i t + m \sin(pt+\theta)] \quad \text{.....(16)}$$

where $$m \sin(pt+\theta) = m_1 \sin(pt+\phi) - m_2 \sin pt \quad \text{...(17)}$$

To find the response, eqn. (16) is expanded into sidebands.

$$e_{i.f.} = \sum_{n=-\infty}^{+\infty} J_n(m) \cos[(\omega_i + np)t + n\theta] \quad \text{.....(18)}$$

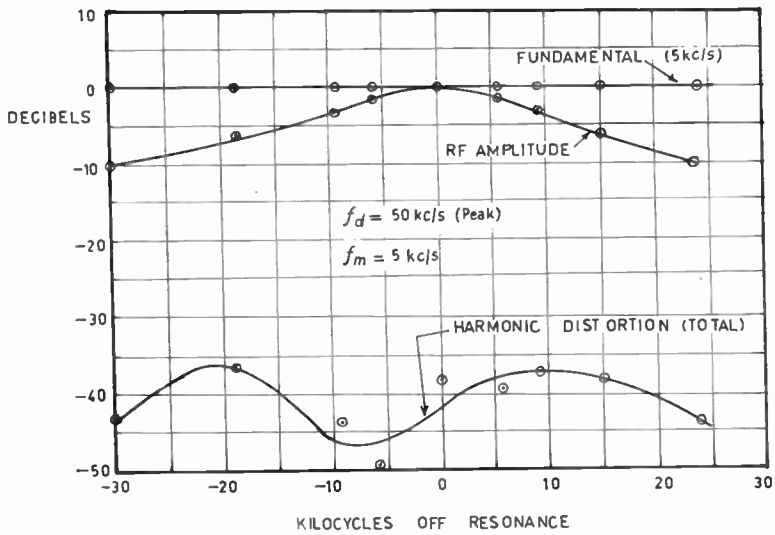

Fig. 8. Effect of detuning dynamic filter.

Thus the output signal is given by:

$$e_{out} = \sum_{n=-\infty}^{+\infty} J_n(m) A_n \cos[(\omega_i + np)t + n\theta + \phi_n] \quad (19)$$

where A_n and ϕ_n are the amplitude and phase changes of the nth sideband due to the i.f. filter.

2.3.2. Dynamic filter response to frequency modulation

If the dynamic filter centre frequency deviation is different from the i.f. deviation, then the response may be found by using a similar procedure to the v.c.o. fixed i.f. case. However, whereas it was convenient to expand the i.f. signal into sidebands of constant frequency, for the dynamic filter it is more convenient to expand the i.f. signal into components of varying frequency. This is so, since if the centre frequency of the dynamic filter is given by:

$$\omega_c(t) = \frac{d}{dt}(\omega_i t + m_2 \sin pt) \qquad \ldots\ldots(20)$$

then the response of the filter to any f.m. wave whose instantaneous frequency differs from $\omega_c(t)$ by a constant amount may be found by using the results of Section 2.1.

Suppose the i.f. signal is given by:

$$e_{i.f.} = \cos[\omega_i t + m_1 \sin(pt + \phi)] \qquad \ldots\ldots(21)$$

Using eqn. (17) this may be rewritten as:

$$e_{i.f.} = \cos[\omega_i t + m \sin(pt + \theta) + m_2 \sin pt]$$

$$= \sum_{n=-\infty}^{+\infty} J_n(m) \cos[(\omega_i + np)t + m_2 \sin pt + n\theta] \quad (22)$$

The response to each of these components can now be calculated in turn and the results superimposed (this is valid since eqn. (3) is a *linear* differential equation), i.e.

$$e_{out} = \sum_{n=-\infty}^{+\infty} J_n(m) A_n \cos[(\omega_i + np)t + + m_2 \sin pt + n\theta + \theta_n] \quad (23)$$

where A_n and ϕ_n are the same as before.

Comparison of eqns. (19) and (23) indicates that they are identical except the instantaneous frequencies differ by $m_2 p \cos pt$, i.e. the difference of the instantaneous output frequency and the instantaneous i.f. filter centre frequency is the same for both systems. Thus the systems are equivalent in behaviour, but the fact that the i.f. centre frequency is varying in one and fixed in the other leads to some interesting possibilities. The important result is that the response of the dynamic filter can be found by finding the response of the equivalent v.c.o. fixed i.f. system (using the method of Section 2.3.1 or any other method[4]).

3. Dynamic Filter Circuits Applied to F.M. Detection

3.1. *A Dynamic Selector Circuit*

A circuit for improving the threshold of f.m. detectors has been suggested by Baghdady[6] along the lines of Fig. 9. The operation of the circuit relies on the output of the frequency detector aligning the dynamic filter to the instantaneous intermediate frequency. Since the filter bandwidth may be smaller than the i.f. bandwidth, an improvement in threshold should be obtained.

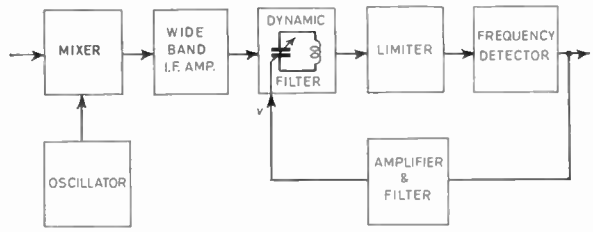

Fig. 9. Dynamic selector for f.m. detection.

Successful operation of the circuit requires that the difference of the filter centre frequency and the instantaneous frequency of the i.f. signal be less that the filter semi-bandwidth for all modulating frequencies. This therefore makes it essential that the gain and phase variations over the modulation bandwidth be small. In fact for a peak-to-peak frequency deviation of ten times the filter bandwidth, the maximum tolerable variations are 1 dB in gain and 5 deg in phase. The amplifier circuits will therefore have a wide frequency response and the resulting large amount of noise will cause the centre frequency of the filter to jitter. This will cause a threshold effect similar to the feedback threshold of a feedback f.m. detector.[2] Gain variations with carrier level and temperature will also upset the operation of the system. Examination of the circuit shows that the feedback does not achieve any improvement in gain stability.

An experimental model of this system was constructed, but it was found that it was impossible to obtain satisfactory results. The gain stability required was very difficult to maintain and the wideband amplifier circuits caused the threshold to occur at a higher level than for a normal f.m. system.

3.2. *A Tracking Dynamic Filter*

To have a successful tracking filter it is essential to have a device which is sensitive to the *difference* of the instantaneous frequency and the filter centre frequency. For the fixed i.f. in a feedback f.m.

system this is simply a frequency detector, but is more complex in the dynamic filter arrangement. A circuit which accomplishes this is shown in Fig. 10.

The detector operates on the principle that if the dynamic filter centre frequency is the same as the instantaneous frequency then the phase shift is zero, but either leads or lags if the frequencies are different.

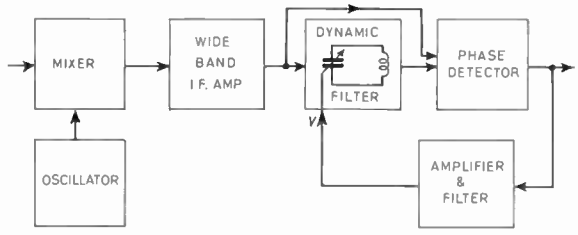

Fig. 10. Dynamic filter detector for f.m.

The linearity of the circuit is not good, since the phase difference θ is equal to arctan $(\Delta f/f_0)$, where Δf is the frequency difference and f_0 the filter semi-bandwidth. The phase detector gives a voltage proportional to sin θ and so the voltage-frequency law is as follows:

$$v = \frac{k\Delta f}{\sqrt{f_0^2 + \Delta f^2}} \qquad \text{.....(24)}$$

Examination of the circuit shows that it is exactly equivalent to a feedback f.m. system, the only difference being that the i.f. filter centre frequency is varying in one case and fixed in the other. The negative feedback present in the circuit makes the gain stability and frequency response requirements much less stringent than for the previous case.

An experimental model of this system was constructed, and its performance was found to approximate closely to the theoretical response of an equivalent feedback f.m. system, except that the detector non-linearity reduced the allowable frequency deviation by about 30%.

4. Conclusions

A method of finding the response of a dynamic filter to a frequency-modulated wave has been derived. It has been shown that the dynamic filter is equivalent to a v.c.o. fixed i.f. system and when used in a tracking filter circuit will give identical results to a feedback f.m. detector. Operation in a dynamic selector circuit using an ordinary frequency detector does not yield a satisfactory system. In the case of a feedback f.m. system the requirements are a linear voltage-controlled oscillator and a linear frequency discriminator. For a tracking filter the requirements are a dynamic filter with a linear frequency/voltage characteristic and a detecting device which will give a voltage linearly dependent on the difference of the instantaneous frequency of the i.f. signal and the filter centre frequency. From a practical viewpoint, therefore, the dynamic filter is capable of the same threshold improvement as a feedback f.m. system, but with possibly greater circuit complexity.

5. Acknowledgment

This research was conducted under a C.S.I.R.O. Post-Graduate Studentship in the Electrical Engineering Department of the University of Adelaide.

6. References

1. F. L. Stumpers, "Theory of f.m. noise", *Proc. Inst. Radio Engrs*, **36**, p. 1081, September 1948.
2. L. H. Enloe, "Decreasing the threshold in f.m. by frequency feedback", *Proc. I.R.E.*, **50**, p. 18, January 1962.
3. C. L. Ruthroff, "F.m. demodulators with negative feedback", *Bell Syst. Tech. J.*, **40**, p. 1149, July 1961.
4. E. J. Baghdady, "On the response of a linear system to an f.m. signal", *Trans. I.R.E. on Circuit Theory*, **CT-6**, p. 387, December 1959.
5. W. J. Cunningham, "Introduction to Non-linear Analysis", pp. 245–280 (McGraw-Hill, New York, 1958).
6. E. J. Baghdady, "Lectures on Communication System Theory", p. 548 (McGraw-Hill, New York, 1961).

Manuscript first received by the Institution on 6th December 1963, in revised form on 4th May 1964 and in final form on 31st August 1964. (Paper No. 947.)

U.D.C. 621.373.4: 621.385.3

The Design of Triode Harmonic Generators

By

T. WILLIAMS, B.Sc., Ph.D.†

Summary: Existing analytical methods for predetermining the anode and grid currents of a triode harmonic generator are examined. These methods are found to give large unpredictable errors which may be of the order of 25%. A new analytical method is devised, based on a power series representation of the valve characteristics, whereby the anode current components can be forecast with a maximum error of less than 6% for harmonic generation up to fifth order. This method is also applied to the prediction of grid currents and is found to be more accurate than previous analytical methods. Transistor harmonic generators are discussed briefly.

List of Symbols

n order of harmonic generation

E_B anode supply voltage

$V_{a(\max)}$ peak value of r.f. voltage developed at the anode.

V_0 minimum value of instantaneous anode voltage $= E_B - V_{a(\max)}$

V_a instantaneous anode voltage

E_g grid bias voltage

$V_{g(\max)}$ peak value of r.f. input voltage

$E_{g(\max)}$ most positive grid voltage attained during r.f. cycle $= V_{g(\max)} - E_g$

V_g instantaneous grid voltage

I_{ap} value of anode current at pulse centre

$I_{a(\text{d.c.})}$ d.c. component of anode current

$I_{an(\max)}$ peak value of nth harmonic component of anode current

$I'_{a(\text{d.c.})}$ d.c. component of anode current derived from linear-law characteristic

$I''_{a(\text{d.c.})}$ d.c. component of anode current derived from square-law characteristic

$I'''_{a(\text{d.c.})}$ d.c. component of anode current derived from cubic-law characteristic

$I'_{an(\max)}$ peak value of nth harmonic component of anode current derived from linear-law characteristic

$I''_{an(\max)}$ peak value of nth harmonic component of anode current derived from square-law characteristic

$I'''_{an(\max)}$ peak value of nth harmonic component of anode current derived from cubic-law characteristic

I'_{ap} value of anode current, derived from linear-law characteristic, at pulse centre

I''_{ap} value of anode current, derived from square-law characteristic, at pulse centre

I'''_{ap} value of anode current, derived from cubic-law characteristic, at pulse centre

i_a instantaneous anode current

I_{gp} value of grid current at pulse centre

$I_{g(\text{d.c.})}$ d.c. component of grid current

$I_{g(\max)}$ peak value of first harmonic component of grid current

i_g instantaneous grid current

$\alpha' = I'_{a(\text{d.c.})}/I'_{ap}$

$\alpha'' = I''_{a(\text{d.c.})}/I''_{ap}$

$\alpha''' = I'''_{a(\text{d.c.})}/I'''_{ap}$

$\beta'_n = I'_{an(\max)}/I'_{ap}$

$\beta''_n = I''_{an(\max)}/I''_{ap}$

$\beta'''_n = I'''_{an(\max)}/I'''_{ap}$

k_0 value of anode current at $V_g = 0$

k' coefficient of linear-law term in valve characteristic power series

k'' coefficient of square-law term in valve characteristic power series

k''' coefficient of cubic-law term in valve characteristic power series

E'_{co} cut-off voltage of linear-law component of anode current

ω angular frequency

θ angle of flow of anode current

θ_g angle of flow of grid current

θ' angle of flow of linear-law component of anode current

θ'' angle of flow of square-law component of anode current

θ''' angle of flow of cubic-law component of anode current

† Department of Light Electrical Engineering, The Queen's University of Belfast.

1. Introduction

Harmonic generators similar to that shown in Fig. 1 have many applications in the radio-frequency field, e.g. as frequency multipliers in broadcast transmitters.

It is desirable, especially at high power levels, that the power input, power output and grid driving power under given operating conditions be predetermined with reasonable accuracy. The only exact method of calculating these quantities is the lengthy 'point-by-point' method.[1] Since, however, in order to optimize the design the calculations are often repeated several times, the design work becomes laborious. Consequently, there have been many attempts to produce an analytical method which would reduce time to a minimum whilst preserving an accuracy approaching that of the 'point-by-point' method. It has been shown, however, that the existing analytical methods are not dependable when applied to harmonic generators using screen-grid valves and give unpredictable errors of magnitude up to 30%.[2] In the present paper the validity of existing analytical methods for triode harmonic generators is investigated and these are found to be undependable also. A new design method is devised whereby anode current components might be forecast with a maximum error of less than 6% for harmonic generation up to fifth order. This new method is applied to the predetermination of grid currents and proves to be more accurate than previous analytical methods.

2. Existing Design Methods

Methods for pre-determining the direct and alternating components of triode harmonic generator current pulses fall into two categories:

(*a*) Graphical methods, in which the current pulse is plotted from static valve characteristics and the component values extracted by a graphical Fourier analysis. There are two such methods:

(i) the 'point-by-point' method, which makes use of the static I_a/V_a characteristics;

(ii) a method employing constant-current charts.[3]

(*b*) Analytical methods, in which the valve characteristics are assumed to follow a mathematical law.

Many papers have been written describing these methods. The first of these assumed that the composite characteristic of the valve was linear.[4] Later a method was formulated on the assumption that the static characteristics followed a $\frac{3}{2}$-power law and included the modification that the anode current reached a saturation value which formed the upper limit of the characteristic.[5] Since then numerous papers have been published[6–19] which have been variations of these two methods.

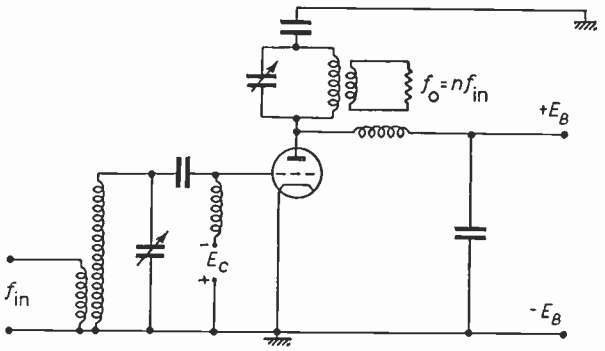

Fig. 1. Simple triode harmonic generator.

3. Validity of Existing Methods

The 'point-by-point' method is exact and has been verified[2, 20] so may be accepted as completely accurate and used as a means of comparison for the analytical methods.

Using this method, fifty designs were carried out on different triodes of various power ratings and amplification factors, five per harmonic, for harmonic generation up to fifth order.

The designs were repeated using the $\frac{3}{2}$-law method[11] and also using a linear-law method which was devised by the writer as a modified form of the $\frac{3}{2}$-law method. Ten designs were performed for each harmonic, and in order to show the errors that can arise the moduli of the maximum errors given by each method for each harmonic are shown in Fig. 2. These results show that existing analytical methods are not dependable and give rise to unpredictable errors which in some cases are of the order of 25%.

4. Power Series Method

Since those methods which assume that the static characteristics of a triode are either linear or follow a $\frac{3}{2}$-law proved undependable, the possibility of representing the valve curves by a power series was investigated.

This means of representation is not entirely unknown. A third order power series has been used to determine the output voltage of an audio-frequency doubler operating class-A,[21] and to calculate the harmonic distortion arising in a class-A amplifier.[22] A power-series representation of triode characteristics has also been derived.[23]

In the second of these cases the analysis is relatively simple because it is applied to a class-A amplifier; the first and third cases depend for their accuracy on valve parameters such as amplification factor, a.c. resistance and mutual conductance remaining constant throughout the operating cycle.

In the case of a triode harmonic generator the curve which is of most use is the *mutual dynamic characteristic*, i.e. the curve relating the variation of anode current to grid and anode voltages. This may be written as

$$i_a = k_0 + k'V_g + k''V_g^2 + \ldots + k^{(r)}V_g^r + \ldots \quad \ldots\ldots(1)$$

where i_a = instantaneous anode current corresponding to

$$V_g = V_{g(\max)} \cos \omega t - E_g \quad \ldots\ldots(2)$$

and

$$V_a = E_B - V_{a(\max)} \cos n\omega t \quad \ldots\ldots(3)$$

where $V_{g(\max)}$ = peak value of r.f. input voltage

E_g = grid bias voltage

E_B = anode supply voltage

$V_{a(\max)}$ = peak value of r.f. voltage developed at anode

n = order of harmonic generation

k_0, k', etc., are constants for a particular curve.

Consider a third-order power series, i.e.

$$i_a = k_0 + k'V_g + k''V_g^2 + k'''V_g^3 \quad \ldots\ldots(4)$$

At $V_g = 0$, $i_a = k_0$, which may be read from the valve curves.

k', k'', and k''' may be found by solving three simultaneous equations, namely:

$$i_1 - k_0 = k'V_1 + k''V_1^2 + k'''V_1^3 \quad \ldots\ldots(5)$$

$$i_2 - k_0 = k'V_2 + k''V_2^2 + k'''V_2^3 \quad \ldots\ldots(6)$$

$$i_3 - k_0 = k'V_3 + k''V_3^2 + k'''V_3^3 \quad \ldots\ldots(7)$$

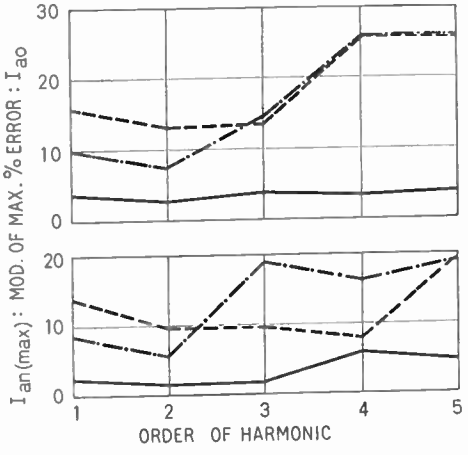

Fig. 2. Modulus of maximum percentage error in anode current components.

———— power series
— — — — 3/2 law
— . — . — linear law

where (i_1, V_1), (i_2, V_2), (i_3, V_3) are particular points on the mutual dynamic characteristic.

The solutions of eqns. (5), (6) and (7) are:

$$k''' = \frac{1}{(V_1 - V_3)} \left\{ M - \frac{1}{(V_2 - V_3)} \left[N - \frac{(i_3 - i_0)}{V_3} \right] \right\} \quad \ldots(8)$$

where

$$M = \frac{1}{(V_1 - V_2)} \left[\frac{(i_1 - i_0)}{V_1} - \frac{(i_2 - i_0)}{V_2} \right]$$

$$N = \frac{(i_2 - i_0)}{V_2}$$

$$k'' = M - k'''(V_1 + V_2) \quad \ldots\ldots(9)$$

$$k' = N - k''V_2 - k'''V_2^2 \quad \ldots\ldots(10)$$

Combining eqns. (2) and (3):

$$V_{ar} = E_B - V_{a(\max)} \cos n \cos^{-1} \frac{(V_{gr} + E_g)}{V_{g(\max)}} \quad \ldots(11)$$

where V_{gr} is the value of a particular constant grid-voltage curve on the i_a/V_a characteristics. Thus i_{ar}, the instantaneous anode current corresponding to V_{gr} and V_{ar}, may be read off the i_a/V_a curves. If four such points are taken then the mutual dynamic characteristic may be determined.

Since anode current flows for only a fraction of a cycle in a radio-frequency harmonic generator it is necessary to represent the mutual dynamic curve only in the region of current flow, i.e. between I_{ap}, the value of anode current at the pulse centre, and cut-off. Thus two obvious points are one at the pulse centre and another near cut-off. In general, a triode harmonic generator will produce a pulse of anode current with a dip at the centre, and so if an accurate representation of the pulse is to be made a point should be taken at the greatest instantaneous anode current reached during the cycle. This usually occurs at, or very close to, the constant grid-voltage characteristic below the one at which the pulse centre occurs. (Although the interval between constant grid-voltage characteristics is arbitrary, the above has been found to be invariably the case for all manufacturers' curves used in the designs carried out.) The fourth point is the instantaneous anode current corresponding to $V_g = 0$ and is k_0 in eqn. (4).

The mutual dynamic curve given by eqn. (4) may be resolved into

(*a*) a linear-law component,

$$i'_a = k_0 + k'V_g \quad \ldots\ldots(12)$$

(*b*) a square-law component,

$$i''_a = k''V_g^2 \quad \ldots\ldots(13)$$

(*c*) a cubic-law component,

$$i'''_a = k'''V_g^3 \quad \ldots\ldots(14)$$

The linear-law component has an angle of flow θ' given by

$$\cos\frac{\theta'}{2}=\frac{E'_{co}+E_g}{V_{g(\max)}} \qquad \text{.....(15)}$$

where $E'_{co}=-k_0/k'$, the cut-off voltage for the linear-law component.

Cut-off is defined as that voltage at which the current reaches zero value. Thus in eqns. (13) and (14) $i''_a=i'''_a=0$ when $V_g=0$ and so the square- and cubic-law components have the same angle of flow, θ_g, as the grid current (where $\theta_g=2\cos^{-1}E_g/V_{g(\max)}$). This does not mean that i''_a and i'''_a flow only when V_g is positive, because being components they may have either positive or negative values in the represented region of the curve.

The component peak currents may be found by substituting $V_g=E_{g(\max)}$ in eqns. (12), (13) and (14) giving

$$I'_{ap}=k_0+k'E_{g(\max)} \qquad \text{.....(16)}$$

$$I''_{ap}=k''.E^2_{g(\max)} \qquad \text{.....(17)}$$

$$I'''_{ap}=k'''.E^3_{g(\max)} \qquad \text{.....(18)}$$

where $E_{g(\max)}$ is the most positive grid voltage attained during the r.f. cycle, $(E_{g(\max)}=V_{g(\max)}-E_g)$,

and

$$I'_{ap}+I''_{ap}+I'''_{ap}=I_{ap} \qquad \text{.....(19)}$$

I_{ap} is the value of anode current at the pulse centre and may be obtained from the valve characteristic at $V_g=E_{g(\max)}$ and $V_a=E_B-V_{a(\max)}$. Equation (19) may be used as a check on the calculation of the power series constants.

Values of $\frac{I^{(r)}_{a(\text{d.c.})}}{I^{(r)}_{ap}}$ $(=\alpha^{(r)})$ and $\frac{I^{(r)}_{an(\max)}}{I^{(r)}_{ap}}$ $(=\beta^{(r)}_n)$ for linear-, square- and cubic-law characteristics are given in Tables 1, 2 and 3 respectively, where

$I^{(r)}_{a(\text{d.c.})}$ = direct component of anode current derived from rth law characteristic

and

$I^{(r)}_{an(\max)}$ = peak value of nth harmonic component of anode current derived from rth law characteristic.

Knowing the angles of flow of the components, values of α', α'', α''', β'_n, β''_n, and β'''_n may be obtained from Tables 1, 2 and 3 for the appropriate harmonic.

The direct current components are then given by

$$I'_{a(\text{d.c.})}=\alpha'.I'_{ap} \qquad \text{.....(20)}$$

$$I''_{a(\text{d.c.})}=\alpha''.I''_{ap} \qquad \text{.....(21)}$$

$$I'''_{a(\text{d.c.})}=\alpha'''.I'''_{ap} \qquad \text{.....(22)}$$

Thus the direct component of the anode current pulse, $I_{a(\text{d.c.})}$ is given by

$$I_{a(\text{d.c.})}=I'_{a(\text{d.c.})}+I''_{a(\text{d.c.})}+I'''_{a(\text{d.c.})} \qquad \text{.....(23)}$$

Similarly the harmonic components are

$$I'_{an(\max)}=\beta'_n.I'_{ap} \qquad \text{.....(24)}$$

$$I''_{an(\max)}=\beta''_n.I''_{ap} \qquad \text{.....(25)}$$

$$I'''_{an(\max)}=\beta'''_n.I'''_{ap} \qquad \text{.....(26)}$$

and the peak harmonic current component of the anode current pulse, $I_{an(\max)}$, is

$$I_{an(\max)}=I'_{an(\max)}+I''_{an(\max)}+I'''_{an(\max)} \qquad \text{.....(27)}$$

Table 1

Values of α' and β'_n and the corresponding angle of anode current flow, $\theta°$

$\theta°$	α'	β'_1	β'_2	β'_3	β'_4	β'_5
20	0·0371	0·0738	0·0733	0·0721	0·0706	0·0687
30	0·0555	0·1103	0·1079	0·1043	0·0993	0·0932
40	0·0739	0·1461	0·1408	0·1323	0·1210	0·1075
50	0·0923	0·1811	0·1710	0·1549	0·1343	0·1107
60	0·1106	0·2152	0·1980	0·1715	0·1386	0·1029
70	0·1288	0·2482	0·2214	0·1814	0·1340	0·0859
80	0·1469	0·2799	0·2409	0·1845	0·1215	0·0625
90	0·1649	0·3102	0·2562	0·1811	0·1025	0·0362
100	0·1828	0·3389	0·2670	0·1717	0·0790	0·0105
110	0·2005	0·3658	0·2735	0·1569	0·0533	−0·0115
120	0·2180	0·3910	0·2757	0·1378	0·0276	−0·0276
130	0·2353	0·4142	0·2736	0·1156	0·0039	−0·0363
140	0·2524	0·4356	0·2676	0·0915	−0·0160	−0·0378

Table 2

Values of α'' and β_n'' and the corresponding angle of anode current flow, $\theta°$

$\theta°$	α''	β_1''	β_2''	β_3''	β_4''	β_5''
20	0·0298	0·0590	0·0588	0·0579	0·0570	0·0560
30	0·0444	0·0881	0·0870	0·0851	0·0819	0·0784
40	0·0591	0·1171	0·1141	0·1092	0·1027	0·0946
50	0·0743	0·1461	0·1400	0·1309	0·1182	0·1041
60	0·0883	0·1740	0·1633	0·1483	0·1280	0·1057
70	0·1027	0·2003	0·1846	0·1611	0·1317	0·1004
80	0·1172	0·2263	0·2039	0·1701	0·1303	0·0897
90	0·1313	0·2515	0·2203	0·1749	0·1237	0·0750
100	0·1454	0·2755	0·2340	0·1754	0·1128	0·0578
110	0·1593	0·2987	0·2450	0·1722	0·0988	0·0402
120	0·1730	0·3206	0·2532	0·1654	0·0827	0·0236
130	0·1865	0·3412	0·2586	0·1557	0·0658	0·0095
140	0·1998	0·3606	0·2614	0·1437	0·0491	−0·0013

Table 3

Values of α''' and β_n''' and the corresponding angle of anode current flow, $\theta°$

$\theta°$	α'''	β_1'''	β_2'''	β_3'''	β_4'''	β_5'''
20	0·0250	0·0500	0·0490	0·0495	0·0460	0·0475
30	0·0375	0·0770	0·0740	0·0748	0·0690	0·0684
40	0·0500	0·1032	0·0980	0·0977	0·0895	0·0862
50	0·0627	0·1267	0·1212	0·1148	0·1060	0·0969
60	0·0756	0·1491	0·1430	0·1310	0·1182	0·1032
70	0·0877	0·1720	0·1625	0·1453	0·1264	0·1027
80	0·1004	0·1949	0·1805	0·1566	0·1293	0·0979
90	0·1123	0·2171	0·1962	0·1648	0·1279	0·0903
100	0·1240	0·2381	0·2100	0·1698	0·1235	0·0793
110	0·1359	0·2588	0·2225	0·1715	0·1161	0·0665
120	0·1476	0·2785	0·2329	0·1705	0·1063	0·0531
130	0·1591	0·2972	0·2411	0·1670	0·0949	0·0401
140	0·1702	0·3148	0·2473	0·1613	0·0826	0·0282

5. Validity of the Power Series Method

The designs already carried out using the $\frac{3}{2}$- and linear-law methods were again repeated using the power series method and the percentage errors in $I_{a(\text{d.c.})}$ and $I_{an(\max)}$ calculated in each case. The moduli of the maximum errors given by the power series method for each harmonic are shown in Fig. 2. From these results it can be seen that the power series method is dependable, and approaches the accuracy of the point-by-point method for the cases taken up to the fifth harmonic.

6. Prediction of Grid Currents

A knowledge of the grid current components is necessary in order to determine the grid driving power, grid dissipation and value of the grid leak resistor to provide the necessary bias (or part of it). Very little has been done, however, on the problem of forecasting the grid driving power required for a given design of harmonic generator. Simple formulæ for its calculation have been published.[24,25] These formulæ, however, require a knowledge of the direct component of the grid current, $I_{g(\text{d.c.})}$, and no method for its determination is given. In a paper dealing with the predetermination of the grid current components, $I_{g(\text{d.c.})}$ and $I_{g(\max)}$,[26] it was stated that the point-by-point method given by Prince[1] is applicable but lengthy. The grid current waveform was assumed to lie between a triangular shape and a cosine-squared wave within the angle of grid current flow for the

cases of interest where $E_{g(\max)}$ is a fairly large portion of V_0, V_0 being the minimum value of instantaneous anode voltage ($= E_B - V_{a(\max)}$). Both the triangular and the cosine-squared waveforms are characterized by the fact that the ratio of the maximum value to the average value of current during the interval of current flow is 2. This treatment, however, considers only first-harmonic generation. Square-law characteristics have been assumed elsewhere[6,11] for all harmonics.

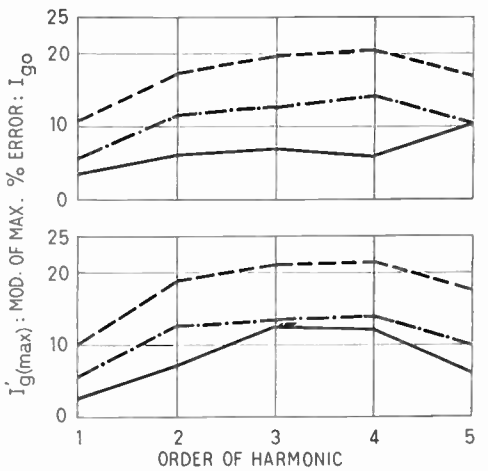

Fig. 3. Modulus of maximum percentage error in grid current components.

———— power series
— — — — square law
— . — . — triangular wave

6.1. *Validity of Existing Analytical Methods*

In order to test the validity of the analytical methods the grid-current components were predicted in a number of designs of harmonic generator, up to fifth order, using valves whose grid-current characteristics were available. The only analytical method previously used for harmonic generation above first was the square-law method. Results obtained by assuming a triangular pulse for higher harmonic designs are also given for comparison. As for the case of the anode current components the point-by-point method was taken as the standard of comparison for the analytical methods. Twenty-five designs were carried out, five per harmonic and, as for the anode current component, the moduli of the maximum errors given by each analytical method for each harmonic are shown in Fig. 3. Overall results show that, apart from the predictions given by the triangular-wave method in the first harmonic designs, the existing analytical methods are far from exact. Of the two known methods, however, the hitherto untried triangular-pulse analysis yields the better results.

6.2. *Power Series Method*

Since the known analytical methods of predicting the grid-current components also proved undependable, the power series method was applied to the grid current designs. It can be seen that since k_0 is the value of i_g at $V_g = 0$, then $k_0 = 0$. Thus linear-, square- and cubic-law components all have the same angle of flow as the actual grid current.

6.3. *Validity of Power Series Method*

To test the validity of the power series method it was applied to the design examples already used to estimate the accuracy of the other analytical methods. The moduli of the maximum errors given by the power series method for each harmonic are shown in Fig. 3. Whilst the predictions given by this method for the grid current components are not as accurate as those obtained for the anode current, the method is an improvement on existing analyses.

7. Analyses using Power Series of Orders other than Third

Anode- and grid-current components were predicted, in a few cases, using a second-order power series method; the results obtained, however, were no better than those given by existing analytical methods. Increased accuracy could be expected by the use of a method involving a fourth-order power series, but this would be as lengthy and laborious as the point-by-point method without, necessarily, having the same accuracy.

8. Limitation of the Point-by-point Method in the Calculation of Grid-current Components

Since grid current flows only when the instantaneous grid voltage exceeds the bias voltage, the angle of grid current flow, θ_g, will always be less than the angle of anode current flow, θ. This means that the instantaneous angle of current flow at the next less-positive constant grid-voltage characteristic below that at which the pulse centre occurs will be a greater fraction of θ_g than of θ. Also since the grid-current pulse is more peaky than that of the anode current, the ratio i_2/I_p will be less for the grid-current than for the anode-current pulse (where i_2 is the instantaneous current at the next less positive constant grid-voltage characteristic below that at which I_p, the current at the pulse centre occurs). This is shown in Fig. 4 where it may be seen that, for a typical design, the first two points, a and b, in the point-by-point trace of the current pulse are reasonably close together in the anode-current case, but are more widely spaced in the grid-current case. Thus if the interval between constant grid-voltage characteristics is large, which is often the case, so that perhaps only four such curves are available from which to form the pulse of grid

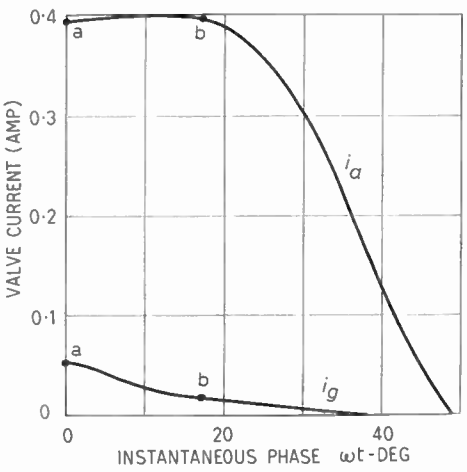

Fig. 4. Typical anode and grid current half-pulses.

current, the portion between a and b in Fig. 4 is indeterminate. This is particularly true for the higher harmonics where the anode moves rapidly in comparison with the grid, so that i_2 often occurs in the almost horizontal portions of the grid-current characteristics, whereas I_{gp} will occur in the regions of greatest slope. In such cases, although the point-by-point method has been taken as the standard to which all other methods have been compared, it is not strictly true to say that the graphical method is completely accurate.

As an example of the variation in the prediction of grid-current components given by the point-by-point method, the indeterminate portion of a typical current pulse was redrawn and the new values of grid current together with the corresponding percentage errors were calculated. These are shown below in Tables 4 and 5 in comparison with the original predictions.

Table 4

Variation in prediction of grid currents

Design	$I_{g(d.c.)}$ (mA)	$I_{g(max)}$ (mA)
Original	3·98	7·74
Redrawn	4·15	8·08

For such designs, where adequate characteristics are not available, the only true criteria are practical test results obtained with the various valves for the given design conditions. Such tests were not necessary, however, since the number of grid-current designs carried out on valves which had adequate characteristics was great enough to establish the fact that existing methods were not dependable and that the power series method gave more accurate results than those known analytical methods. The point-by-point method used as a basis of comparison in such cases is, however, still quite valuable. For instance, in the above example, the original grid-current pulse was probably drawn too narrow, thus explaining the large positive errors given by the analytical methods. But the errors given by the power series method are the lowest of the three, showing that it is the most accurate of these methods.

In a number of grid-current predictions the power series method gives errors much greater than those arising in the anode-current components, suggesting that some of the inaccuracy lies in the point-by-point method. This is not unreasonable, because when the designer draws the grid-current pulse, in the course of the graphical method, he makes a guess at the indeterminate portion of the curve (a—b in Fig. 4). This situation arises, exactly, in the power series method, i.e. when the points a and b are used in the analysis a 'guess' is made by the resulting power series as to the intervening path.

9. Transistor Harmonic Generators and Prediction of Harmonic Output

Since the development of the high-frequency power transistor, r.f. power amplifiers and harmonic generators have come into use. A typical tuned-input, tuned-output type is shown in Fig. 5. The circuit design for such an arrangement is rather more involved than for the valve harmonic generator since it is necessary, for example, to match the input of the transistor to the source at the fundamental frequency.

There is no written evidence to suggest that any attempt has been made to predict the power output of a transistor frequency multiplier or power amplifier.

Table 5

Variation of errors in predicted grid currents

Design	Power series		Square law		Triangular wave	
	% Error in $I_{g(d.c.)}$	% Error in $I_{g(max)}$	% Error in $I_{g(d.c.)}$	% Error in $I_{g(max)}$	% Error in $I_{g(d.c.)}$	% Error in $I_{g(max)}$
Original	+ 7·04	+ 12·29	+ 19·86	+ 20·94	+ 12·81	+ 13·18
Redrawn	+ 2·65	+ 7·54	+ 14·94	+ 15·84	+ 8·19	+ 8·42

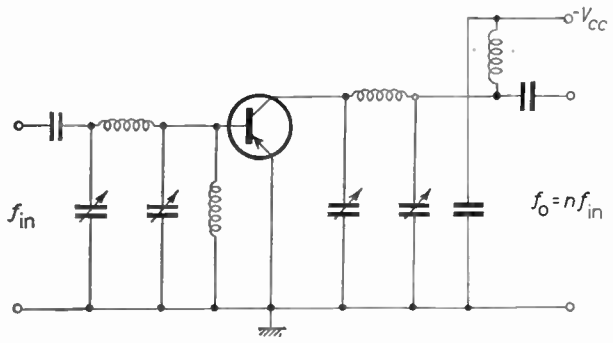

Fig. 5. Simple transistor harmonic generator.

The point-by-point method will be applicable, requiring the emitter-base diode characteristic and the emitter-current/collector-current curve of the transistor, as shown in Fig. 6. For a given bias, the pulse of emitter current may be derived from the I_E/V_{EB} curve and hence the collector-current pulse from the I_E/I_C relationship. The harmonic and direct components of the approximate current pulse may then be extracted by a graphical Fourier analysis.

It would be of practical interest to determine the accuracy of the power series method, especially in cases where the transistor is overdriven and produces a flat-topped collector current pulse.

Work also remains to be done in examining a simpler analytical approach, perhaps of a nature similar to the linear-law method.

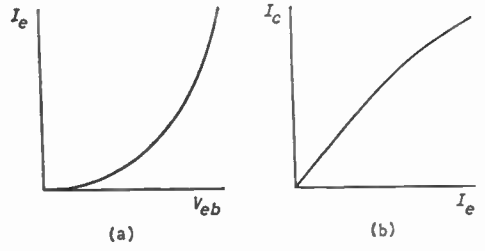

Fig. 6. Transistor characteristics.
(a) Emitter-base diode characteristic.
(b) Collector-current/emitter-current characteristic.

10. Conclusions

On the results obtained from 50 anode-current and 25 grid-current designs on a number of triodes used as harmonic generators up to fifth order, it was concluded that existing analytical methods of predetermining these current components were not dependable, giving errors of the order of 25% in both cases.

A method, based on a power series representation of the particular mutual dynamic characteristic of the valve used in the harmonic generator, gave errors of less than 6% in the components of anode current and less than 13% in the case of grid currents.

In the prediction of the grid-current components the point-by-point method was unreliable in some instances and measurements of absolute accuracy were impossible from paper designs alone. The power series method was, however, more accurate than any other analytical method irrespective of this lack of absolute accuracy.

The power series method may also be applied to pentodes and beam tetrodes to calculate anode, control-grid and screen-grid currents.

Now that high-frequency power transistors are available analytical methods for predicting the harmonic output of a transistor harmonic generator are required.

11. References and Bibliography

1. D. C. Prince, "Vacuum tube as a power amplifier", *Proc. Inst. Radio Engrs*, **11**, pp. 275–313, June 1923.
2. S. M. Ali, "Frequency multiplication and harmonic generation in thermionic valves", to be published.
3. R. H. Brown, "Harmonic amplifier design", *Proc. I.R.E.*, **35**, pp. 771–7, August 1947.
4. J. Marique, "Note sur le calcul des étages multiplicateurs de fréquence à triodes", *L'Onde Electrique*, **8**, pp. 1–19, January 1929.
5. Y. Kusunose, "Calculation of characteristics and the design of triodes," *Proc. I.R.E.*, **17**, pp. 1706–49, October 1929.
6. W. G. Wagener, "Simplified methods for computing performance of transmitting tubes", *Proc. I.R.E.*, **25**, pp. 47–77, January 1937.
7. W. L. Everitt, "Optimum operating conditions for class-C amplifiers", *Proc. I.R.E.*, **22**, pp. 152–76, February 1934.
8. F. E. Terman and W. C. Roake, "Calculation and design of class-C amplifiers", *Proc. I.R.E.*, **24**, pp. 621–32, April 1936.
9. H. J. Scott and L. J. Black, "Harmonic generation", *Proc. I.R.E.*, **26**, pp. 449–68, April 1938.
10. H. Uchida, "Analysis of frequency multipliers", *Electrotech. J. Inst. Elect. Engrs Japan*, **3**, pp. 156–64, July 1939.
11. F. E. Terman, "Analysis and design of harmonic generators", *Trans. Amer. Inst. Elect. Engrs*, **57**, pp. 640–4, November 1938.
12. F. M. Kósa, "H.f. power amplifiers", *Wireless Engineer*, **14**, pp. 647–56, December 1937.
13. G. W. O. Howe, "The optimum conditions for class-C operation", *Wireless Engineer*, **20**, pp. 267–72, June 1943.
14. Y. Fukuta, "Harmonic analysis of the plate current of a triode power amplifier", *Nippon Elect. Commun. Engng*, **10**, pp. 187–8, April 1938.
15. P. Baudoux, "Caractéristiques généralisées des amplificateurs non linéaires à triode", *L'Onde Electrique*, **16**, pp. 611–30, November 1937 and pp. 666–80, December 1937.

16. R. Mesny, "Au sujet de la multiplication des fréquences par les triodes", *L'Onde Electrique*, 9, pp. 18–22, January 1930.

17. B. P. Asséef, "Note sur le calcul d'un doubleur de fréquence", *L'Onde Electrique*. 10, pp. 36–47, January 1931,

18. M. Meloni, "Sul funzionamento dei triplicatori di frequenza a triodi", *Alta Frequenza*, 4, pp. 389–405, August 1935.

19. C. Matteini, "Conversione di potenza mezzo du triode", *Alta Frequenza*, 5, pp. 68–103 and pp. 180–207, February and March 1936.

20. G. L. Edgecombe and J. C. Downes, "Application of the Radiotron type 807 valve as a frequency doubler", *A.W.A. Tech. Rev.*, 7, pp. 251–79, 1947.

21. C. K. Steadman, "A thermionic frequency doubler", *Physics*, 2, pp. 42–47, January 1932.

22. D. C. Espley, "The calculation of harmonic production in thermionic valves with resistive loads", *Proc. I.R.E.*, 21, pp. 1439–46, October 1933.

23. F. E. Terman, "Radio and Electronic Engineering", pp. 205–206 and pp. 327–329, 4th Edn. (McGraw-Hill, New York, 1955.)

24. H. P. Thomas, "Determination of grid driving power in r.f. power amplifiers", *Proc. I.R.E.*, 21, pp. 1134–41, August 1933.

25. E. E. Spitzer, "Grid losses in power amplifiers", *Proc. I.R.E.*, 17, pp. 985–1005, June 1929.

26. W. L. Everitt and K. Spangenberg, "Grid current flow as a factor in the design of vacuum tube power amplifiers", *Proc. I.R.E.*, 26, pp. 612–39, May 1938.

12. Appendix

12.1. *To Find an Expression for E_g*

The grid-bias voltage, E_g, may be calculated on the assumption that the static characteristics are of the form

$$i_a = f(\mu V_g + V_a)^a$$

substituting

$$V_g = V_{g(max)} \cos \omega t - E_g$$

$$V_a = E_B - V_{a(max)} \cos n\omega t$$

$$i_a = f[\mu(V_{g(max)} \cos \omega t - E_g) + E_B - V_{a(max)} \cos n\omega t]^a$$

At cut-off, $i_a = 0$ and $\omega t = \theta/2$.

Putting $V_{g(max)} = E_g + E_{g(max)}$

$$\mu E_g \cos \theta/2 + \mu E_{g(max)} \cos \theta/2 - \mu E_g + E_B - V_{a(max)} \cos n\theta/2 = 0$$

giving

$$E_g = \frac{E_{g(max)} \cos \theta/2}{(1 - \cos \theta/2)} + \frac{E_B - V_{a(max)} \cos n\theta/2}{\mu(1 - \cos \theta/2)}$$

12.2. *Design Example*

The following design example is given in order to demonstrate the use of the power series method:

To design a third harmonic generator using valve type DET 17.

The maximum value of the anode voltage, E_B, as laid down in the manufacturer's data is 2000 V; this will be the value used in the design. The peak value of the anode voltage, $V_{a(max)}$ will be taken as $0{\cdot}8E_B$, i.e. $V_{a(max)} = 1600$ V. The angle of anode current flow is chosen as 90 deg and the bias voltage calculated to be 478 V.

The first step is to choose the particular points: from reasons given in Section 4 they will be taken as $V_1 = +75$ V, $V_2 = +50$ V, $V_3 = -100$ V and the zero grid-voltage point. The instantaneous anode currents corresponding to these instantaneous grid voltages are derived using eqn. (11). This derivation may be carried out as shown below in Table 6.

The power series constants are calculated from eqns. (8), (9) and (10) to be

$$k''' = -0{\cdot}000\ 126\ 9$$

$$k'' = -0{\cdot}012\ 68$$

and $$k' = 2{\cdot}851$$

Therefore

$$i_a = 305 + 2{\cdot}851 V_g - 0{\cdot}012\ 68 V_g^2 - 0{\cdot}000\ 126\ 9 V_g^3$$

From eqns. (16), (17) and (18)

$$I'_{ap} = 305 + 2{\cdot}851 \times 75 = 518{\cdot}8 \text{ mA}$$

$$I''_{ap} = -0{\cdot}012\ 68 \times 75^2 = -71{\cdot}33 \text{ mA}$$

$$I'''_{ap} = -0{\cdot}000\ 126\ 9 \times 75^3 = -53{\cdot}54 \text{ mA}$$

Equation (19) gives:

$$I_{ap} = 518{\cdot}8 - 71{\cdot}33 - 53{\cdot}54$$

$$= 393{\cdot}93 \text{ mA}$$

(cf. 394·0 mA read from the valve characteristics at $E_{g(max)} = 75$ V and $V_0 = 400$ V)

$$E'_{co} = \frac{-305}{2{\cdot}851} = -107$$

Table 6

Calculation of particular points

V_{gr}	$\omega t = \phi°$	$3\omega t = 3\phi°$	$V_{a(max)} \cos 3\omega t$	V_{ar}	i_a (mA)
$V_1 = +75$	0	0	1600	400	$394 = i_1$
$V_2 = +50$	17° 12′	51° 36′	994	1006	$400 = i_2$
0	30° 12′	90° 36′	−17	2017	$305 = i_0$
$V_3 = -100$	46° 54′	140° 42′	−1237	3237	$20 = i_3$

Therefore in eqn. (15)

$$\cos\frac{\theta'}{2} = \frac{478-107}{553} = \frac{371}{553}$$

$$\theta' = 95^\circ\ 36'$$

$$\theta'' = \theta''' = \theta_g = 2\cos^{-1}\frac{E_g}{V_{g(\max)}}$$

$$= 2\cos^{-1}\frac{478}{553}$$

$$= 60^\circ\ 24'$$

From Tables 1, 2 and 3

$\alpha' = 0{\cdot}173\ 0$ $\quad \beta_3' = 0{\cdot}176\ 5$ at $\theta = 95^\circ\ 36'$

$\alpha'' = 0{\cdot}087\ 5$ $\quad \beta_3'' = 0{\cdot}149\ 0$ at $\theta = 60^\circ\ 24'$

$\alpha''' = 0{\cdot}075\ 5$ $\quad \beta_3''' = 0{\cdot}132\ 0$ at $\theta = 60^\circ\ 24'$

Equations (20), (21) and (22) give:

$$I'_{a(\text{d.c.})} = 0{\cdot}173\ 0 \times 518{\cdot}8 = 89{\cdot}70 \text{ mA}$$

$$I''_{a(\text{d.c.})} = -0{\cdot}087\ 5 \times 71{\cdot}33 = -6{\cdot}24 \text{ mA}$$

$$I'''_{a(\text{d.c.})} = -0{\cdot}075\ 5 \times 53{\cdot}54 = -4{\cdot}04 \text{ mA}$$

and from eqn. (23)

$$I_{a(\text{d.c.})} = 89{\cdot}70 - 6{\cdot}24 - 4{\cdot}04$$

$$= 79{\cdot}42 \text{ mA}$$

Equations (24), (25) and (26) give:

$$I'_{a3(\max)} = 0{\cdot}176\ 5 \times 518{\cdot}8 = 91{\cdot}50 \text{ mA}$$

$$I''_{a3(\max)} = -0{\cdot}149\ 0 \times 71{\cdot}33 = -10{\cdot}62 \text{ mA}$$

$$I'''_{a3(\max)} = -0{\cdot}132\ 0 \times 53{\cdot}54 = -7{\cdot}06 \text{ mA}$$

and from eqn. (27)

$$I_{a3(\max)} = 91{\cdot}50 - 10{\cdot}62 - 7{\cdot}06$$

$$= 73{\cdot}82 \text{ mA}$$

The point-by-point method gives:

$$I_{a(\text{d.c.})} = 78{\cdot}57 \text{ mA and } I_{a3(\max)} = 74{\cdot}76 \text{ mA}$$

Therefore

$$\%\text{ error in } I_{a(\text{d.c.})} = +1{\cdot}08\%$$

and $$\%\text{ error in } I_{a3(\max)} = -1{\cdot}26\%$$

The $\frac{3}{2}$ law method gives:

$$\%\text{ error in } I_{a(\text{d.c.})} = -13{\cdot}62\%$$

$$\%\text{ error in } I_{a3(\max)} = +0{\cdot}35\%$$

and the linear-law method gives:

$$\%\text{ error in } I_{a(\text{d.c.})} = -9{\cdot}87\%$$

$$\%\text{ error in } I_{a3(\max)} = -2{\cdot}90\%$$

Manuscript first received by the Institution on 20th May 1964 and in final form on 14th August 1964. (Paper No. 948.)

U.D.C. 629.135/6: 681.32

A Special-purpose Digital Computer for Flight Simulation

By

D. J. SYKES, B.Sc.†

Presented at the Joint Symposium of the Radar and Navigational Aids and Computer Groups of the Institution and the Computer Design Group of the Institution of Electrical Engineers on "Simulators for Training Purposes" held in London on 21st April 1964.

Summary: The advantages of digital techniques in simulators are stated and computer requirements considered in relation to the simulator to be controlled. The computer described employs core and drum stores. Its output provides both arithmetical and Boolean functions. The system has been designed for programming by non-specialists.

1. Introduction

Electronic flight simulators for crew training have traditionally been based on analogue techniques, the computing equipment being divided into four main areas:

1. Aerodynamics, flight instruments and autopilot;
2. Engine performance and instrumentation;
3. Accessory systems: hydraulics, fuel, electrics, etc.;
4. Navigational aids.

A typical simulator would include some 700 operational amplifiers, 80 servos, 600 non-linear potentiometers, 10 000 precision resistors and 600 relays.

Computing accuracy has not been a major problem except in the navigational aids, and the ease of the dynamic solution of the flight equations by analogue methods has more than compensated for the marginal accuracy obtained. However, simulation of navigational aids has always posed a problem of accuracy and recently digital techniques have been applied in this area alone to overcome the difficulty.

By far the largest disadvantage of an analogue simulator is that the resistor and capacitor networks, relay systems and non-linear potentiometers must be designed and built individually for each type of aircraft to be simulated, and this involves 'freezing' the data several months prior to the customer's acceptance in order to meet the drawing and manufacturing schedule. In many cases this means that the design is fixed before the aircraft has flown and an extensive program of equipment modifications must be carried out when flight-test data become available.

With a fully digital approach, the same computer can be used for simulating a variety of aircraft, the machine being programmed to represent the data concerned. Up-dating the program can be done continuously and changes can be fed into the computer in a matter of minutes. With the digital computer there is no problem with accuracy, the only limit on this being set by the electromechanical read-out devices for which figures of 0·25% to 2% are typical but the errors are confined to each individual channel. In a large scale analogue system there are cumulative computing errors due to drift and component tolerances of between 1% and 5% in addition to the errors in the read-out devices. Furthermore a great deal of maintenance effort is necessary to avoid deterioration of performance of the analogue system whereas the digital computer will provide consistent results over an indefinite period. The improved reliability of digital machines is such as to give an availability of between 98% and 99%. Fault diagnosis is facilitated by test programs; an equivalent procedure in an analogue machine is completely impracticable.

A large amount of data describing radio transmitting stations is easily stored in a digital computer thus avoiding the constant setting in of this information by an operator.

Other benefits of the digital computer are a saving of some 40% in floor area, power consumption and heat dissipation.

2. The Necessity for a Special-purpose Computer

The digital computer for this application must have sufficient capacity to store the large number of program instructions and constants for the entire simulator, and sufficient speed and accuracy to produce a stable solution of the equations and to give smoothly changing outputs with negligible lag. The computer should also be capable of handling large numbers of

† General Precision Systems Ltd., Aylesbury, Buckinghamshire.

inputs and outputs, both analogue and digital so that the exercise of coupling the machine into the simulator is minimized.

Special facilities are necessary for efficient simulation of aircraft electrical and hydraulic systems involving the programming of logical operations with single bits and direct addressing of individual bits. Aerodynamic and engine equations contain many non-linear functions and in order to avoid time-consuming 'table look-up' methods, some special hardware is essential. In order to decide which ground transmitter (if any) should be received by each of the aircraft receivers at any instant, many comparisons of frequency and position have to be performed. Here again, special purpose equipment can be used to advantage.

All these facts indicate that a general-purpose computer would not be an economic proposition for a training simulator although certain g.p. computers could be very useful in research applications. A further disadvantage of such a machine is that a large amount of skill and experience is required in programming, so precluding the possibility of simulator engineers writing their own programs (programming languages would be of only limited use in this field).

In order to overcome these problems a special-purpose computer, the Mark 1, was developed and is currently being used to simulate the Boeing *727*, *707*, the *C141*, the *C135B* aircraft and the *Gemini* spacecraft in the U.S.A., and the *TSR2* in Great Britain.

3. Incorporation of the Mark 1 Computer into the Simulator

Figure 1 shows the computer in relation to the remainder of the simulator. Analogue voltages from the cockpit controls are fed into the machine together with Boolean inputs from the cockpit switches, circuit breakers, instructor's switches, etc. The effect of these in the simulator is governed entirely by the program fed into the computer and it is thus possible to alter the function of any input from the cockpit without changing any wiring. The computer outputs are both analogue and Boolean; the former are used for driving the cockpit instruments, control loading, motion and audio equipment whereas the latter provide switching control of lamps, flags, etc.

It is necessary to provide amplifiers and servo units to drive the instruments but it should be emphasized that this analogue equipment is solely for matching external equipment to the computer and not for further computation. This permits a high degree of standardization of analogue modules. If a visual system is fitted to the simulator, then analogue outputs are used to position servos on the television camera and associated optical systems.

4. The Mark 1 Computer

The computer can be divided into the following sections as shown in Fig. 2:

1. Working store;
2. Input/output sections;

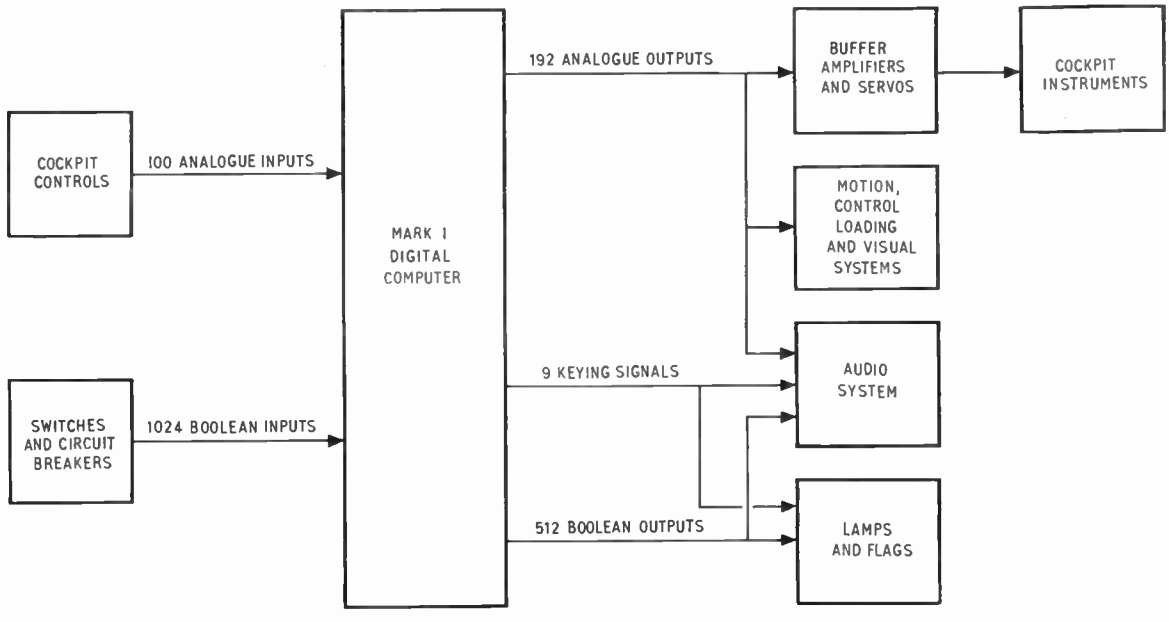

Fig. 1. Digital flight simulator.

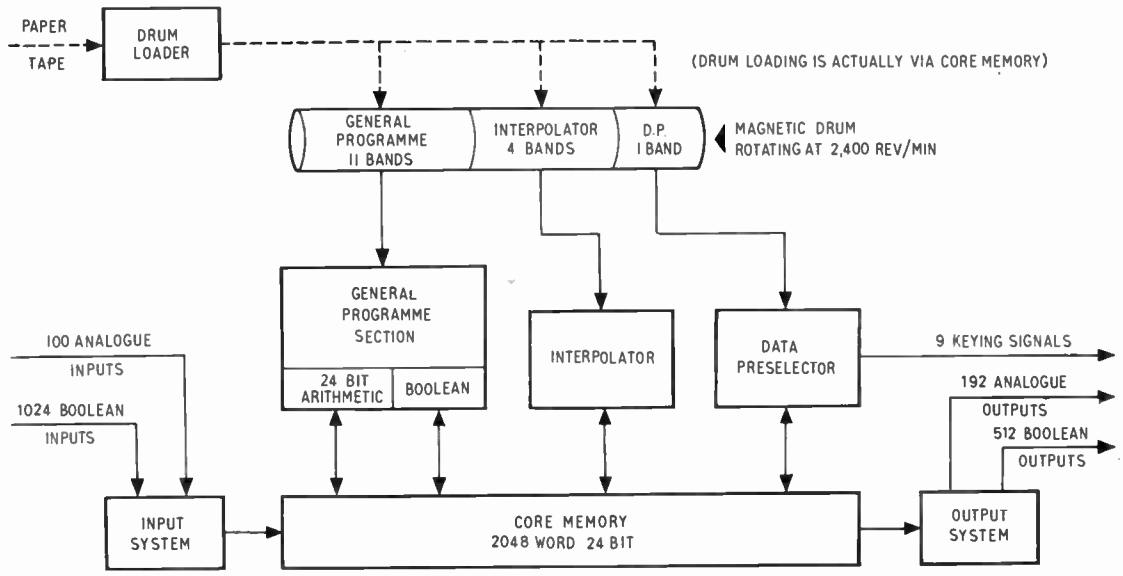

Fig. 2. Block diagram of the Mark 1 computer.

3. Program and data store;
4. Computing sections—all working simultaneously;
   (*a*) General program section for solving arithmetic, differential and logical equations for all areas of simulation;
   (*b*) Interpolator for handling the numerous non-linear aerodynamic and engine functions;
   (*c*) Data preselector for selecting the appropriate radio facilities.

(*b*) and (*c*) relieve the general program section of a vast number of time-consuming operations.

4.1. *Working Store*

This is a 2048-word, 24-bit core store with a 5-microsecond cycle time, and acts as a buffer between the various computing sections and the input/output sections. This necessitates the use of a priority system to control the access of each section. A special facility is provided for addressing any single bit in a particular section of the store.

4.2. *Input/Output System*

4.2.1. Analogue inputs

100 analogue channels are all scanned 20 times a second, converted to 14-bit binary numbers and placed in specific core-store locations.

4.2.2. Boolean inputs

1024 switches or other on/off devices are all interrogated 20 times a second in groups of 16 and their states stored as 16-bit words.

4.2.3. Analogue outputs

192 direct voltages are produced which are the equivalent of 192 words in specific core-store locations. All channels are read out 80 times a second.

4.2.4. Boolean outputs

512 relays whose contacts are available for external use are set in one state or the other according to whether the appropriate bit in the core store is a '0' or a '1'. The relay states are updated 10 times every second.

4.3. *Program and Data Store*

A magnetic drum with a capacity of approximately one million bits and rotating at 40 revolutions per second is used to store all program instructions and constants. There are 4096 bits on each of the 240 tracks, giving a cell-time of 6 μs and a corresponding clock frequency of 164 kc/s. No changes are made to the stored information during computation so there is no danger of inadvertent modification of the program, since in order to write on the drum, the computer must be stopped and a special mode selected. The program is prepared on punched paper tape and the entire drum can be loaded in six minutes but small program changes can be written on the drum in a matter of seconds. The core store is used as a buffer during the transfer from the tape to drum. The drum is used by the three computing sections and its capacity is divided as follows.

4.3.1. General program

176 of the tracks are grouped into 11 bands of 16 and these 16 tracks are read in parallel. Only one band

is read at a time but the order of reading the 11 bands is interlaced to give different up-dating rates for dealing with areas of simulation having different rates of change. A typical pattern would be as follows:

Fast: one band read every 50 ms.

Medium: two bands each read every 200 ms.

Slow: eight bands each read every 800 ms.

Other interlace patterns can be selected to give the best ratio of iteration rate to capacity for the simulator in question.

4.3.2. Interpolator

Four bands each of 4096, 11-bit words are read sequentially which results in a rate of up-dating of 10 times/second for all functions.

The capacity of the four bands is adequate for storing 800 single variable functions.

4.3.3. Data preselector

One band of 4096, 20-bit words is read every revolution. This band capacity is sufficient to store complete data, including call letters, for 350 transmitting facilities of five types (i.e., l.f., v.h.f., middle, outer and airways markers).

4.4. *General Program Section*

This is divided into two units, one for arithmetic functions and the other for Boolean functions.

4.4.1. 24-bit parallel arithmetic unit

This executes the arithmetic instructions in the order in which they are read from the drum. The current values of the variables are obtained from the core store and the results of the computation are placed in the core store.

The basic instruction time is 6 μs including access and the multiply time is 30 μs including access. There are 21 instruction types each consisting of a 5-bit code and an 11-bit address. An addressable salvage register is provided which is used to minimize core access requirements.

4.4.2. Boolean unit

This is used for performing operations in the simulator to deal with the aircraft switching systems, etc. There are five instruction types and the address used with these instructions specifies a single bit in the core memory or one of four salvage registers. It is possible to control the arithmetic section from the Boolean section and generate Boolean functions as a result of arithmetic operations.

4.5. *Interpolator* (Fig. 3)

Non-linear functions are stored on the drum as the ordinates at nine breakpoints which are equispaced along the abscissa. The current value of the variable is obtained from the core store, a linear interpolation carried out between the appropriate breakpoints, and the result placed in the core store. The relevant addresses are written on the drum before and after the curve data. The interpolator can deal with functions of one, two or three variables and an indexing system is provided which enables the same curve data to be used for four independent sets of up to three variables.

4.6. *Data Preselector*

Each receiver frequency is compared in turn with all transmitter frequencies and at the same time the aircraft latitude and longitude are compared with the corresponding figures for all transmitters. If a station is within prescribed limits for all three quantities, the complete data describing that station are transferred from the drum to specific core-store locations where it can be used by the general program. Also in this section is a 'keying function' generator which produces d.c. keying signals corresponding to the call letters of the preselected stations.

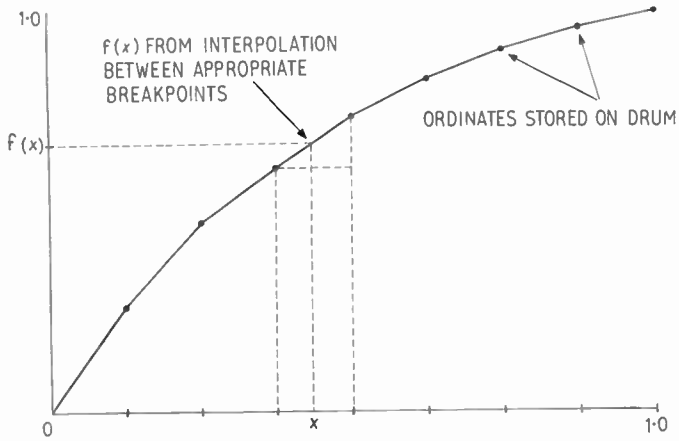

Fig. 3. Operation of interpolator.

5. Programming the Mark 1 Computer

From the outset, the Mark 1 computer was designed for programming by people who are not specialist programmers. Engineers with an analogue background but who are familiar with the particular problems of flight simulation are finding it an easy matter to adapt themselves to the digital approach. Customers' maintenance technicians also can carry out program modifications without having to bring in specialist programmers.

Since the program is lengthy, many engineers are involved in its preparation, and the method of program storage used means that work can be carried out independently without mutual interference. With a general-purpose computer there is always a danger of a variable being stored inadvertently in an instruction location which could then cause the subsequent program to get hopelessly out of sequence.

In the Mark 1 computer there is no need for the programmer to concern himself with the transfer of data in and out of the computer; this is all done automatically by the priority system. Similarly there is no need for 'administrative routines'; all the capacity of the program store can be used for solving the actual equations involved.

All arithmetic programming is performed by only 21 types of instruction and integration is achieved simply by adding a computed increment to the existing value of the integral. The fixed interval between readings of a given instruction on a particular band obviates the necessity for computing increments of time during the integration process. The fast band rate of 20 iterations per second permits the use of simple integration formulæ for obtaining stable solutions for the fastest areas of the flight dynamics with accuracies in damping and frequency better than can be achieved by analogue methods.

Aircraft switching systems are programmed by writing the logical equation for the system and arranging a series of Boolean instructions (AND, OR, INVERT) to solve the equation.

Branching in the general program section is achieved by skipping a group of instructions.

The interpolator does not require programming as such but merely the preparation of curve data in the form of nine ordinates.

Some function shapes may not lend themselves readily to representation with equispaced breakpoints and in such cases the function has to be split and considered as two more separate functions.

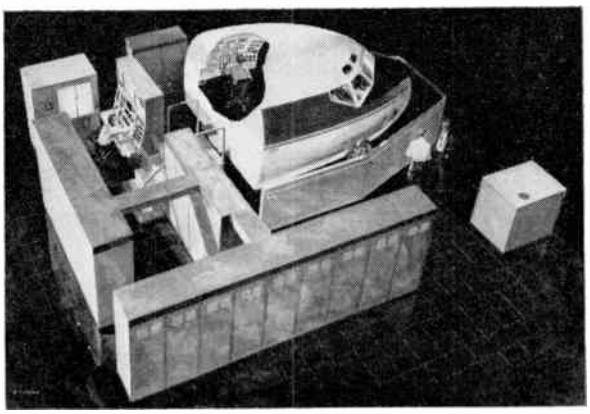

Fig. 4. Artist's impression of digital flight simulator for Boeing *707*.

Data preparation for the radio aids consists solely in the assignment of limits to the various facilities, the representation of station details in a prescribed form and the coding of the station call letters as pseudo-binary numbers.

6. Tape Preparation Unit

To provide a high degree of flexibility in the Mark 1 computer, convenient methods are provided for tape preparation. The program is first punched on standard cards and then transferred to paper tape so as to give flexibility combined with a high speed of loading into the computer. It is also possible to copy tapes or to modify them by keyboard input. These facilities are contained in the tape preparation unit which also can produce a hard copy print-out of the data on the tape.

7. The Mark 2 Computer

The Mark 2 computer was developed from the Mark 1 to provide double-speed operation but has the same actual storage capacity. An improved order code, however, results in a greater effective capacity being achieved. The extra speed, although not necessary for flight simulators for training purposes, does find application in research simulators, particularly for spacecraft.

8. Conclusions

The advantages of digital rather than analogue computation for flight simulation are:

(*a*) Flexibility for ease of up-dating.

(*b*) Improved accuracy.

(*c*) Repeatable results over an indefinite period.

(*d*) Improved reliability and ease of maintenance.

(*e*) Ease of storage of radio aids data.

(*f*) Reduced floor area, power consumption and heat dissipation.

The advantages of the special-purpose Mark I computer over a similarly priced general-purpose computer are:

(*a*) High overall effective speed by virtue of three computing sections operating simultaneously.

(*b*) Large program capacity.

(*c*) Large numbers of input and output channels, both analogue and digital.

(*d*) Separate storage for program and data.

(*e*) Ease of programming, particularly for integration and interpolation.

(*f*) Program instructions cannot be inadvertently overwritten.

(*g*) Economic handling of Boolean functions.

The outstanding advantages of digital computation over analogue for flight simulation will result in a marked swing towards a fully digital approach over the next few years. The initial cost of a digital installation may be some 20% higher than a corresponding analogue one, but this will be offset by reduced maintenance costs, a saving in 'down-time' for modifications and also by the fact that the computer will still be of further use at the end of the life of the original simulator. It is not claimed that these special-purpose computers have introduced any novel basic techniques, but that they offer an economic solution for this large-scale real-time application.

9. Acknowledgments

The author wishes to thank the directors of General Precision Systems Limited, for permission to publish this paper and to acknowledge the work done by the staff of the Link Group of General Precision Inc., Binghampton, New York, in particular under Dr. John M. Hunt, Technical Vice-President.

Manuscript first received by the Institution on 21st April 1964 and in final form on 15th September 1964. (Paper No. 949/C74.)

U.D.C. 621.391.821

Measurements of Atmospheric Noise Levels

By

OLU IBUKUN, Ph.D., D.I.C., B.Sc.(Eng.) (*Associate Member*) †

Summary: Two separate standard equipments have been simultaneously used for the measurement of atmospheric radio noise parameters at Ibadan (7°N, 6°E) during the spring and summer seasons of 1958 to 1961. The first was designed by the Department of Scientific and Industrial Research of Great Britain (D.S.I.R.) for obtaining, by manual operation, the amplitude probability distribution of noise envelopes from which noise parameters may be derived. The second equipment is an automatic noise recorder (ARN-2) designed by the Central Radio Propagation Laboratories of the United States of America (C.R.P.L.). Values of atmospheric noise power and other noise parameters have been directly obtained from the equipment.

It is shown that both equipments can be operated to provide consistent and reliable values of atmospheric noise parameters in a tropical area. Comparisons of the results of noise power and r.m.s./average ratios at chosen frequencies (113 kc/s, 11 Mc/s and 20 Mc/s) indicate that the discrepancies are significant only at 20 Mc/s and that at this frequency station interference is the major source of error on the C.R.P.L. equipment.

1. Introduction

Since about 1922, measurements of atmospheric radio noise have been made at a number of locations throughout the world. Although early measurements made in England and the North-Eastern part of the United States between 1923 and 1932 were confined to low frequencies in the range 15 to 60 kc/s, the radio frequency range from 15 kc/s to 20 Mc/s has been covered in more recent times. The early measurements were surveyed in 1947 by Thomas and Burgess,[1] who found that there had been no correlation between existing measurements at different places. It was difficult to make comparisons between results and deductions at one place with those of another place because different methods were used by different workers. As a result of various measurements made before 1952, it was realized that owing to the statistical nature of atmospheric noise, it could not be described adequately by one single parameter like average or root mean square voltage. In 1952, Hoff and Johnson[2] described a method and equipment suitable for the measurement of the amplitude probability distribution of noise. Yuhara, Ishida and Higashimura,[3] in 1956, also described a simple equipment for the measurement of the amplitude probability distribution (a.p.d.) of noise. In the same year, Horner and Harwood[4] of the Department of Scientific and Industrial Research, England (D.S.I.R.) were the first to describe an elaborate method for the measurement of a.p.d. but within the range 10–35 kc/s only. The D.S.I.R. later developed another noise measuring equipment[5] operating on a different principle from the former and suitable for the frequency range 15 kc/s to 20 Mc/s.

The latter D.S.I.R. equipment has been used in Nigeria to measure certain parameters of atmospheric radio noise between 1958 and 1961. The system of measurement has been based on taking the percentage occupation time for varying threshold levels and from the resulting cumulative probability curve, deductions were made of the average, the root mean square and the r.m.s. to average ratio of the envelope voltage.

An alternative system of noise measurement was developed by the Central Radio Propagation Laboratory (C.R.P.L.) of the United States of America. During and since the International Geophysical Year, a network of noise recording stations using this system has been provided. The equipment operates on eight chosen frequencies in radio frequency bands from 51 kc/s to 20 Mc/s over a narrow power bandwidth of 200 c/s. Measurements of noise power, the deviation of average voltage in decibels below the mean power, and deviation of the average logarithm of voltage below the mean power have been obtained from similar equipment at Ibadan between 1958 and 1961.

The two equipments were installed about 190 m apart on a wide open site at Ibadan, far from known man-made noise sources. Values of noise parameters deduced from the two types of equipment are compared with a view to the possibility of interchanging the results from one type of equipment with those from the other.

† Department of Physics, University of Ibadan, Nigeria.

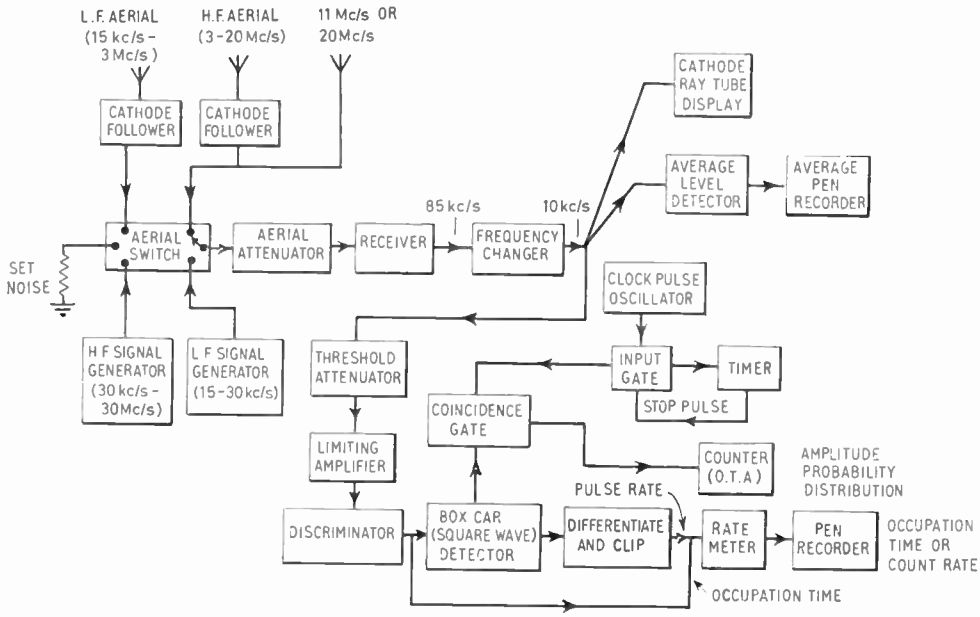

Fig. 1. Block diagram of D.S.I.R. noise equipment.

2. The D.S.I.R. Equipment

2.1. *Description of Equipment*

This equipment, developed by the Radio Research Station, Slough, England, has been described in detail by Clarke[5] and also by Harwood and Nicolson.[6] A block diagram of the whole equipment is shown in Fig. 1. The procedure followed in taking observations was also similar to the techniques of measurement already described by Clarke[5] for the plotting of the amplitude probability distribution curves. A low-frequency aerial consisting of a vertical mast about 30 ft long is used to cover the kilocycles range. Two separate aerials were used for 11 Mc/s and 20 Mc/s; the aerials are approximately one quarter wavelength and use an earth mat consisting of eight 50 ft radial wires. The aerials are omnidirectional and are connected to a heterodyne receiver with intermediate frequency output at 85 kc/s, and then to a frequency changer with output at 10 kc/s in a 3-dB bandwidth of about 340 c/s. The signal is then applied to an amplitude discriminator through an attenuator and limiting amplifier. The discriminator is operated at a fixed threshold while the signal amplitude was varied by the threshold attenuator. The discriminator output is fed to a square wave detector where parts of the noise envelope exceeding a set threshold are converted to rectangular pulses, passed through a coincidence gate and used to control a train of clock pulses. The number of clock pulses, which succeed in passing through the coincidence gate and recorded on the counter channel, is compared with the number in a fixed sample time and recorded on the timer channel. The ratio of these two readings which is the percentage of the time the noise envelope is above the threshold, is the percentage occupation time. A plot of this parameter as a function of threshold voltage gives the cumulative amplitude probability distribution.

2.2. *Operational Procedure*

The receiver was tuned to a clear channel and with threshold attenuator at zero, the aerial attenuator (in 10 dB and 1 dB steps up to 90 dB) was set at a value to produce a percentage occupation time between 90% and 99%. A sample time of 30 seconds was used at these lower thresholds. The aerial attenuator was then varied in 10 dB steps using sample times of 50 seconds between 10% and 1%; 100 seconds between 1% and 0·01% and 3 × 100 seconds (median of three 100 seconds sample time) for values between 0·01% and 0·0001%. The threshold attenuator with 2 dB steps was used only when the aerial attenuation was insufficient. This modification in procedure was made at Ibadan to prevent the effects of overloading since, in the tropics, the noise envelopes have high peaks, especially at the lower frequencies.

One a.p.d. run normally took about 20 minutes, although only about 9 minutes were required for percentages above 0·01%. Special care was taken at the higher thresholds since that portion of the a.p.d. curve has greater effect on the derived power.

Results obtained in this way for a tropical area have already been discussed by the author.[7]

2.3. *Calibration*

Measurements made on the equipment had to be related to actual field strength by calibrating in terms of a signal generator voltage corresponding to a known threshold voltage.

The noise field at the output of the receiver will be different from that at the aerial as a result of losses in the cables and mismatch between the aerial and the receiver. A fixed factor for each frequency was then applied to relate generator inputs to equivalent aerial field strengths, in decibels relative to 1 μV/m. Checks of cable attenuation and cathode follower gains, where used, were made from time to time.

2.4. *Deductions from A.P.D.*

The instantaneous noise voltage induced in a receiving antenna and also the voltage envelope at the detector output and measured as already described will occur in a random fashion. The probability that the value of the variate (voltage of noise envelope) will fall within an infinitesimal interval v to $(v+\mathrm{d}v)$ for a sample of noise can be expressed by $P(v)\mathrm{d}v$

where $P(v)\mathrm{d}v$ is the probability of occurrence,

and $P(v)$ is the probability density function of various values of voltage v.

Assuming that, during the usual hourly period of measurement, the probability density of the noise ensemble is the same no matter at what instant observations are made, then the noise ensemble may be said to be stationary; and the outcome is a stationary random process.

The rth moment of such distribution is given by

$$M_r = \int_0^\infty v^r P(v)\,\mathrm{d}v$$

Cramer[8] has shown that, to describe such series completely, all the moments ($r = 1, 2, 3, \ldots$) should be specified. However, for most problems of communication, Lee[9] has indicated that first and second moments only, namely

$$M_1 = \int_0^\infty vP(v)\,\mathrm{d}v \quad \text{mean or average value } (\bar{v})$$

$$M_2 = \int_0^\infty v^2 P(v)\,\mathrm{d}v \quad \text{mean square value } (\overline{v^2})$$

yield adequate information.

M_1 is taken as signifying amplitude, M_2 power level indication and the ratio $(\sqrt{M_2})/M_1$ as specification of noise structure.

2.4.1. Evaluations of average and root mean square values

For the purpose of these measurements,

$$M_1 = \bar{v} = \int_0^\infty vP(v)\,\mathrm{d}v$$

Now $$P(v) = -\frac{\mathrm{d}}{\mathrm{d}v}Q(v)$$

where $Q(v)$ is the cumulative distribution function or the integrated probability density.

Therefore
$$\bar{v} = -\int_0^\infty v\frac{\mathrm{d}}{\mathrm{d}v}Q(v)\,\mathrm{d}v$$
$$= \int_{Q(v)=0}^{Q(v)=1} v\,\mathrm{d}Q(v) \qquad \ldots\ldots(1)$$

This is the area under the a.p.d. curve

Similarly
$$M_2 = \overline{v^2} = \int_0^\infty v^2 P(v)\,\mathrm{d}v$$
$$= \Big[v^2Q(v)\Big]_0^\infty + \int_0^\infty 2vQ(v)\,\mathrm{d}v$$
$$= 2\int_{Q(v)=1}^{Q(v)=0} vQ(v)\,\mathrm{d}v$$

Hence the mean square of the noise voltage

$$\overline{v^2} = 2\int_{Q(v)=1}^{Q(v)=0} vQ(v)\,\mathrm{d}v \qquad \ldots\ldots(2)$$

The relationships in equations (1) and (2) may be evaluated graphically, based on Dufton's formula for approximate integration.[10] For a smooth curve represented by $y = \mathrm{f}(x)$, the area A, enclosed between the x-axis, the curve and the ordinates defined by $x = a$ and $x = b$, is expressed by

$$A = \int_a^b \mathrm{f}(x)\,\mathrm{d}x \simeq \frac{b-a}{4}[\mathrm{f}(x_1)+\mathrm{f}(x_2)+\mathrm{f}(x_3)+\mathrm{f}(x_4)]$$

where
$$x_1 = a+\tfrac{1}{10}(b-a)$$
$$x_2 = a+\tfrac{4}{10}(b-a)$$
$$x_3 = a+\tfrac{6}{10}(b-a)$$
$$x_4 = a+\tfrac{9}{10}(b-a)$$

A typical a.p.d. curve is shown in Fig. 2 and is divided into decades. For a threshold voltage decade with limits at

$$a = 1, \quad b = 10,$$

then

$$x_1 = 1{\cdot}9, \quad x_2 = 4{\cdot}6, \quad x_3 = 6{\cdot}4, \quad x_4 = 9{\cdot}1.$$

Taking 1 volt as the reference, the area below the a.p.d. curve is the sum of all the areas in each decade relative to the reference. The average voltage as obtained from equation (1) is evaluated as in Table 1.

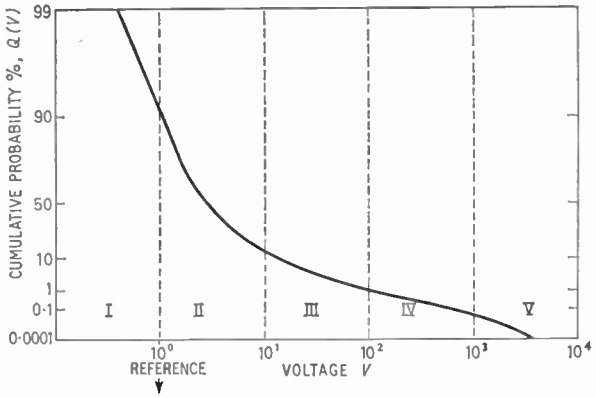

Fig. 2. Typical a.p.d. curve.

The procedure adopted for the mean square of noise envelope $\overline{v^2}$ is to obtain $vQ(v)$ for each decade, apply the appropriate decade factor and sum as indicated for the first few decades only in Table 2.

Then $$\overline{v^2} = \tfrac{9}{2}vQ(v)_{11}$$

Hence $\overline{v^2}$ in dB relative to reference

$$= 20\log_{10}[vQ(v)_{11}] + 13$$

The root mean square of noise voltage in dB relative to reference

$$= 10\log_{10}[vQ(v)_{11}] + 6{\cdot}5$$

2.4.2. Possible errors in the evaluations

Some of the errors in the evaluation of noise parameters as outlined above arise from errors in Dufton's approximate formula. It may be shown that the fractional error Δ in the approximate formula when a function $y = f(x^n)$ is integrated over the limits $x = a$ and $x = b$ is given by

$$\Delta = \delta - 1$$

where

$$\delta = \frac{(n+1)(b-a)}{4\times 10^n} - \frac{(9a+b)^n+(6a+4b)^n+(4a+6b)^n+(a+9b)^n}{(b^{n+1}-a^{n+1})}$$

A rigorous estimation of Δ can be made by summing the errors in each decade, taking limits as appropriate for individual decades. However, as an indication of the maximum possible error, a range of v from 0·01 to 10^5 relative the reference may be taken, i.e. $a = 0{\cdot}01$, $b = 10^5$ and $10a$ is then negligible with respect to b.

Then $$\delta = \frac{n+1}{4\times 10^n}(1+4^n+6^n+9^n)$$

The maximum percentage errors for given functions are tabulated below.

f(x)	x	x^2	x^3	x^4	x^5	x^6	..
Δ %	0	0·5	1·0	1·4	1·8	1·9	..

For polynomial expressions of the order n represented by $\sum_{r=1}^{r=n} k_r x_r$ the maximum percentage error

Table 1

Evaluation of Average of Noise Envelope

Decade Number	I	II	III	IV	V	..
Values of $Q(v)$	$Q(0{\cdot}19)$	$Q(1{\cdot}9)$	$Q(19)$	$Q(190)$	$Q(1900)$	..
	$Q(0{\cdot}46)$	$Q(4{\cdot}6)$	$Q(46)$	$Q(460)$	$Q(4600)$	..
	$Q(0{\cdot}64)$	$Q(6{\cdot}4)$	$Q(64)$	$Q(640)$	$Q(6400)$	..
	$Q(0{\cdot}91)$	$Q(9{\cdot}1)$	$Q(91)$	$Q(910)$	$Q(9100)$	..
First summation	$Q(v)_1$	$Q(v)_2$	$Q(v)_3$	$Q(v)_4$	$Q(v)_5$	..
Decade factors	10^{-1}	10^0	10^1	10^2	10^3	..
Second summation (first summation × decade factor)	$Q(v)_1^1$	$Q(v)_2^1$	$Q(v)_3^1$	$Q(v)_4^1$	$Q(v)_5^1$	..
Final summation	$Q(v)_{11} = Q(v)_1^1 + Q(v)_2^1 + Q(v)_3^1 + Q(v)_4^1 + Q(v)_5^1 + \ldots$					

$$\text{Total area} = \frac{10-1}{4}Q(v)_{11} = \tfrac{9}{4}Q(v)_{11}$$

Hence average voltage in dB relative to the reference

$$= 20\log_{10}Q(v)_{11} + 7$$

Table 2

Evaluation of Mean Square of Noise Envelope

Decade Number	I	II	III	IV	V
Values of $vQ(v)$ for each decade	0·19 Q(0·19) 0·46 Q(0·46) 0·64 Q(0·64) 0·91 Q(0·91)	1·9 Q(1·9) 4·6 Q(4·6) 6·4 Q(6·4) 9·1 Q(9·1)	19 Q(19) 46 Q(46) 64 Q(64) 91 Q(91)	190 Q(190) 460 Q(460) 640 Q(640) 910 Q(910)	.. ..
First summation	$v_1\ Q(v_1)$	$v_2\ Q(v_2)$	$v_3\ Q(v_3)$	$v_4\ Q(v_4)$	..
Decade factor	10^{-2}	10^0	10^2	10^4	..
Second summation (first summation × decade factor)	$v_1\ Q(v_1)_1$	$v_2\ Q(v_2)_1$	$v_3\ Q(v_3)_1$	$v_4\ Q(v_4)_1$	
Final summation	$vQ(v)_{11} = v_1Q(v_1)_1 + v_2Q(v_2)_1 + v_3Q(v_3)_1 + v_4Q(v_4)_1 + \ldots$				

could be the sum of the errors for individual terms. This could never exceed $\sum_{r=1}^{r=n} \Delta_r$

Hence for a complicated distribution curve of the form

$$y = k_0 + k_1x + k_2x^2 + k_3x^3 + k_4x^4 + k_5x^5 \quad \text{(i.e. } n = 5\text{)}$$

the maximum percentage error is less than 4·7%. This lies within the limit of 0·5 dB to which all noise measurements have been made.

3. C.R.P.L. Equipment

3.1. *Description of Equipment*

The main equipment has been described fully by Ahlbeck *et al.*[11] A block diagram of the main equipment is also shown in Fig. 3. The main equipment is designed to make automatic hourly recordings of the average atmospheric radio noise power for eight frequencies:

51 kc/s	113 kc/s	246 kc/s	545 kc/s
2·5 Mc/s	5 Mc/s	10 Mc/s	20 Mc/s

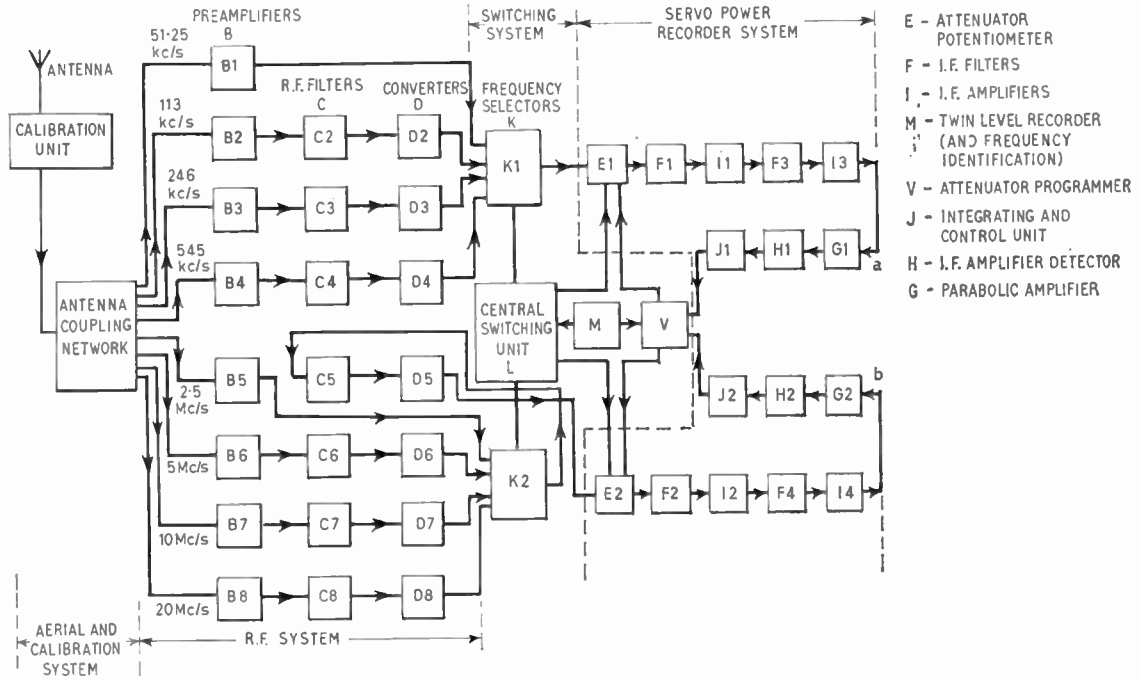

Fig. 3. Block diagram of C.R.P.L. system (ARN-2).

These are covered by a time-sharing arrangement which simultaneously records one of the low frequencies and one of the high frequencies as paired above. The four high frequencies lie on I.T.U. allocations for standard frequencies and should be frequencies least contaminated by signal interference in the radio spectrum. A telescopic aluminium whip 21·75 ft long mounted on a metal roof is used as the antenna system and the output is connected to the input of the noise recorder through a short coaxial cable. The calibration unit contains a standard noise generator and a set of eight dummy antenna networks transforming the noise generator output impedance to simulate the antenna impedance.

The antenna coupling network A switches the appropriate pair of the preamplifiers B1–8 on to the antenna, provides isolation through an isolation coil between the low-frequency and high-frequency pair of preamplifiers and grounds the input terminals of the other preamplifiers. The outputs of B2–B4, B6–B8 are fed through radio-frequency filters to converters D. The filters reject the first-order image frequency and all frequencies prior to the converter units by 126 dB. The frequency selectors K select the correct frequency channels for recording while the central switching unit L controls all the switching operations in the antenna coupling unit and frequency selector units and also causes the attenuators to track back to zero as operating frequencies are changed.

The attenuator potentiometer E provides the actuating voltage for the pen of the recorder. When it is in zero position, the potentiometer applies full-scale current to the recorder and reduces this current with increase in attenuation. The attenuator programmer V reduces the effect of intermittent signals arising from interference from man-made and other sources. At the instant of switching for change of frequency, relays hold the attenuator programmer inoperative. Two minutes later, when the attenuator potentiometer is now indicating noise power at about normal level, a flasher in the attenuator programmer is operated to give pulses to the attenuator potentiometer causing the potentiometer to slip three or four steps (6 to 8 dB) above the indicated noise level. After this, the relay system in the programmer locks the potentiometer to prevent any further forward stepping, but the potentiometer can step downwards towards the originally indicated level which is more likely to be the true atmospheric noise level.

3.2. *Evaluation of Records*

For all the records, code lines on the edges of the chart indicate the frequency channel under reference. A 15-minute recording is made on each frequency each hour and these samples are taken as representing

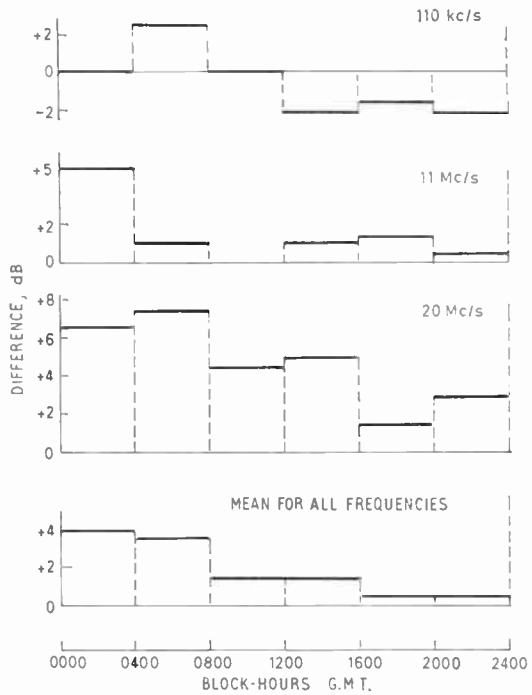

Fig. 4. Differences in measured r.m.s. fields (Spring).

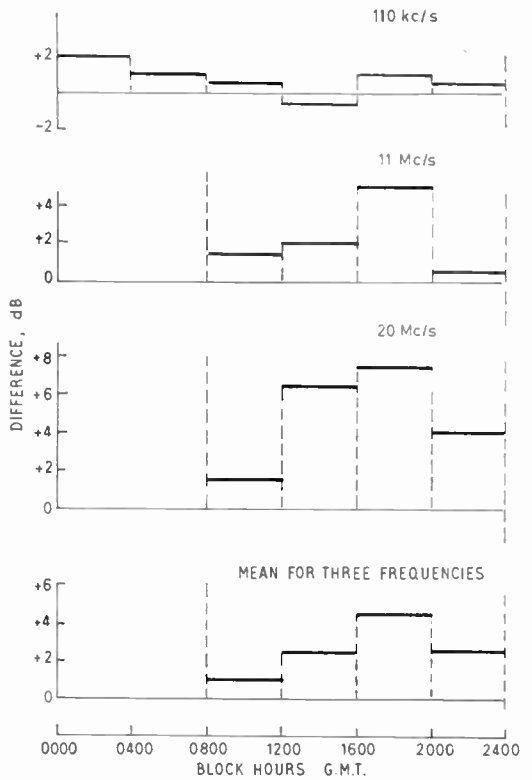

Fig. 5. Differences in measured r.m.s. fields (Summer).

noise conditions for the full hour. The last step value during each 15-minute recording interval for a given frequency is recorded on the 2 dB interval chart; and pairs of frequencies are recorded as follows:

51 kc/s and 2·5 Mc/s—first 15 minutes of the hour

113 kc/s and 5·0 Mc/s—15–30 minutes of the hour

246 kc/s and 10·0 Mc/s—30–45 minutes of the hour

545 kc/s and 20·0 Mc/s—last 15 minutes of the hour

For the power records, the decibel values on the daily chart were read off and converted to effective antenna noise figure F_a defined as the noise power available from an equivalent lossless antenna relative to kTB, the thermal noise power in watts in a passive resistance where

k = Boltzmann's constant = $1{\cdot}38 \times 10^{-23}$ joules per degree Kelvin.

T = absolute temperature in degrees Kelvin (taken as 290°).

B = effective noise bandwidth in cycles per second.

F_a in dB is related to the r.m.s. field strength at the antenna by the equation[12]

$$E_n = F_a + 20 \log_{10} f - 65{\cdot}5$$

where E_n = equivalent vertically polarized ground wave r.m.s. noise field strength in dB above 1 microvolt per metre for 1 kc/s bandwidth.

f = frequency in megacycles per second.

The method is therefore suitable for comparing measurements made with the two equipments described, provided bandwidths are taken into account. The mean voltage and mean logarithm of voltage, V_d and L_d, expressed in dB below mean power, were also measured in a log-linear auxiliary section on a separate rack from the main equipment.

4. Discrepancies in Measured Parameters

The parameters which have been compared are the r.m.s. field and the r.m.s./average ratios of atmospheric noise envelope obtained from the two systems already described. For the r.m.s. field, the results from both systems are expressed in terms of F_a, in dB above kTB, which is independent of bandwidth. In the case of the r.m.s./average ratio, the results from the C.R.P.L. equipment at 200 c/s power bandwidth have been converted for bandwidth of 340 c/s which is that of the D.S.I.R. equipment, using curves provided by Spaulding *et al.*[13] The amplitude probability distributions derived from the log-linear records on the C.R.P.L. equipment and modified for bandwidth, have been compared with those obtained directly from the D.S.I.R. equipment.

4.1. *R.M.S. Field Values*

For convenience, when values from the C.R.P.L. equipment are greater than corresponding values on the D.S.I.R. equipment, the discrepancies between values from the two systems are denoted positive (+). The mean discrepancies between simultaneous hour-by-hour values of r.m.s. field obtained from measurements during May 1958, April 1959, March, April, May 1960 and April, May 1961—being Spring months—are plotted in Fig. 4, while the mean discrepancies obtained during June and July 1959, 1960 and 1961—all Summer months—are shown in Fig. 5.

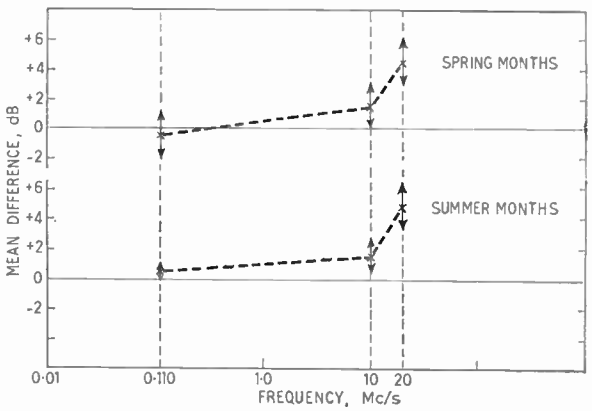

Fig. 6. Mean differences in measured fields.

Three frequencies for each season were considered and values have been averaged over C.C.I.R. four-hour time-blocks for both seasons. Substantial results were not obtained for 0000–0400 and 0400–0800 time-blocks for 11 Mc/s and 20 Mc/s during the Summer seasons. A difference of 1 dB has been allowed for in the plots for 11 Mc/s since the C.R.P.L. equipment recorded at 10 Mc/s while the D.S.I.R. was operated at 11 Mc/s. All the discrepancies for each frequency (for all time-blocks) have been averaged for the Summer and Spring months as shown in Fig. 6. The arrows indicate the statistical limits of variation of discrepancies obtained from the Standard Error of the difference between the means of measurements by each system. A total of about 1500 hours of comparison has been considered for each of the two seasons.

4.2. *R.M.S./Average Ratio*

The r.m.s./average ratios have also been compared for Summer months on same three frequencies. Consistent results for the three seasonal months were obtained in Summer 1960 on the C.R.P.L. equipment and in Summer 1961 on the D.S.I.R. equipment. The time-block averages of discrepancies in the ratios

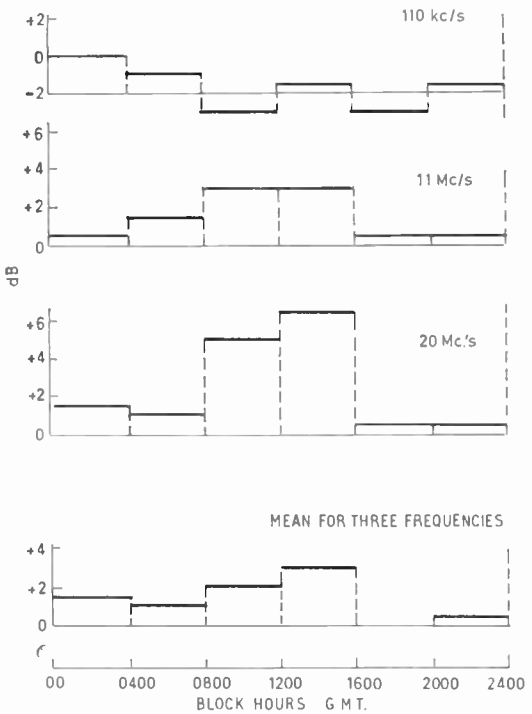

Fig. 7. Discrepancies in measured r.m.s./average ratios.

have been shown in Fig. 7, with positive values again assigned to cases where r.m.s./average ratio values are higher on the C.R.P.L. equipment. However, an average of twenty values for each frequency obtained simultaneously on both systems on hour-by-hour basis during Summer 1961 have also been compared. These discrepancies are indicated in Table 4 together with seasonal discrepancies. A total of about 600 hours of comparison has been considered at Ibadan.

4.3. *Significance of the Discrepancies*

It is necessary to test statistically whether these discrepancies taken as differences of sample means are significant. The *u*-test based on range estimates in place of the root-mean-square estimates of the *t*-test and which was developed by Lord,[14] has been applied here.

Table 3

Discrepancies between Measured R.M.S. Values

Frequency Mc/s	Mean and Range of All Discrepancies in dB		Significance Limit, dB $D_n\left(\frac{w_1+w_2}{2}\right)$
	Spring months	Summer months	
0·110	$-0{\cdot}5 \pm 1{\cdot}5$	$+0{\cdot}5 \pm 0{\cdot}5$	5·5
11(10)	$+1{\cdot}5 \pm 1{\cdot}5$	$+1{\cdot}5 \pm 1{\cdot}0$	5·0
20	$+4{\cdot}5 \pm 1{\cdot}5$	$+4{\cdot}8 \pm 1{\cdot}5$	3·5

If two samples of equal size have means $\bar{x}_1$, $\bar{x}_2$ and ranges w_1, w_2 and each sample may be considered as a random selection from the same normal population, the probability is 95% that if they are also drawn from the same population,

$$|\bar{x}_1 - \bar{x}_2| \leqslant D_n \frac{(w_1 + w_2)}{2}$$

where D_n is the mean range in samples from a normal population of unit standard deviation. It depends on the size of sample and is predetermined. Mean group ranges are used and the difference between the means (in dB) is assumed to have a standard error which follows a normal law (in dB). Greater discrepancies than indicated by $\left[D_n \frac{w_1+w_2}{2}\right]$ are unlikely to have arisen through chance and therefore indicate real differences.

The measured discrepancies for each frequency and estimated values of significance limits are given in Table 3 for the r.m.s. values and Table 4 for r.m.s./average ratios. The mean of the discrepancies fall within limit of experimental error in the cases of 110 kc/s and 11(10) Mc/s. This is further supported by the 'tests of significance' which show that it is only in the case of 20 Mc/s that the mean of the discrepancies exceeds the significance limit.

4.4. *Comparison of A.P.D. Curves*

An empirically-derived graphical method of obtaining an amplitude probability distribution from three statistical moments—F_a, $\bar{v}$, $\overline{\log v}$—obtained directly from the C.R.P.L. equipment has been published by Crichlow *et al.*[15] Also Spaulding *et al.*[13] have presented a method for the conversion of a.p.d. from one bandwidth to the other. By the application of these two processes, an a.p.d. was derived and directly comparable in all respects with the a.p.d. obtained from the D.S.I.R. equipment. An a.p.d. curve obtained directly in a 3-dB bandwidth of 340 c/s at 108 kc/s between 1600–2000 hours G.m.t. averaged for summer 1961 and another derived from the C.R.P.L. equipment at 200 c/s bandwidth and 113 kc/s

Table 4

Discrepancies between Measured R.M.S./Average Ratios

Frequency M/cs	Mean Differences for All Time Blocks, dB		Significance Limit, dB
	Seasonal comparison	Hourly comparison	
0·110	+0·3	+0·25	3·0
11(10)	+1·5	+1·0	2·0
20	+2·5	+2·0	1·5

between 1600–2000 hours, averaged over same season and converted to 340 c/s bandwidth, have been compared in Fig. 8. Corresponding curves for 20 Mc/s averaged for the whole summer season are shown in Fig. 9.

5. Discussion of Results

The results indicate that both equipments can provide consistent and reliable results in the tropics and that good agreement exists between measured parameters obtained with the two systems in all but one of the frequencies investigated. The discrepancies in r.m.s. values and also r.m.s./average ratios are significant only at 20 Mc/s.

In a report to Commission IV of the U.R.S.I. XIIIth General Assembly in 1960, Horner[16] indicated from comparative measurements made at Singapore on an hour-by-hour basis that the median C.R.P.L. values of r.m.s. field are higher than the corresponding D.S.I.R. values at low and high frequencies. The discrepancies from the series of measurements are of mean amount:

24 kc/s	2·5 dB	145 kc/s	2·0 dB
11 Mc/s	5·0 dB	20 Mc/s	4·5 dB

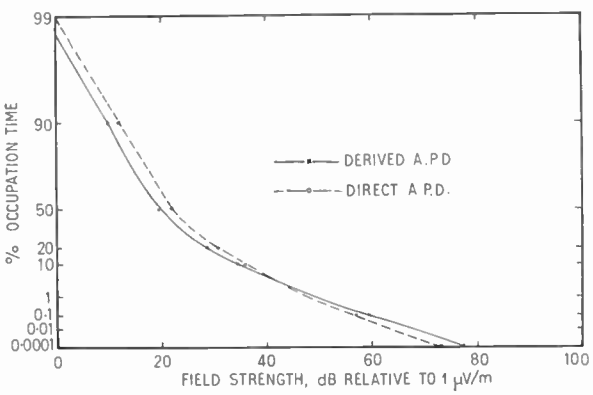

Fig. 8. Comparative (direct and derived) a.p.d. at 110 kc/s.

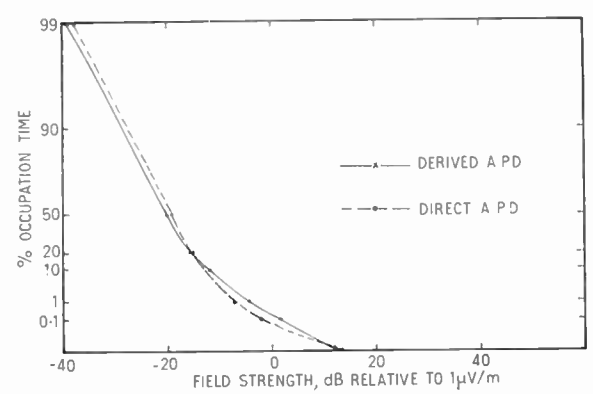

Fig. 9. Comparative (direct and derived) a.p.d. at 20 Mc/s.

The mean amount of discrepancies at Ibadan also indicates greater differences at the high frequencies with the higher values on the C.R.P.L. equipment. The r.m.s./average ratios also show greater values on the C.R.P.L. equipment and the results in Table 4 show that the mean difference of about +2 dB is significant only at 20 Mc/s. The plot in Fig. 7 shows that the overall discrepancy is least during late afternoons (1600–2000) in Spring, which is a season when local thunderstorm activity is most intense in the area investigated, and is low through the night-time when the noise levels are normally high. This trend indicates interference as a source of error, so that at high noise levels such interference becomes less important.

The direct and derived a.p.d. curves comparing both structure and amplitude averaged over the same seasonal period for 110 kc/s and 20 Mc/s are shown in Figs. 8 and 9 and show good agreement. At 110 kc/s there is higher threshold on the C.R.P.L. derived curve for a given percentage occupation time than in the case of the D.S.I.R. At 20 Mc/s, however, the D.S.I.R. curve has a smaller r.m.s./average ratio and hence its r.m.s. and average values are influenced to a greater extent than the derived C.R.P.L. curve by the higher threshold contributions.

The results show that the discrepancies are significant only at 20 Mc/s when the mean amount of 4·5 dB agrees with the result obtained at Singapore, and the trend of variation of discrepancies indicates interference at 20 Mc/s from stations as a source of error causing higher noise value on the C.R.P.L. equipment, the interference being less important at high noise levels. Normally propagated interference signal level on 20 Mc/s would be expected to increase at night, say between 2000–2400 hours, when the propagation of long-distance signals is good. However, the attenuator programmer rejects an interfering signal rise of 6 to 8 dB.

The equipments have been situated close to each other and siting effects are negligible. It is generally believed that cosmic noise, arising from disturbances originating outside the Earth, contributes to noise fields from between 15 Mc/s to 30 Mc/s. Any differences in the noise contribution as received on both equipments are bound to be negligible. Another possible cause of discrepancy is an error in the overall 20 Mc/s calibration of one or both equipments (e.g. due to non-infinite impedance of noise diode used for calibration in the C.R.P.L. equipment), but such errors should be constant throughout the day and not be subject to diurnal variations. If the receiver of the D.S.I.R. equipment were saturated on the peaks of noise, it would have an observed effect of tending to decrease the measured level of noise on the D.S.I.R. equipment. Such saturation is far more likely at lower frequencies than 20 Mc/s at which frequency

the noise is of a quasi-fluctuation type with little dynamic range. Various operational precautions were taken at all frequencies to avoid saturation and observations made at saturation were easily rejected from the visual display of the waveforms of noise envelope during the process of measurement.

All the observations taken on the D.S.I.R. equipment during Spring seasons and averaged for the differences in measured fields plotted in Fig. 4 have been further examined for the effect of interference. On certain occasions, observations were interrupted or discontinued at a particular frequency as a result of noticeable interference. The percentage of such occasions for all observations are 2·5% at 24 kc/s, 4·5% at 110 kc/s, 7·5% at 11 Mc/s and 28% at 20 Mc/s. Although the D.S.I.R. and the C.R.P.L.

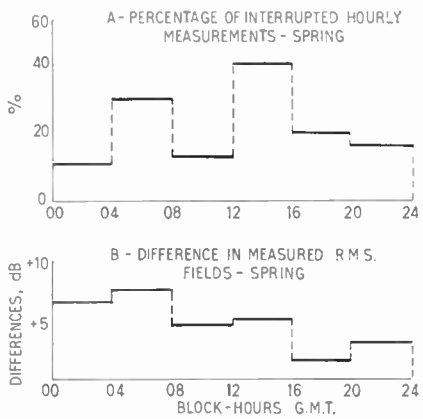

Fig. 10. Interference effect and discrepancies in measured fields at 20 Mc/s.

equipments operated at different bandwidths in the same neighbourhood, these percentages have been obtained at a fixed bandwidth for one of the equipments. The relatively high percentage at 20 Mc/s will support the idea that 20 Mc/s was more susceptible to interference than any of the lower frequencies investigated. The time-block distribution of these interruptions at 20 Mc/s is shown in Fig. 10, where it is compared with the differences in measured r.m.s. fields from both systems at 20 Mc/s over the same seasonal period. Apart from the 2000–2400 time-block, rise or fall in measured differences corresponds to increase or decrease in the percentage of interrupted measurements.

Automatic measurements on the C.R.P.L. equipment have been made in a narrow bandwidth of 200 c/s with high selectivity. Further, the action of the attenuator programmer sets an upper limit of 6 to 8 dB rise in noise level within a 15-minute period of measurement. Nevertheless, a risk of error could arise from an interfering signal persisting through the period of measurement at a particular frequency and tending to increase the apparent noise level.

Although the D.S.I.R. equipment has been used, unattended, to obtain average levels of noise at a fixed frequency, it is designed primarily for manual operation. To obtain sufficient number of values of noise parameters to average statistically for a range of frequencies, this equipment requires a number of operators. On the other hand, the C.R.P.L. automatic equipment would more easily provide the large number of results required for noise values for eight different frequencies. The C.R.P.L. equipment, therefore, is to be recommended for atmospheric noise studies on a world-wide scale provided a system for automatic discrimination of contaminated noise signals at least in the 20 Mc/s band can be incorporated.

6. Conclusions

Both the D.S.I.R. and the C.R.P.L. standard noise equipments have been operated satisfactorily for the measurement of noise levels and parameters in a tropical area. Higher values of noise power and r.m.s./average ratios are generally obtained with the C.R.P.L. equipment, but the discrepancies are significant only at 20 Mc/s when the difference has a mean value of +4·5 dB for noise power and +2·0 dB for r.m.s. to average ratio. A major source of the discrepancy is the error in the C.R.P.L. equipment arising from station interference at 20 Mc/s and causing the C.R.P.L. values to be higher. It is suggested that an additional system for automatic discrimination of interference should be incorporated in the C.R.P.L. equipment to enhance its suitability as the standard equipment for the measurement of atmospheric noise parameters on a world-wide scale.

7. Acknowledgments

The author wishes to thank the Department of Scientific and Industrial Research of Great Britain and the Central Radio Propagation Laboratories of U.S.A., who made the equipments available as their contributions to the Nigerian programmes of the International Geophysical Year 1957–58, and also a number of his colleagues for valuable assistance during the programme.

8. References and Bibliography

1. H. A. Thomas and R. E. Burgess, "Study of Existing Information and Data on Radio Noise over the Frequency Range 1–30 Mc/s", D.S.I.R. Radio Research Report No. 15, 1947.
2. R. S. Hoff and R. C. Johnson, "A statistical approach to the measurement of atmospheric noise", *Proc. Inst. Radio Engrs*, 40, p. 185, 1952.

3. H. Yuhara, T. Ishida and M. Higashimura, "Measurement of amplitude probability distribution of atmospheric noise" *J. Radio Research Laboratories (Japan)*, 3, p. 101, 1956.
4. F. Horner and J. Harwood, "Investigation of atmospheric radio noise at very low frequencies", *Proc. Instn Elect. Engrs*, 103B, p. 743, 1956.
5. C. Clarke, "Atmospheric noise structure", *Electronic Technology*, 37, p. 197, 1960.
6. J. Harwood and C. Nicolson, "Atmospheric radio noise: (equipment for the measurement of amplitude probability distributions)", *Electronic Radio Engr*, 35, p. 183, 1958.
7. O. Ibukun, "Studies of Atmospheric Radio Noise in a Tropical Area", Ph.D. Thesis, University of London Faculty of Engineering, December 1963.
8. H. Cramer, "Mathematical Methods of Statistics", p. 176 (Princeton University Press, 1947).
9. Y. W. Lee, "Statistical Theory of Communication", p. 148 (J. Wiley, New York, 1960).
10. L. M. Milne-Thomson and L. J. Comrie, "Standard Four-figure Mathematical Tables", p. 225 (Macmillan, London, 1931).
11. W. H. Ahlbeck, W. Q. Crichlow, R. T. Disney, F. F. Fulton Jr. and C. A. Samson, "Operating Instructions for ARN-2 Noise Recorder", National Bureau of Standards Report 5545, 1958.
12. C.C.I.R., "Revision of Atmospheric Radio Noise Data" C.C.I.R. Report No. 65, I.T.U., Geneva, 1957.
13. A. D. Spaulding, C. J. Roubique and W. Q. Crichlow, "Conversion of the amplitude probability distribution function for atmospheric radio noise from one bandwidth to another", *J. Res. Nat. Bur. Stds*, **66D**, p. 713, 1962.
14. E. Lord, "The use of range in place of standard deviation in the *t*-test", *Biometrika*, 34, p. 41, 1947.
15. W. Q. Crichlow, C. J. Roubique, A. D. Spaulding and W. M. Berry, "Determination of the amplitude probability distribution function for atmospheric radio noise from statistical moments", *J. Res. Nat. Bur. Stds*, **64D**, p. 49, 1960.
16. F. Horner, "Properties of Natural Noise: Results of the IGY Atmospheric Noise Programme", Report of Commission IV, URSI XIIIth General Assembly, London, 1960.

Manuscript first received by the Institution on 13th April 1964 and in final form on 16th September 1964. (Paper No. 950.)

STANDARD FREQUENCY TRANSMISSIONS

(Communication from the National Physical Laboratory)

Deviations, in parts in 10^{10}, from nominal frequency for **November 1964**

November 1964	GBR 16kc/s 24-hour mean centred on 0300 U.T.	MSF 60 kc/s 1430–1530 U.T.	Droitwich 200 kc/s 1000–1100 U.T.	November 1964	GBR 16 kc/s 24-hour mean centred on 0300 U.T.	MSF 60 kc/s 1430–1530 U.T.	Droitwich 200 kc/s 1000–1100 U.T.
1	− 149·9	− 149·7	—	16	− 150·1	− 151·2	+ 1
2	− 149·4	− 149·4	− 3	17	− 151·0	− 151·2	+ 1
3	− 150·1	− 149·2	− 2	18	—	—	+ 1
4	− 151·2	− 151·1	− 2	19	− 149·6	− 150·7	+ 2
5	− 151·3	− 150·3	− 2	20	− 151·9	− 151·9	+ 2
6	− 150·4	− 150·0	− 1	21	− 150·4	− 148·8	+ 3
7	− 149·8	− 149·1	—	22	− 149·9	− 150·2	+ 4
8	− 149·1	− 149·2	—	23	—	− 150·2	+ 4
9	− 149·7	− 150·7	0	24	− 149·9	− 151·2	+ 4
10	− 149·5	− 149·3	0	25	− 152·1	− 151·2	+ 4
11	− 149·9	− 150·3	0	26	− 150·0	− 149·8	+ 4
12	− 151·8	− 151·1	0	27	− 150·2	− 149·9	+ 5
13	− 149·6	− 150·0	+ 1	28	− 149·1	—	+ 6
14	− 150·9	− 150·8	+ 1	29	− 148·0	− 148·7	+ 7
15	− 150·2	− 150·4	+ 1	30	− 148·4	− 149·2	+ 6

Nominal frequency corresponds to a value of 9 192 631 770 c/s for the caesium F,m (4,0)–F,m (3,0) transition at zero field.

Notes: The phase of the GBR/MFS time signals will be retarded by 100 milliseconds at 00 00 UT on 1st January 1965.

The frequency offset for 1965 will be -150×10^{-10}

U.D.C. 621.372.542.21

A Full-section Prototype Filter with Chebyshev Behaviour and Finite Inductor Q

By

D. W. W. ROGERS
(*Associate Member*)†

Summary: A method of achieving an exact wide-band Chebyshev response in a full-section filter is described, in which the dissipation for each arm is taken into account. The work follows on from that of Mole, in which the shunt dissipation is assumed to be zero. A similar treatment has been carried out by Head, in which the design parameters are presented in a series form. The method of analysis employed by the author is less elegant, for the case considered, than that of Dishal, but has the advantage of being more direct, and providing a simpler expression for attenuation.

Graphs are included which indicate the correct dissipation for each arm and the insertion loss of the filter in terms of the normalized terminations and shunt conductance.

List of Symbols

R_n nominal impedance for a constant k prototype half-section (ohms).

$L = R_n/\omega_c$, $C_0 = 1/R_n\omega_c$ element values of prototype, low or high-pass filters.

$\omega_c = 2\pi f_c$, where f_c is the cut-off frequency of a prototype filter (radians).

A_1 peak-to-peak ripple amplitude measured from zero frequency to the frequency f_1 at which the ripple is defined in the case of a low-pass filter (dB). (See Fig. 1.)

$x = f/f_c$, operating frequency variable.

$x_1 = f_1/f_c$ fractional ripple bandwidth.

x_{10}, x_{20}, x_{40} are frequencies at which the loss exceeds that at zero frequency by 10, 20 and 40 dB respectively.

P ratio of the effective source or load resistance to the nominal impedance for a T-network, and its reciprocal for a π-network.

P_1, P_2 modified P values as plotted in Fig. 3.

A attenuation relative to the loss at zero frequency in the case of a low-pass filter (dB).

G_1 shunt conductance of the full-section filter (mhos).

G' ratio of the effective shunt conductance G_1 to the nominal impedance (mhos)^2.

1. Introduction

Dishal[3] has analysed the multi-element ladder network in which the dissipation of each element may be taken into account. This latter aspect relating to dissipation is of great practical significance in so much that a filter may be designed with low-Q inductors and still have, theoretically at least, exact Chebyshev properties. A Chebyshev response has a ripple of constant magnitude over prescribed limits in the pass band and offers the greatest attenuation slope in the stop-band. Such a response provides the best approximation to an ideal rectangular characteristic and is suitable for many requirements in which m derivation is unnecessary. To this end, the symmetrical full-section filter is perhaps a good compromise between simplicity and efficiency, and the author will give some simplified graphical design information of this case. The method of analysis employed in this paper is to compare the coefficients of the modulus squared of the transfer function for the low-pass filter shown in Fig. 2 with the coefficients of the Chebyshev polynomial of the first kind, order 6 (see Section 2). The two resulting equations in terms of the normalized terminations P_1, P_2, shunt conductance G_1 and fractional bandwidth x_1, are combined into one equation by eliminating the fractional bandwidth. When the latter equation, a cubic in P_1, P_2 and G_1, is solved for P_1 and P_2 in terms of G_1, it is found that the values of the normalized filter terminations P_1 and P_2 given by the above equation present a design which is almost equivalent to a full-section symmetrical filter with Chebyshev response and infinite shunt Q, i.e. $G_1 = 0$.

In order to overcome the usual difficulties associated with the presentation of filters with Chebyshev behaviour, the properties of the Chebyshev polynomial employed, are discussed at length from a tutorial point of view.

† Oldham Technical College, Lancashire. The author holds the Diploma of Graduate Studies of the University of Birmingham.

2. Some Properties of the Chebyshev Polynomial of the First Kind, Order 6

The modulus of the transfer function of the full-section filter is shown in Section 3 to have the form $P_2/2|\,f(x)|$, where $|\,f(x)|^2$ is to be represented by the Chebyshev polynomial given below.

$$|\,f(x)|^2 = x^6 - \tfrac{3}{2}x_1^2x^4 + \tfrac{9}{16}x_1^4x^2 + C \quad \text{.....(1)}$$

where

$$x = f/f_c \quad \text{and} \quad x_1 = f_1/f_c$$

Differentiating twice with respect to x, the frequency variable,

$$\frac{d(|\,f(x)|^2)}{dx} = 6x^5 - 6x_1^2x^3 + \tfrac{9}{8}x_1^4x \quad \text{.....(2)}$$

and

$$\frac{d^2(|\,f(x)|^2)}{dx^2} = 30x^4 - 18x_1^2x^2 + \tfrac{9}{8}x_1^4 \quad \text{.....(3)}$$

Equating $\dfrac{d(|\,f(x)|^2)}{dx}$ to zero, the roots are $x = 0$, $\dfrac{x_1}{2}$, $\dfrac{\sqrt{3}x_1}{2}$ and represent zero frequency at which the first minimum occurs, one half the ripple bandwidth at which the first maximum occurs and 0·866 of the ripple bandwidth at which the second minimum occurs, respectively. This form of ripple is shown in Fig. 1.

Substituting $x = 0, \dfrac{x_1}{2}, \dfrac{\sqrt{3}x_1}{2}$, into eqn. (3) gives for $\dfrac{d^2(|\,f(x)|^2)}{dx^2}$, $\tfrac{9}{8}x_1^4$, $-\tfrac{3}{2}x_1^4$ and $\tfrac{9}{2}x_1^4$ respectively, which confirm the two minima and one maximum shown in Fig. 1.

The values of $|\,f(x)|^2$ at the above frequencies are as follows:—

x	$\lvert f(x)\rvert^2$
0	C
$\dfrac{x_1}{2}$	$\dfrac{x_1^6}{16} + C$
$\dfrac{\sqrt{3}}{2}x_1$	C
x_1	$\dfrac{x_1^6}{16} + C$

.....(4)

which illustrates the 'equi-ripple'.

3. Analysis of Full-section Low-pass Filter with Chebyshev Behaviour

A lossy shunt capacitor is assumed in order that the analysis may if required be applicable to a band-pass filter by suitable transformation formulæ, in which the shunt inductor is of finite Q. The T-network shown in Fig. 2 is used for analysis although the results are equally applicable to a π-network.

Consider an arbitrary series inductive arm $R+j\omega L$. For a prototype low-pass filter, $L = R_n/\omega_c$, where ω_c is the cut-off frequency. Substituting P_1R_n for R, the left-hand series arm may be represented by

$$P_1R_n + j(\omega/\omega_c)R_n \quad \text{or} \quad P_1R_n + jxR_n \quad \text{.....(5)}$$

and the right-hand arm by $P_2R_n + jxR_n$. Similarly an arbitrary lossy shunt capacitive arm may be represented by $G' + j\omega C_0$ in a half-section prototype filter. Substituting $C_0 = 1/\omega_cR_n$ and $G' = G_1/R_n$ the shunt arm may be represented by

$$2G_1/R_n + j2\omega/\omega_cR_n, \quad \text{or} \quad 2G_1/R_n + j2x/R_n \quad \text{.....(6)}$$

the factor of 2 being present on account of the full-section. The variables P_1, P_2 and G_1 are introduced in order that a relation may be found between them such that a Chebyshev response for the low-pass filter of Fig. 2 is obtained. The transfer function of the filter may be shown to be

$$V_{out}/V_{in} = P_2/[P_2 + jx + (P_1 + jx) \times \times (1 + 2(P_2 + jx)(G_1 + jx))] \quad \text{.....(7)}$$

where the modulus of the transfer function is of the form $P_2/2|\,f(x)|$ and

$$|\,f(x)|^2 = x^6 - (2 - P_1^2 - P_2^2 - G_1^2)x^4 + (P_1^2P_2^2 + P_1^2G_1^2 + P_2^2G_1^2 + (P_2 + P_1)G_1 - P_1^2 - P_2^2 + 1)x^2 + ((P_1 + P_2)/2 + P_1P_2G_1)^2 \quad \text{.....(8)}$$

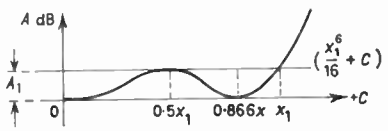

Fig. 1. Chebyshev response.

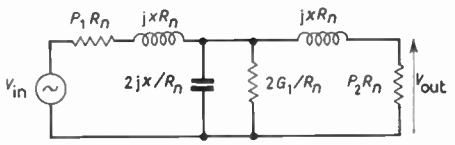

Fig. 2. Normalized filter circuit.

The phase of the filter in this case is of minor interest, although it is clear from Bode's integral theorem relating magnitude to phase, that the phase must also ripple correspondingly. If the coefficients of $|\,f(x)|^2$ eqn. (8) are now compared with that of the Chebyshev polynomial of the first kind, order 6, eqn. (1), the following three equations are obtained, which must be simultaneously satisfied in order that the modulus of eqn. (7) will have the desired Chebyshev behaviour.

$$2 - P_1^2 - P_2^2 - G_1^2 = \tfrac{3}{2}x_1^2 \quad \text{.....(9)}$$

$$P_1^2 P_2^2 + P_1^2 G_1^2 + P_2^2 G_1^2 + P_2 G_1 + + P_1 G_1 - P_1^2 - P_2^2 + 1 = \tfrac{9}{16} x_1^4 \quad \text{.....(10)}$$

$$((P_1 + P_2)/2 + P_1 P_2 G_1)^2 = C \quad \text{.....(11)}$$

Eliminating x_1 from eqns. (9) and (10) and rearranging

$$P_1^4 + P_2^4 + G_1^4 - 2P_1^2 P_2^2 - 2P_2^2 G_1^2 - 2P_1^2 G_1^2 = 4G_1(P_1 + P_2 + G_1) \quad \text{.....(12)}$$

This is the required relationship between the normalized variables P_1, P_2 and G_1. It is convenient to factorize eqn. (12) as follows:

$$(P_1 + P_2 + G_1)[(P_2 - P_1 + G_1)(P_2 - P_1 - G_1) \times \times (P_1 + P_2 - G_1) - 4G_1] = 0 \quad \text{.....(13)}$$

This equation clearly has four solutions in terms of the terminations P_1, P_2 and G_1. However, only the solution in which P_1, P_2 and G_1 are all positive is of immediate interest. The following two cases are considered:

(*a*) Shunt conductance zero $P_1 = P_2$.

(*b*) „ „ positive $P_1 \neq P_2$.

3.1. *Shunt Conductance Zero* $P_1 = P_2$

This is the degenerate case considered by Mole[1] for which the root $(P_1 - P_2)$ gives a remarkably simple solution of eqn. (13). Although for many practical cases the assumption that G_1 is zero leads to unsatisfactory filter designs, it is shown in Section 3.2 that the formula derived for the ripple bandwidth and stop-band attenuation for this case may be employed with negligible error to case (*b*), in which the solution of eqn. (13) gives specific values of P_1, P_2 and G_1, for the normalized terminations. It is necessary therefore to review case (*a*) in some detail in preparation for case (*b*) by deriving the ripple and stop-band attenuation.

Substituting $P_1 = P_2$ and $G_1 = 0$ in eqn. (9)

$$P_1 = P_2 = \sqrt{1 - \tfrac{3}{4}x_1^2} \quad \text{.....(14)}$$

This equation enables the terminations to be chosen in terms of the normalized ripple bandwidth x_1. Substituting $P_1 = P_2$ and $G_1 = 0$, in eqn. (11), $C = P_1^2$ and the transfer function may be written as

$$V_{out}/V_{in} = P_1/(2\sqrt{(x^2 - \tfrac{3}{4}x_1^2)^2 x^2 + P_1^2}) \quad \text{.....(15)}$$

In particular it is interesting to examine the case for which the bandwidth just vanishes, i.e. $x_1 = 0$. Then from eqn. (14) $P_1 = P_2 = 1$, and the transfer function is of the form $1/(2\sqrt{1 + x^{2n}})$. This is the familiar Butterworth response for $n = 3$, the factor 2 representing the 6 dB matching loss for equal resistive terminations (i.e. $R_1 = R_2 = R_n$). The transfer function of eqn. (15) may be rewritten as

$$V_{out}/V_{in} = 1/\left(2\sqrt{1 + \frac{(x^2 - \tfrac{3}{4}x_1^2)^2 x^2)}{P_1^2}}\right) \quad \text{.....(16)}$$

$$= 1/(2\sqrt{1 + F^2})$$

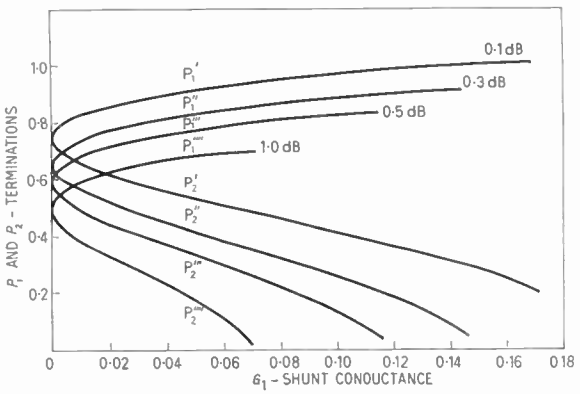

Fig. 3. Graph of terminations versus conductance.

where

$$F = \frac{x(x^2 - \tfrac{3}{4}x_1^2)}{P_1} = \frac{x(x^2 - \tfrac{3}{4}x_1^2)}{\sqrt{1 - \tfrac{3}{4}x_1^2}} \quad \text{.....(17)}$$

Finally, expressing the attenuation of the filter relative to the loss at zero frequency, which in this case merely excludes the 6 dB matching loss, the loss is given by

$$A = 10 \log_{10}(1 + F^2) \text{ dB} \quad \text{.....(18)}$$

Referring now to Fig. 1, the peak-to-peak ripple amplitude expressed as a power ratio in decibels is given by

$$20 \log_{10} \sqrt{\frac{\frac{x_1^6}{16} + C}{C}} = 10 \log_{10}(1 + F_1^2) \quad \text{.....(19)}$$

where

$$F_1^2 = \frac{x_1^6}{16 - 12x_1^2} \quad \text{.....(20)}$$

3.2. *Shunt Conductance Positive* $P_1 \neq P_2$

Substituting $P_2 - P_1 = a$ and $P_2 + P_1 = b$, the factor $[(P_2 - P_1 + G_1)(P_2 - P_1 - G_1)(P_1 + P_2 - G_1) - 4G_1] = 0$ in eqn. (13) becomes

$$(a^2 - G_1^2)(b - G_1) = 4G_1 \quad \text{.....(21)}$$

and may be solved as the following cubic equation

$$G_1^3 - G_1^2 b - G_1(4 + a^2) + a^2 b = 0 \quad \text{.....(22)}$$

in which given values of a and b are substituted to find G_1. Finally triads of P_1, P_2 and G_1 are plotted as in Fig. 3 for various values of ripple. An alternative graphical solution for the positive values of P_1, P_2 and G_1 was suggested by D. Hiscock of A.U.W.E., Portland. Equation (21) is written in the form

$$y^2 = a^2 - G_1^2 = 4G_1/(b - G_1) \quad \text{.....(23)}$$

The intersections of the circle $y^2 + G_1^2 = a^2$ and $y^2 = 4G_1/(b - G_1)$, give the values of a and b in terms of G_1, as shown in Fig. 4.

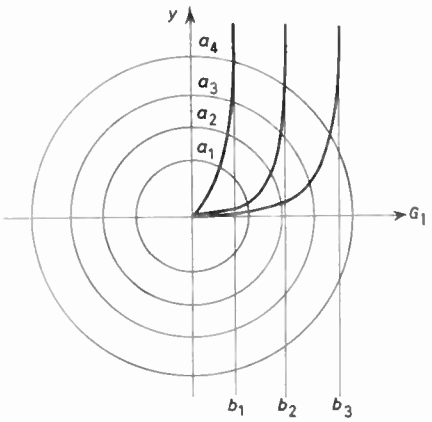

Fig. 4. Graphical solution of $y^2 = a^2 - G_1^2 = 4G_1/(b - G_1)$.

The ripple bandwidth in this case may be determined for case (*b*) from eqn. (9)

$$x_1^2 = \tfrac{4}{3} - \tfrac{2}{3}(P_1^2 + P_2^2 + G_2^2) \qquad \text{.....(24)}$$

Fortunately, because the value of the expression $(P_1^2 + P_2^2 + G_1^2)$ turns out to be within 1% of the value of P_1 given in eqn. (14), the value of x_1 may be justifiably taken as

$$x_1 = \sqrt{\tfrac{4}{3}(1 - P_1^2)} \qquad \text{.....(25)}$$

as in case (*a*).

The error involved in this approximation is masked in any case by the practical variation of inductor Q over the ripple bandwidth. Similarly because the value of

$$C = \left(\frac{P_1 + P_2}{2} + P_1 P_2 G_1\right)^2$$

approximates to P_1 in eqn. (14), the values of the peak-to-peak ripple amplitude and attenuation are closely approximated by eqns. (18) and (19) respectively. The attenuation loss and ripple amplitude are given in Table 1 for 0·1, 0·3, 0·5 and 1·0 dB.

Table 1

A_1(dB)	P	x_1	x_1/P	$2Px_1$	x_{10}/x_1	x_{20}/x_1	x_{30}/x_1	x_{40}/x_1	x_3/x_1
0·1	0·74	0·77	1·02	1·14	1·9	2·7	3·8	5·5	1·39
0·3	0·65	0·88	1·36	1·14	1·6	2·2	3·2	4·5	1·23
0·5	0·59	0·94	1·58	1·1	1·5	2·1	2·9	4·1	1·17
1·0	0·49	1·01	2·04	0·99	1·3	1·9	2·6	3·7	1·1

4. Mid-band Voltage Transfer

From eqn. (7),

$$V_{in}/V_{out} = P_2/(P_1 + P_2 + 2P_1 P_2 G_1) \simeq P_2/(P_1 + P_2) \qquad \text{.....(26)}$$

as $2P_1P_2G_1 \ll P_1 + P_2$.

4.1. *Insertion Loss*

The insertion loss is plotted for various values of ripple and in Fig. 5 an expression for this factor is derived as follows:

$$\text{available power} = V_{in}^2/4P_1,$$

$$\text{power out} = V_{in}^2 P_2^2/P_2(P_1 + P_2 + 2P_1 P_2 G_1)^2,$$

therefore

$$\text{insertion loss} = \frac{\text{available power}}{\text{power out}} = 20 \log_{10} \frac{(P_1 + P_2 + 2P_1 P_2 G_1)}{2\sqrt{P_1 P_2}}$$

5. A Practical Example

It is supposed that a low-pass filter is to be designed with a bandwidth of 400 c/s, an approximate source impedance of 100 ohms and an attenuation at 1·5 kc/s of > 28 dB. The Q of the available inductors is 50.

Assuming that the Q of the inductors remains adequately constant over the 400 c/s bandwidth, then from eqn. (6)

$$G_1 = R_n G' = G'/\omega_c C_0 = 1/Q_{shunt} = 0{\cdot}02$$

The values of P_1 and P_2 corresponding to $G_1 = 0{\cdot}02$ and a ripple of 0·1 dB in Fig. 3 are 0·62 and 0·85 respectively. This particular design includes an RC shunt arm, instead of just a shunt capacitor in order that the design may be transformed if necessary into a bandpass filter. For the case of the capacitor alone, the values of P_1 and P_2 corresponding to $G_1 = 0$ and 0·1 dB ripple coalesce on Fig. 3 to 0·74 as in Table 1.[1] Reverting to the shunt RC case, however, P_1 and P_2 represent from eqn. (5) the reciprocals of the series arm Q, i.e.

$$P_1 = R/\omega_c L = 1/Q_{series}$$

The effective Q of the series arms corresponding to P_1 and P_2 are 1·61 and 1·18 respectively. From Fig. 5 the insertion loss is 0·3 dB. The mid-band voltage

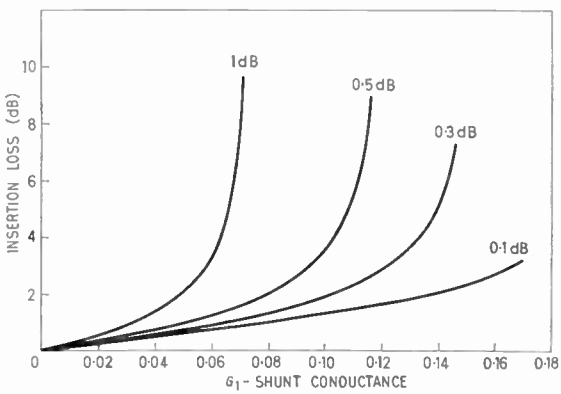

Fig. 5. Graph of power loss versus conductance.

transfer from eqn. (26) is given by

$$20 \log_{10} [P_2/(P_1+P_2)] = 20 \log_{10} [0{\cdot}85/(0{\cdot}62+0{\cdot}85)] \simeq -4{\cdot}5 \text{ dB}$$

From Table 1, $x_1 = 0{\cdot}77 = f_1/f_c = 400/f_c$, i.e. $f_c = 519$ c/s. Therefore $L = 100/6{\cdot}28 \times 519 = 3{\cdot}07$ mH, and $C_0 = 1/6{\cdot}28 \times 519 \times 100 = 3{\cdot}07$ μF. Further, $x_3 = 1{\cdot}39 \times 0{\cdot}77 = 1{\cdot}07$ and $x_{30} = 3{\cdot}8 \times 0{\cdot}77 = 2{\cdot}92$, corresponding to $519 \times 1{\cdot}07 = 555$ c/s at 3 dB attenuation, and $519 \times 2{\cdot}92 = 1520$ c/s at 30dB attenuation respectively. The required design is shown in Fig. 6.

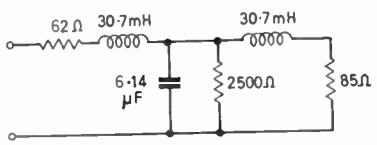

Fig. 6. Final low-pass filter design.

In practice, of course, the filter terminations are smaller than the values shown by an amount corresponding to the inherent resistive component of the resistors chosen. If it is required to transform to a bandpass filter, the inductor in the low-pass filter should be replaced by a series-resonant circuit with the following element values:

L_1(bandpass) = L(low-pass)/[$2\pi \times$ bandwidth]

C_1(bandpass) = [$2\pi \times$ (bandwidth)]/[L(low-pass) $\times \omega_0^2$]

Similarly, each capacitor should be replaced by a parallel-resonant circuit with the following element values:

L_2(bandpass) = [C(low-pass) $\times 2\pi \times$ bandwidth]/ω_0^2

C_2(bandpass) = 1/[C(low-pass) $\times 2\pi \times$ bandwidth]

where ω_0 is the mid-band circular frequency.

6. Conclusions

It has been shown that the design of a full-section prototype filter with Chebyshev behaviour and with dissipation in each arm, may be designed with simple formulæ, which are very nearly identical to the case when the shunt conductance G_1 is zero. The design has been proved, typical tolerances for satisfactory operation being ±5%, 1% and 0·1% for the resistances, reactive components, and resonant frequencies respectively.

7. Acknowledgment

The author is grateful to Mr. P. Kay of Oldham Technical College for helpful suggestions.

8. References

1. J. H. Mole, "Filter Design Data", pp. 236–8. (Spon, London, 1952.)
2. J. W. Head, "Filter design without filter theory", p. 1474, in "Electronic Engineer's Reference Book", edited by L. E. C. Hughes (2nd edn.). (Heywood, London, 1958.)
3. M. Dishal, "Design of dissipative band-pass filters producing desired exact amplitude-frequency characteristics", *Proc. Inst. Radio Engrs*, 37, pp. 1050–69, September 1949.

Manuscript first received by the Institution on 14th October 1963 and in final form on 7th July 1964. (Paper No. 951.)

SUBJECT INDEX

Papers and major articles are denoted by printing the page numbers in bold type.

Abstracts of papers are denoted by A.

INDEX OF PERSONS

Names of authors of papers published in the volume are indicated by bold numerals for the page reference.

Authors of papers which are given in abstract form are denoted by A.

Contributors to discussion are indicated by D.

INDEX OF ABSTRACTS

This index classifies under subject headings the abstracts published throughout the volume in "Radio Engineering Overseas".

JOURNALS FROM WHICH ABSTRACTS HAVE BEEN TAKEN DURING THE SECOND HALF OF 1964

Archiv der Elektrischen Übertragung (Germany)

Journal of the Institute of Electrical Communication Engineers of Japan

Mitsubishi Denki Laboratory Reports (Japan)

Nachrichtentechnische Zeitschrift (Germany)

L'Onde Électrique (France)

Philips Technical Review (Holland)

Proceedings of the Indian Division of the Institution of Electronic and Radio Engineers

Proceedings of the Institution of Radio and Electronics Engineers Australia

Slaboproudý Obzor (Czechoslovakia)